Power Factor Correction and Power Consumption Characterization of Piezoelectric Actuators
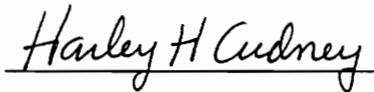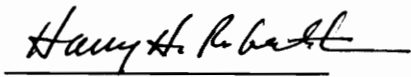
by

Christopher Niezrecki

Thesis submitted to the Faculty of the

Virginia Polytechnic Institute and State University

in partial fulfillment of the requirements for the degree of

MASTER OF SCIENCE

in

Mechanical Engineering

APPROVED:

Harley H Cudney

Dr. H. H. Cudney, Chairman

Harry H. Robertshaw

Dr. H. H. Robertshaw

A. L. Wicks

Dr. A. L. Wicks

September, 1992

Blacksburg, Virginia

Power Factor Correction and Power Consumption Characterization of Piezoelectric Actuators

by

Christopher Niezrecki

Committee Chair: Dr. Harley H. Cudney

Mechanical Engineering

(Abstract)

A piezoceramic actuator used for structural control behaves electrically as a nearly pure capacitance. When conventional amplifiers are used to drive these actuators, the current and voltage is close to 90 degrees out of phase. This causes the power factor (PF) of the load to be close to zero and results in excessive power requirements. This thesis reports the results of a study of the following question: What effect does applying power factor correction methods to piezoceramic actuators have on their power consumption characteristics? A subproblem we explored was to determine the qualitative relationship between the power consumption of a piezoceramic actuator and the damping that actuator added to a structure.

To address the subproblem, a feedback control experiment was built which used a ceramic piezoceramic actuator and a strain rate sensor configured to add damping to a cantilevered beam. A disturbance was provided by a shaker attached to the beam. The power consumption of the actuator was determined by measuring the current and voltage of the signal to the actuator. The energy dissipated in the beam by the feedback control loop

was assumed to be modeled by an ideal structural damping model. A model relating structural damping as a function of the apparent power consumed by the actuator was developed, qualitatively verified, and physically justified.

Power factor correction methods were employed by adding an inductor in both parallel to and in series with the piezoceramic actuator. The inductance values were chosen such that each inductor-capacitor (LC) circuit was in resonance at the second natural frequency of the beam.

Implementing the parallel LC circuit reduced the current consumption of the piezoceramic actuator by 75% when compared to the current consumption of the actuator used without an inductor. Implementing the series LC circuit produced a 300% increase in the voltage applied to the actuator compared to the case when no inductor was used. In both cases, employing power factor correction methods corrected the power factor to near unity and reduced the apparent power by 12 dB. A theoretical model of each circuit was developed. The analytical and empirical results are virtually identical. The results of this study can be used to synthesize circuits to modify piezoceramic actuators, reducing the voltage or current requirements of the amplifiers used to drive those actuators.

Acknowledgments

Table of Contents

List of Figures

List of Tables

Nomenclature

b	beam width
C	capacitance
c	damping coefficient
d_{31}	piezoelectric constant
E_a, E_b, E_p	modulus of elasticity of the adhesive layer, beam, and the PZT actuator
E_{Beam}	energy dissipated within the beam due to natural damping
E_d	energy provided to the beam by the shaker (per cycle)
E_{PZT}	energy dissipated within the beam due to active damping
F_o	magnitude of applied force
F(s)	Laplace domain forcing function
g	strain rate feedback gain
i, I	current
I_b, I_{Eq}	are moment of inertia of the beam and an equivalent area moment of inertia
I_C	current in the capacitive element
I_L	current in the inductor
j	imaginary number
k	mechanical stiffness
K^*, K	proportionality constant
k_1, k_2	first and second mode stiffness
L	inductance
M	mass
M^*, M	equivalent bending moment of the PZT actuator
m_1	first mode modal mass
m_2	second mode modal mass
P	real power

P_a	apparent power
PF	power factor
P_X	reactive power
R	resistance
R_L	internal resistance of the inductor
R_C	internal resistance of the PZT
Ri	resistance
s	Laplace variable
t_a, t_b, t_p	adhesive layer, beam, and PZT actuator thickness
V	voltage
V_C	voltage across a capacitor
V_s	amplifier supply voltage
V_i	input voltage
V_L	voltage across an inductor
V_o	output voltage
V_R	real voltage
V_{Ui}	voltages in the current to voltage converter and voltage reducer
V_X	reactive voltage
X	vibration amplitude
X	reactance
X(s)	Laplace domain output
X_C, X_L	capacitive and inductive reactance
Z	impedance
Z_C, Z_{PZT}	capacitive and PZT actuator impedance
Z_P	impedance of a parallel LC combination
Z_t	impedance of the realistic LC combination

Greek:

α	structural damping constant
Δ	temporary variable representing a denominator
γ	structural damping ratio
ϕ	phase angle between current and voltage
ϑ	phase angle between displacement and force
$\omega, \omega_n, \omega_r$	operating, natural, and resonant frequencies
ζ	viscous damping ratio
Λ	free strain of the actuator

Subscripts:

k	k-th actuator
1,2	top and bottom actuator, respectively
a	adhesive layer
b	beam
p	PZT actuator

Chapter 1

Introduction

1.1 Motivation

Adding structural damping using active control methods has been shown to be effective in reducing vibrations in mechanical structures (Skidmore and Hallauer, 1985, Bailey and Hubbard, 1985). Presently, the amount of control energy required to obtain a desired amount of damping or reduction in structural vibration when using piezoelectric actuators is unclear. This makes the selection of the amplifier a difficult task and inevitably the engineer chooses either an amplifier that is over-designed or unable to meet the design requirements. It is therefore desired to have some kind of guidelines for an engineer to follow in order to choose the appropriate amplifiers for the particular structural control application using piezoelectric actuators.

Several problems may occur when trying to drive lead zirconate titanate (PZT) actuators with amplifiers due to the actuator's capacitive properties. If an amplifier voltage is suddenly applied, sudden increase in voltage contains high frequency components that can cause large PZT currents and exceed the current limitations of the amplifier. A source of damage to the amplifier (depending on the amplifier design) occurs if the charged PZT has no path to discharge through. The piezoelectric actuator can cause a back electromotive force (emf) that exceeds the saturation voltage of the amplifier, causing damage. A third problem is caused when a piezoelectric actuator is driven by a transient or non-sinusoidal signal. The signal may have high frequency content and result in large currents (Trek, Inc., 1991). Finally, the power factor (ratio of real to apparent power) of a typical PZT actuator is near zero. This forces the amplifier to generate large currents to deliver the

required power. If the power factor can be increased, the power needed to drive PZT actuators can be reduced and will result in a reduced amplifier size. This work is motivated by the need to have guidelines in amplifier sizing based on energy dissipation and the desire to reduce control energy in active structural control.

1.2 Objective

The are two primary objectives of this research. The first is to study what effect applying power factor correction methods to piezoelectric actuators has on their power consumption characteristics. The second objective is to determine the qualitative relationship between the power consumption of a piezoelectric actuator and the damping that actuator added to a structure. Theoretical and experimental results will be compared and the differences between them will be discussed. Finally the practical applications of the results will be addressed.

1.3 Approach

The approach taken initially addresses the second objective. Piezoelectric actuators and polyvinylidene fluoride film (PVDF) sensors are mounted on an aluminum cantilever beam. The beam is excited in the second mode with a shaker and a signal proportional to strain rate is fed back to the PZT actuators. The control loop provides active damping to the structure. To measure the power consumption of the PZT actuators, voltage and current measuring circuits are constructed. The consumed power is then determined by measuring the magnitude and phase of the current and the voltage. The amount of added damping will be determined using frequency response functions of accelerance with respect to applied force and a curve fitting algorithm. The relationship between consumed power and added damping can then be developed. For the first objective, impedance

measurements will be performed to determine the electrical characteristics of the PZT actuator. The PZT consumed power will be reduced and power factor corrected by using inductor-capacitor (LC) resonant circuits tuned, to the second structural mode.

1.4 Outline

A review of the related literature and a brief description of industrial power factor correction is presented in Chapter 2. A theoretical development is presented in Chapter 3. A relationship between PZT actuator apparent power and the amount of added structural damping is developed. Series and parallel resonant circuits are investigated and their application to piezoceramic actuators is discussed. The experiments required to verify the concepts developed in Chapter 3 are described in Chapter 4. The experimental and analytical results are presented in Chapter 5. A review of the results and the conclusions are given in Chapter 6.

Chapter 2

Review of Related Literature

2.1 Active Structural Control

Within the last fifteen years much research has been performed in the control of flexible structures. A particular application of flexible structures is found in space. The structures that are constructed on Earth or in space need to be strong and light. This usually results in a structure with very light damping, but which may have stringent pointing requirements and a desired critically damped response (Clark, *et al.*, 1989). Another application of active structural control is in skyscrapers. Actuators are used to dampen out the vibration caused by high winds (Hsu and Lin, 1987, Xu, *et al.*, 1990). The idea of using active structural control has been considered as one means to obtain desired structural response characteristics.

2.2 Active Structural Control Using Piezoceramic Actuators

The area of active structural acoustic control has recently received much attention. In this field piezoceramic materials have been shown to be an effective way to reduce vibration as well as noise. Zhou showed that using an adaptive algorithm in controlling piezoelectric actuators mounted on an elastic plate, the average reduction of sound pressure level is on order of 20 dB and 13 dB at mode (3,1) and (3,3), respectively (Zhou, 1992). Sumali showed that an adaptive controller, actuating with piezoceramic patches, is able to reduce the vibration level in a cylinder by 68 dB (Sumali, 1992).

Several problems may occur when trying to drive PZT actuators with amplifiers due to the actuator's capacitive properties. If an amplifier voltage is suddenly applied, sudden increase in voltage contains high frequency components that can cause large PZT currents

and exceed the current limitations of the amplifier. A source of damage to the amplifier (depending on the amplifier design) occurs if the charged PZT has no path to discharge through. The piezoelectric actuator can cause a back electromotive force (emf) that exceeds the saturation voltage of the amplifier, causing damage. A third problem is caused when a piezoelectric actuator is driven by a transient or non-sinusoidal signal. The signal may have high frequency content and result in large currents (Trek, Inc., 1991).

2.3 Power Factor Correction Principles

Since the beginning of power generation and distribution, the concept of power factor correction has played an important role. In an electrical system the power consumed is defined by the product of the voltage, current, and the ratio of real to apparent power. The ratio of real power to apparent power is defined as the power factor (PF). When the supplied voltage and current are in phase the power factor is unity. The primary reason for wanting a PF close to unity in most industrial applications is the increase in the electrical capacity of the distribution system (lower current requirements). Most electric utilities asses a penalty for a low PF. This penalty may result in a significant portion of the users electric bill. For small facilities with low power requirements, a poor PF may result in penalties of thousands of dollars per year. Unlike purely resistive loads, inductive loads (such as motors, transformers, and industrial furnaces) require reactive or magnetizing currents. The reactive current provides only the electromagnetic field for operating the device and does not perform work or appear on an electric bill. The magnetizing current is also known as wattless, non-usable, or phantom current (Knisley, 1988).

Because most facilities have lagging PF's (inductive loads produce a lagging PF and capacitive loads produce a leading PF), capacitors or synchronous motors are usually placed in parallel with the load to correct the PF (Chapman, 1985). These capacitors

operate at nearly zero PF alone and have a negligible internal resistance. Because there are no resistive losses within the capacitors, the addition of capacitors does not increase the power consumption.

Table 2.1 shows the results of altering the PF from 0.707 lagging to 0.95 lagging by adding a 33.6e-6 F capacitor (Johnson, *et al.*, 1986). Figure 2.1a shows the circuit diagram of an uncorrected load while Fig. 2.1b shows the circuit for a corrected load. The addition of the capacitor to the circuit has reduced the current by 25.6%. In both cases the real power provided to the load is the same. However, the corrected circuit requires less reactive power and causes the apparent power to decrease. This in turn reduces the magnitude of the current consumed by the load and the amount of current that the power company must generate.

The practical significance of power factor correction for piezoelectric actuators is found in resonant inductor-capacitor (LC) circuits. The electrical properties of a piezoceramic actuator is similar to a capacitor. The PF of a PZT (Lead Zirconate Titanate) actuator is approximately zero and is leading. To correct the PF to unity, the PZT load requires the addition of a lagging PF. Therefore the PF of the PZT can be corrected with the addition of the appropriate inductor.

The LC combination is essentially an LC resonant circuit. The properties of the LC resonant circuit has been exploited in electronics since its discovery. Today LC resonant circuits are used widely in electronic filters. There are two elementary configurations (series and parallel resonance) that can be exploited. At resonance, the equivalent impedance of the parallel LC circuit approaches infinity and the current through the circuit goes to zero. This implies that a PZT actuator can have an actuation voltage with very little current consumption. At resonance, the equivalent impedance of the series LC

Table 2.1 Results of Power Factor Correction

	Real Power (W)	Apparent Power (VA)	Reactive Power (VAR)	Current (Amperes)
Uncorrected Load	25.0	35.4	25.0	0.50
Corrected Load	25.0	26.3	8.2	0.37

a.

b.
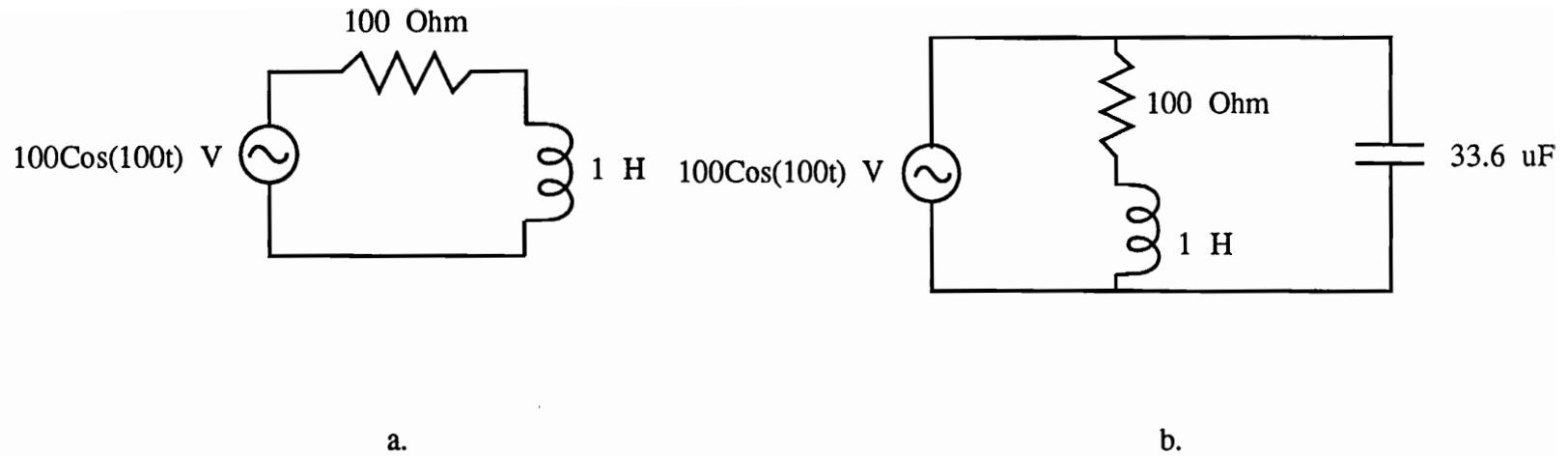
Figure 2.1 Power Factor Correction
a. Uncorrected Load (PF=0.707)
b. Corrected Load (PF=0.95)

circuit goes to zero. Therefore the current passing through the circuit is much larger and is governed by the internal resistance of the circuit and the applied voltage via Ohm's law. The high current in turn causes the capacitor and inductor voltages to be out of phase and also to be larger than the input voltage (Smith, 1983). This implies that a PZT actuator can be excited with a voltage that is much larger than the input voltage.

Application of the power factor correction methods to PZT actuators has not been performed. This research will demonstrate the feasibility of using LC resonant circuits to adjust the power factor of piezoceramic actuators.

2.4 Passive Structural Control Using Piezoceramic Actuators

Hagood and von Flotow investigated the possibility of dissipating mechanical energy with piezoelectric material shunted with passive electrical elements (resistors and inductors). It was shown that the resistor shunting produced a material loss factor as high as 42%, while using a resonant circuit reduced the vibration amplitude by 35 dB (Hagood and von Flotow, 1989). Work done by Cudney demonstrates numerically that passive damping on structures with layers of piezoceramic materials and external electrical circuits can increase damping from 0.11% to 3.67% of critical damping (Cudney, 1989).

2.5 Characterizing Active Structural Damping as a Function of Control Energy

Piezoelectric actuators have been researched for active structural control applications for many years (e.g., Crawley and de Luis, 1987, Bailey and Hubbard, 1985, Lee, *et al.*, 1989, Crawley and Anderson, 1990, Clark and Fuller, 1992). Much research has been done on various control techniques such as rate feedback, optimal, and adaptive control. In most cases work is done on the optimal placement of actuators in order to maximize

9

controllability or on optimal control laws which penalize control energy (Schulz and Heimbold 1983). However, the physical electrical power consumption of the actuator has not been considered.

2.6 Summary

A brief review of the applications and importance of active control techniques has been presented. The significance of applying power factor correction techniques to electrical distribution systems reduces the current requirements and the overall apparent power. The significance of power factor correction to PZT actuators is also described. Power factor correction and power consumption characterization of piezoelectric actuators has not yet been performed. Development of the theory will be presented next.

Chapter 3

Theoretical Development

3.1 Introduction

This chapter presents the theoretical background and concepts developed in this research. Methods to correct the power factor of PZT actuators and the effects caused by the correction are discussed. Both series and parallel resonant circuits are analyzed, and the appropriate electrical elements required to correct the PZT actuator power factor to unity are determined. Finally a relationship between the amount of PZT apparent power and the structural damping in a cantilever beam is developed.

3.2 Correcting the Power Factor of Piezoceramic Actuators

A piezoceramic actuator used for structural control behaves electrically as a nearly pure capacitance. When conventional amplifiers are used to drive these actuators, the current and voltage are close to 90 degrees out of phase. This causes the power factor (PF) of the load to be close to zero and results in excessive power requirements. This section investigates how the PF of the PZT actuator can be changed with the use of series and parallel resonant circuits.

3.2.1 Review of AC Power

In order to fully understand the concepts being presented, it is necessary to have an understanding of alternating current electrical power. For a load that is powered by an AC signal, the power passing through the load consists of real power and reactive power.

The amount of each power component depends on the impedance of the load. For purely resistive loads the voltage and current are in phase and so the element uses only real power. For purely inductive or capacitive loads no real power is consumed and the element only uses reactive power. For a load with both real and reactive components the ratio of the real to reactive impedance is equal to the ratio of the real to reactive power consumed by the load. The magnitude of the vector sum of the real and reactive power components is called the apparent power. Figure 3.1 shows the transition from impedance to power for a load consisting of real and inductive components.

For a load using a given amount of real power, the current and voltage amplitudes are minimized when the phase between the current and voltage is zero. The power factor in this case is unity. An example of a load corrected to a unity power factor is described in section 3.2.2.

3.2.2 Parallel LC Resonance

To understand the properties of the parallel resonant circuit, it is best to investigate the transfer function of V_o/V_i for the circuit in Fig. 3.2a. The impedance of the parallel combination of the inductor and capacitor can be shown to be,

$$Z_P = \frac{-j\omega L}{\omega^2 LC - 1} \tag{3.1}$$

The transfer function of the output voltage to the input voltage is then easily determined to be,

$$\frac{V_o}{V_i} = \frac{-j\omega L}{-j\omega L + \omega^2 RLC - R} \tag{3.2}$$

Figure 3.1 Transition From Impedance to Power Triangle
a. Impedance Triangle
b. Phasor Diagram
c. Power Triangle

a.

b.
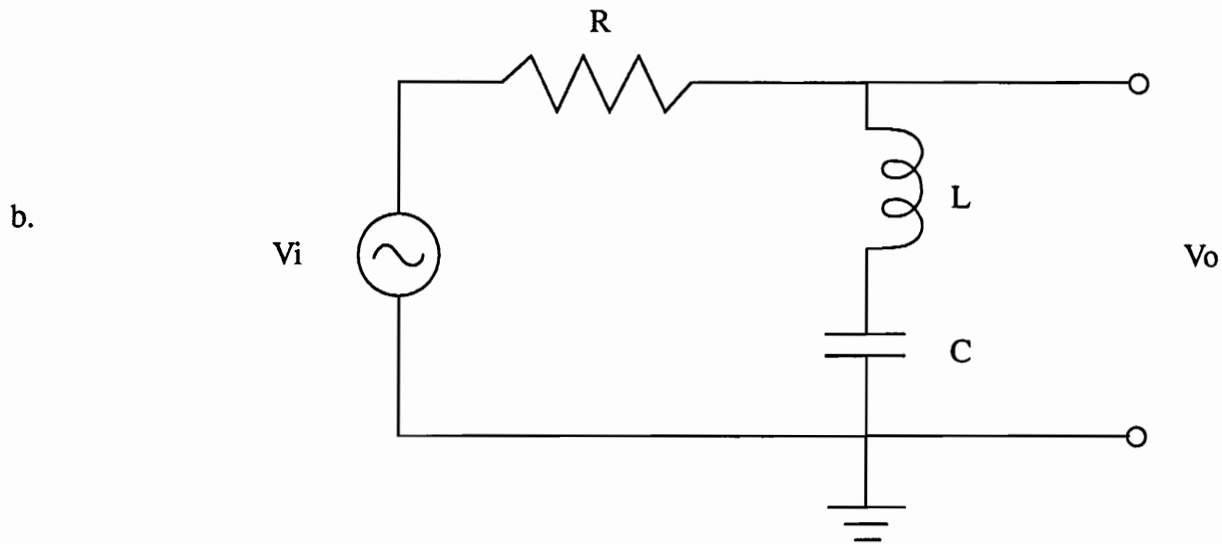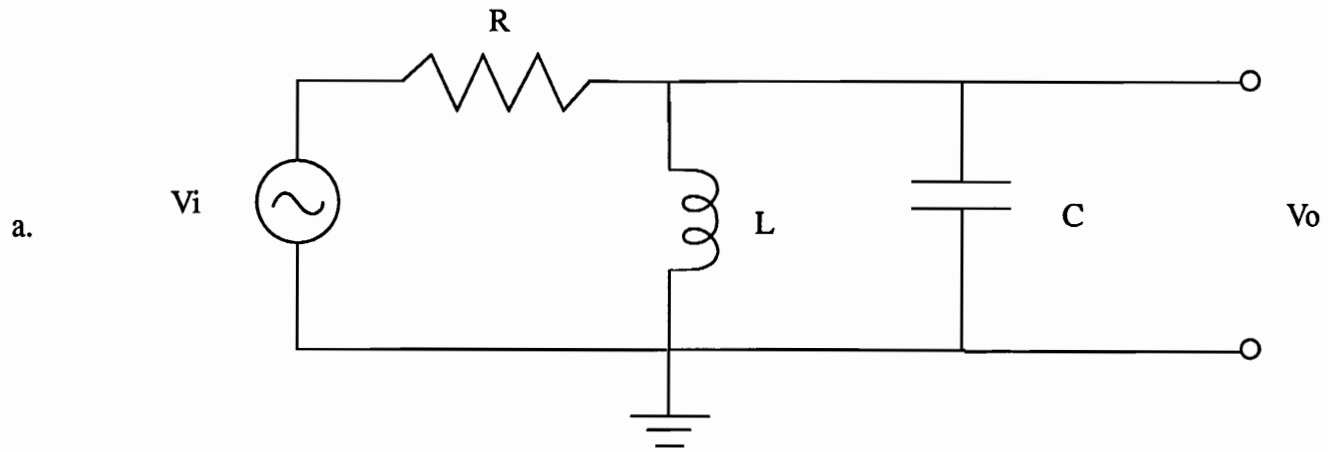
Figure 3.2 Ideal Resonant Circuits
a. Parallel Resonance
b. Series Resonance

The circuit transfer function in Eq. 3.2 reaches unity at the resonant frequency ω_r,

$$\omega_r = \sqrt{\frac{1}{LC}} \qquad (3.3)$$

At the resonant frequency the denominator of Eq. 3.1 goes to zero and the impedance of the parallel combination reaches infinity. Therefore a voltage can be applied across the ideal LC combination with no current consumption. At resonance, the reactive components cancel and the phase between the current and voltage is zero (PF=1). This effect is demonstrated in the phasor diagram of Figure 3.3a. At resonance the current in the inductor and capacitor have equal magnitudes and are 180 degrees out of phase, resulting in zero net currents to the elements.

Figure 3.4 demonstrates how the impedance of the parallel combination is several orders of magnitude higher than the impedance of a capacitor alone. In this example, some internal resistance is added to the capacitor and inductor in the model; this more accurately model real elements and prevents the impedance at resonance from going to infinity. The three cases show the effect of the increasing internal resistance. The modeled values are shown in Table 3.1. Figure 3.5 shows how the phase between the current and the voltage within the LC combination goes to zero at resonance. Three different internal resistance values are simulated. The model shows that the internal resistance simply adds damping to the system and changes the resonant frequency by a negligible amount.

3.2.3 Realistic Parallel Resonance Considerations and Tuning

Because the PZT actuator behaves electrically similar to a capacitor, the benefits of the LC

Table 3.1 Element Properties of RC and RLC Resonant Circuits Used to Show Effects of Resonance on Impedance

	Inductor (H)	Capacitor (nF)	Inductor Int. Resistance (Ohms).	Capacitor Int. Resistance (Ohms)
Case 1	10.0	50.0	50.0	50.0
Case 2	10.0	50.0	1000	1000
Case 3	10.0	50.0	5000	5000
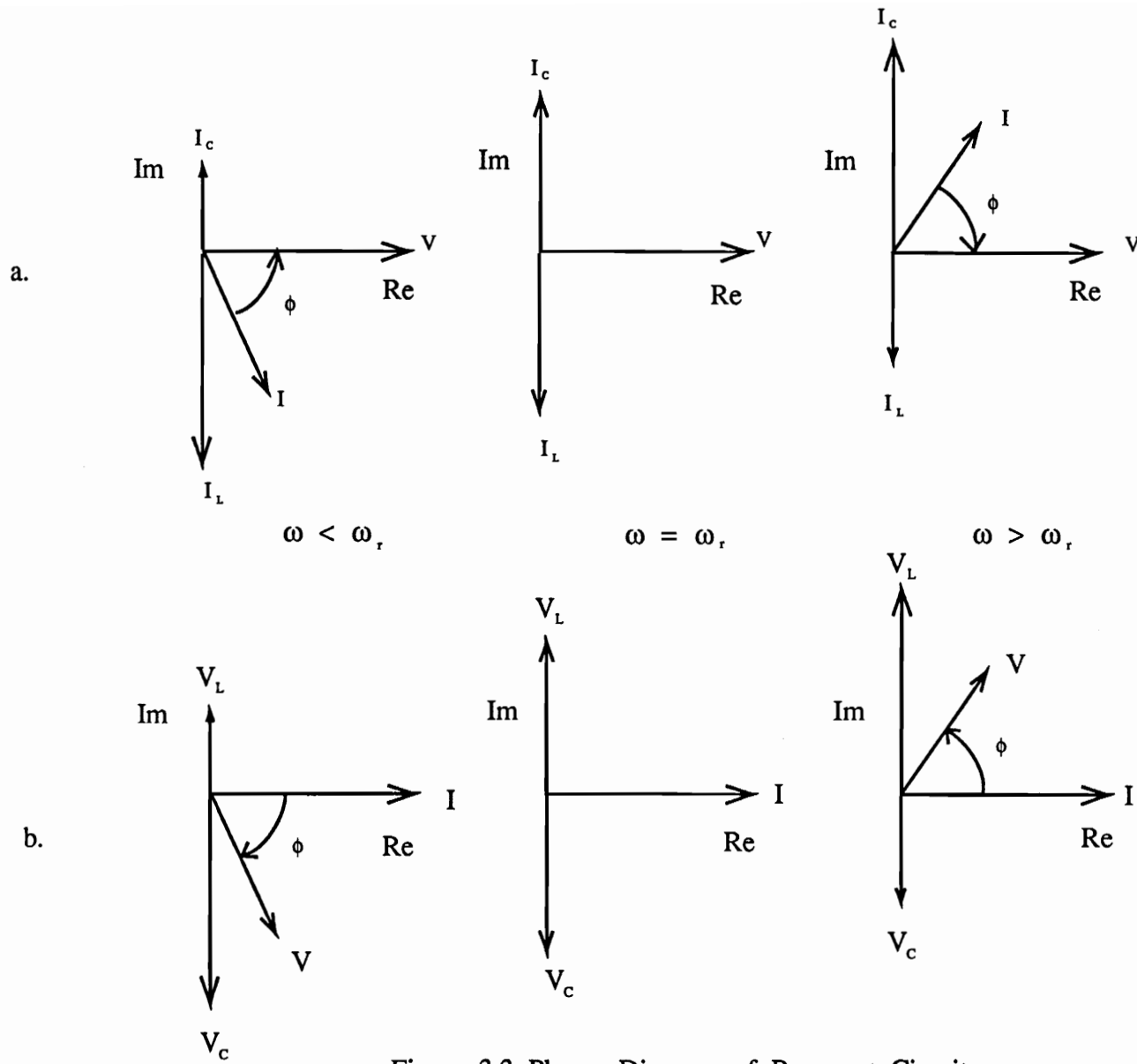
Figure 3.3 Phasor Diagram of Resonant Circuits
a. Parallel Case
b. Series Case
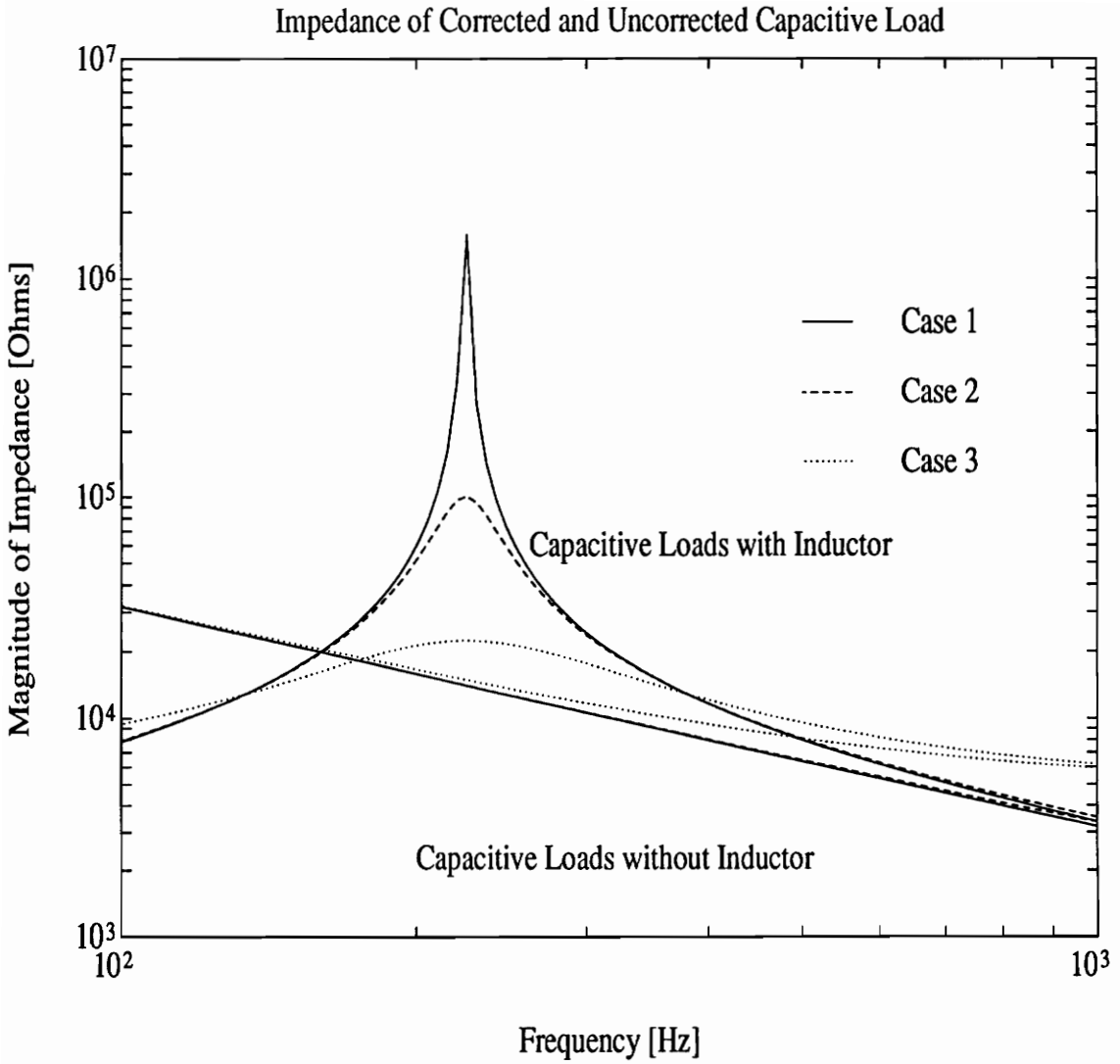
Figure 3.4 Comparison of Impedance for RC and RLC Resonant Circuits,

as a Function of Increasing Internal Resistance
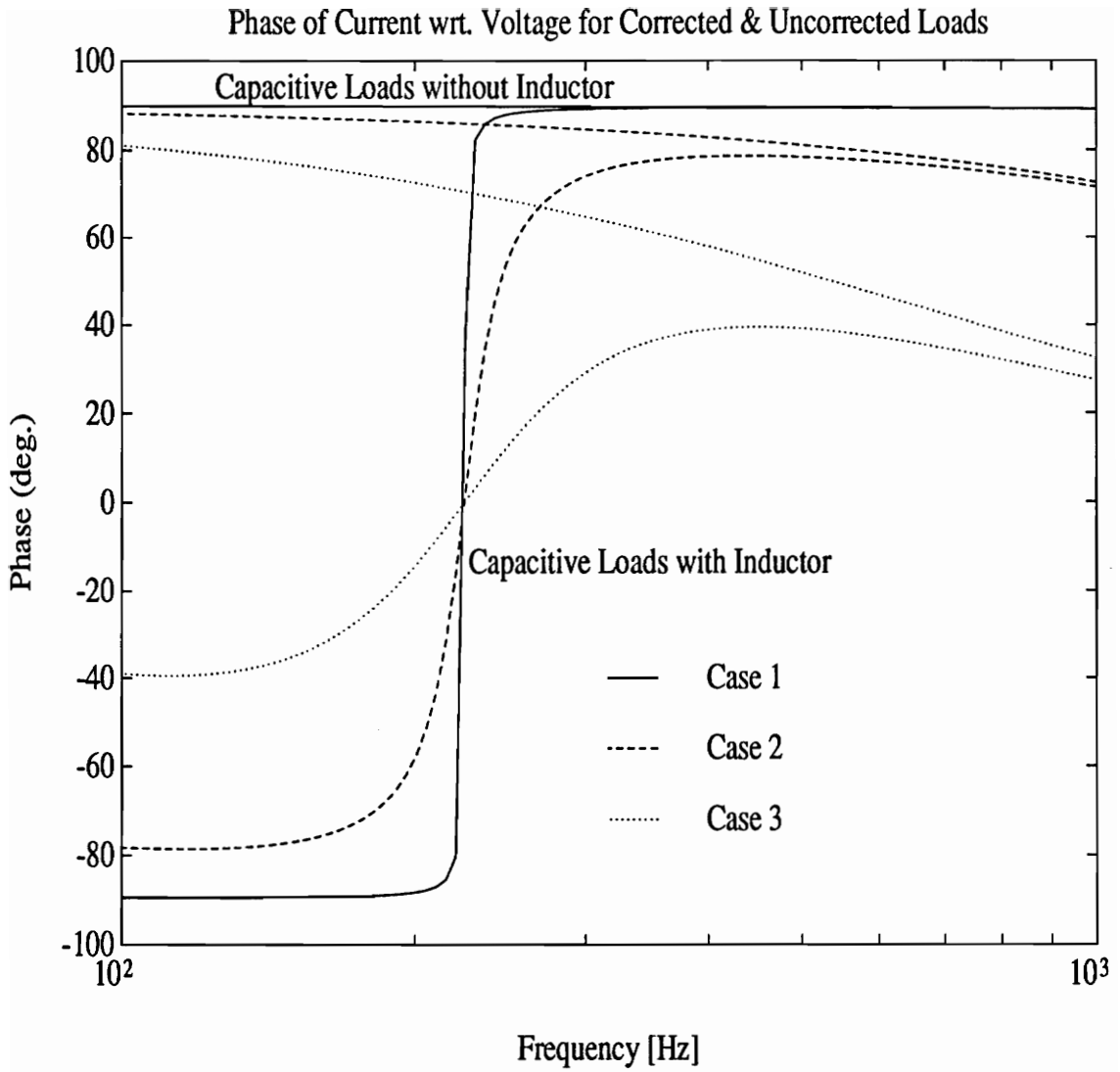
Figure 3.5 Comparison of Phase of RC and RLC Resonant Circuits,

as a Function of Increasing Internal Resistance

parallel resonance can be applied. Several factors must be considered. PZT actuators and all inductors have some internal resistance that is not negligible. This internal resistance must be incorporated for an accurate model. When determining the inductor that is required to create a parallel resonant circuit, several things must be known: the operating frequency, the PZT electrical properties, and the internal resistance of the inductor being considered. Because the internal resistance of the inductor can not be known exactly before choosing the specific inductor, a value must be assumed. A realistic model of an inductor and actuator circuit is shown in Fig. 3.6a. The model chosen for the realistic capacitor has the internal resistance in series with the capacitor instead of in parallel. This model is chosen because the experimental data extracts the impedance of the PZT as a complex number that is most easily represented by a series model. The derivation of the correcting inductor value for a parallel internal resistance model of the actuator is analogous to the one presented.

To solve for the appropriate inductor, the power factor of the LC combination must be driven to unity. This can be done by looking at the impedance of the LC combination. The impedance of the combination can be expressed in terms of the inductive and capacitive reactance,

$$Z_t = \frac{(R_L + jX_L)(R_C + jX_C)}{R_L + R_C + j(X_L + X_C)},$$

(3.4)

where X_C represents the capacitive reactance $(-1/\omega C)$, X_L represents the inductive reactance (ωL), and j is an imaginary number $(\sqrt{-1})$.

The real and imaginary components of Z_t are determined,

$$\text{Re}\{Z_t\} = (R_L^2 R_C + R_L R_C^2 + R_L X_C^2 + R_C X_L^2)/\Delta$$

(3.5)

20
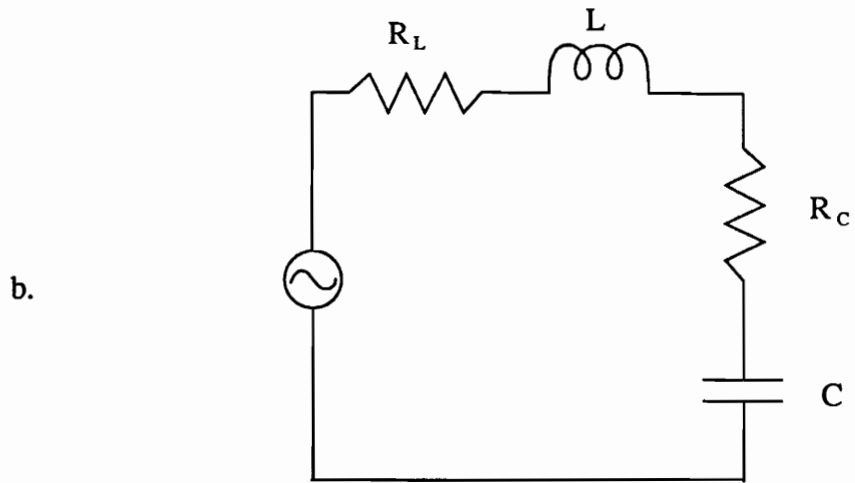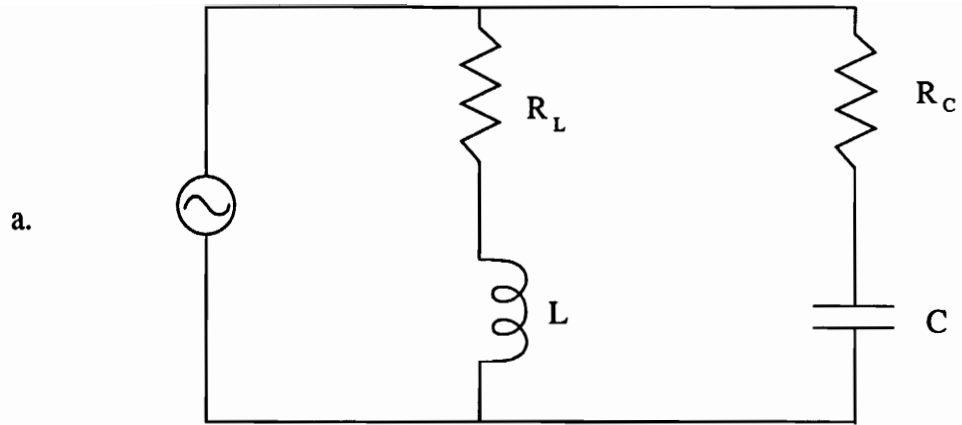
Figure 3.6   Realistic Resonant Circuits
a. Parallel Resonant Circuit
b. Series Resonant Circuit

$$\text{Im}\{Z_t\} = (R_L{}^2 X_C + R_C{}^2 X_L + X_L X_C{}^2 + X_L{}^2 X_C)/ \; \Delta \tag{3.6}$$

where Δ is the square of the magnitude of the denominator in Eq. 3.4.

The governing equation in adjusting the power factor is given by,

$$PF = \cos\{\tan^{-1}(\text{Im}\{Z_t\}/\text{Re}\{Z_t\})\} \tag{3.7}$$

By setting the power factor to unity and rearranging the terms in Eq. 3.7, results in the constraint that $\text{Im}\{Z_t\}$ must be equal to zero,

$$\text{Im}\{Z_t\} = 0 \tag{3.8}$$

Combining Eq. 3.6 and Eq. 3.8 leads to a quadratic equation that can be solved if it is assumed that R_C, R_L, and C are constant. The quadratic equation is given by,

$$L^2(\omega^2) - L(R_C{}^2 \omega^2 C^2 + 1)/C + R_L{}^2 = 0 \tag{3.9}$$

The solution of Eq. 3.9 is given by,

$$L = \frac{R_C{}^2 C}{2} + \frac{1}{2\omega^2 C} \pm \frac{1}{2}\sqrt{\left(R_C{}^2 C + \frac{1}{\omega^2 C}\right)^2 - 4\left(\frac{R_L{}^2}{\omega^2}\right)} \tag{3.10}$$

The solution in Eq. 3.10 has two roots; one root is physically realizable. The solution can be used to determine the inductor required to correct the power factor of a capacitive load with known capacitance and internal resistance. A value of the internal resistance of the inductor must be known prior to the solution. If the internal resistance of the inductor and capacitor are fairly small, an approximate solution can be obtained,

$$L \cong \frac{1}{\omega^2 C} \qquad (3.11)$$

3.2.4 Series LC Resonance

To understand the series resonant circuit, it is best to investigate the transfer function of V_o/V_i for the circuit in Fig. 3.2b. The transfer function can be shown to be,

$$\frac{V_o}{V_i} = \frac{j\left(\omega L - \dfrac{1}{\omega C}\right)}{R + j\left(\omega L - \dfrac{1}{\omega C}\right)} \qquad (3.12)$$

where the resonant frequency is given by,

$$\omega_r = \sqrt{\frac{1}{LC}} \qquad (3.13)$$

When the inductor-capacitor combination reaches resonance, the numerator of Eq. 3.12 approaches zero. The imaginary components cancel and so the voltage and current are in phase (power factor = 1). Using Ohm's law, the current through the circuit is,

$$I = \frac{V_i}{R} \qquad (3.14)$$

The transfer function of the capacitor voltage to the input voltage is given by,

23

$$\frac{V_C}{V_i} = \frac{Z_C}{R} \tag{3.15}$$

where V_C represents the voltage across the capacitor (PZT).

The transfer function in Eq. 3.15 indicates that the voltage across the capacitor can achieve much higher values than the input voltage. The amount of voltage increase is dependent on the value of the resistor chosen. The magnitude of the transfer function can theoretically reach infinity.

3.2.5 Realistic Series Resonance Considerations and Tuning

Again, the internal resistance of the inductor and the PZT must be considered for a valid model. Figure 3.6b shows a realistic model of the series LC resonant circuit that includes internal resistances. Because the internal resistances are in series, they can easily be incorporated into the resistance, R, of the model developed in section 3.2.4. Then, the inductor required to correct the power factor of the PZT to unity is given by,

$$L = \frac{1}{\omega^2 C} \tag{3.16}$$

3.3 Relating Structural Damping and Actuator Power

This section initially provides a brief review of strain rate feedback. An energy balance of the structure is then performed and the damping is modeled. Finally a relationship between the PZT apparent power required for a desired amount of structural damping is developed.

3.3.1 Strain Rate Feedback

The addition of damping by feeding back a signal proportional to strain rate is easily seen by analyzing the relationship for an equation of motion for a single degree of freedom system,

$$m\ddot{x} + c\dot{x} + kx = f(t) \tag{3.17}$$

By taking the Laplace transform of Eq. 3.17 the open loop transfer function of the system is obtained,

$$G(s) = \frac{X(s)}{F(s)} = \frac{1}{s^2 + 2\zeta\omega_n s + \omega_n^2} \tag{3.18}$$

A block diagram of the system with strain rate feedback is shown in Fig. 3.7. The closed loop transfer function is given by,

$$T(s) = \frac{X(s)}{F(s)} = \frac{1}{s^2 + (2\zeta\omega_n + g)s + \omega_n^2} \tag{3.19}$$

where $X(s)$ and $F(s)$ represent the Laplace domain displacement and forcing function, respectively. The term g is the feedback gain and ζ is the damping within the system. The addition of the feedback loop alters the system dynamics. It is clear from the closed loop transfer function that altering the feedback gain, g, will change the damping within the system.

3.3.2 Energy Balance and Damping Model

To determine a relationship between the power consumption of a piezoceramic actuator and the amount of damping in a structure it is necessary to perform an energy balance on

F(s)

+

E(s)

G(s)

X(s)

−

Rate Feedback

gain = g
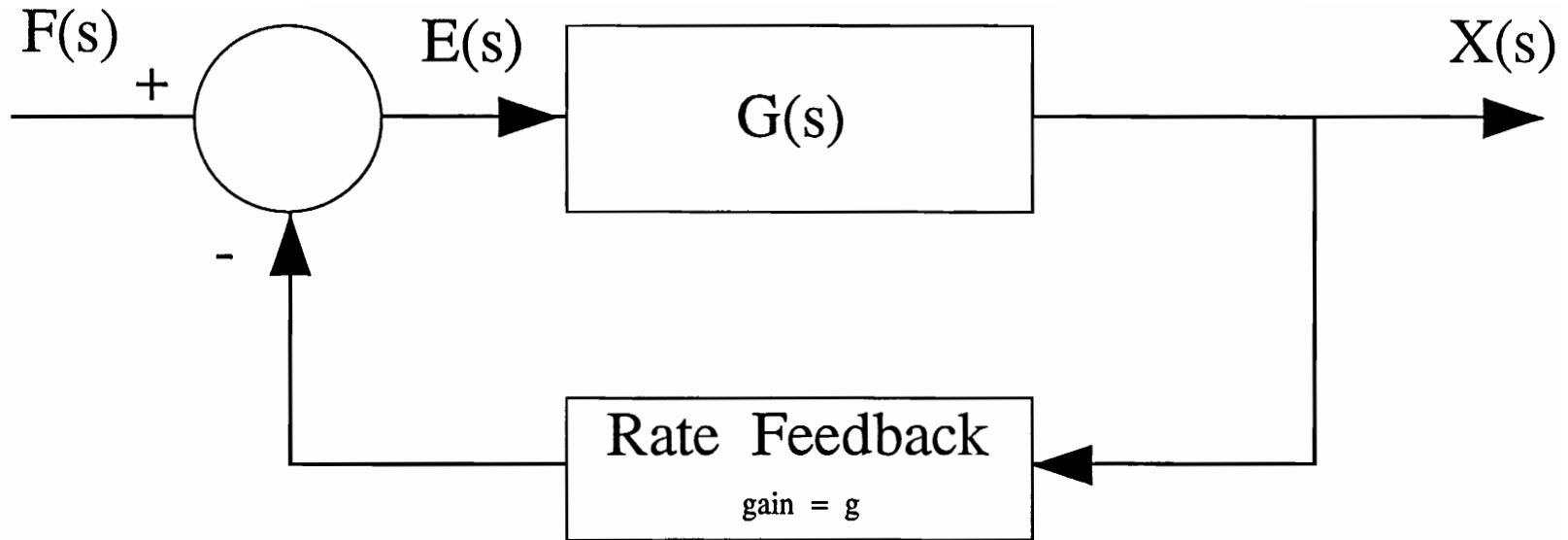
Figure 3.7 Strain Rate Feedback for a Single Degree of Freedom System

the cantilever beam. To perform an energy balance it is also necessary to define the cantilever beam as the control volume to which mechanical energy is being added and removed. Energy is added to the system by the disturbance, represented by a shaker. We assume energy is removed from the system by either of two forms of mechanical energy dissipation. The first form of dissipation is through the natural damping within the structure. The second form of energy dissipation is through active damping caused by the PZT actuator. The PZT uses the strain rate signal to actuate the beam such that it counteracts the vibration caused by the disturbance. For steady state excitation the amount of mechanical energy within the system is fixed. Therefore all the energy provided by the disturbance (shaker) is dissipated through natural damping in the beam and through active PZT damping. The energy balance can be expressed as,

$$\sum Energy = E_d - E_{Beam} - E_{PZT} = 0 \tag{3.20}$$

where E_d, E_{Beam}, and E_{PZT} represent the mechanical energy provided by the disturbance, dissipated via natural damping within the beam, and dissipated via active damping caused by the PZT actuator, respectively.

Assuming a structural damping model, the energy dissipated through natural damping is proportional to the square of the amplitude of vibration (Thomson, 1981), and is given by,

$$E_{Beam} = \alpha X^2 \tag{3.21}$$

where α is the structural damping constant and X is amplitude of vibration.

At a natural frequency of a structure, the amplitude of vibration of that mode can be predicted by a single degree of freedom model (Rao, 1990),

$$X = \frac{F_o}{2k\zeta} \qquad (3.22)$$

where F_o, ζ, and k represent the force applied to the structure, the equivalent viscous damping ratio, and the effective stiffness of the structure at the mode of interest, respectively.

The structural damping ratio is related to α and ζ at resonance via (Thomson, 1981),

$$\gamma = \frac{\alpha}{\pi k} \qquad (3.23)$$

where,

$$\gamma = 2\zeta \qquad (3.24)$$

where γ represents the structural damping ratio.

Combining Eq. 3.22 and Eq. 3.24 results in,

$$X = \frac{F_o}{k\gamma} \qquad (3.25)$$

Equation 3.23 and Eq. 3.25 can now be substituted into Eq. 3.20, resulting in a relationship between the amount of mechanical energy dissipated per cycle in the PZT actuator as a function of the structural damping in the system,

$$E_{PZT} = E_d - \left(\frac{\pi F_o^2}{k} \right) \frac{1}{\gamma}$$

(3.26)

3.3.3 Actuator Power and Damping Relationship

For an elastic mechanical system the vibration amplitude is proportional to the amplitude of the applied force or moment,

$$X \propto M$$

(3.27)

For a system vibrating in steady state, the amount of energy entering the system by the disturbance is equal to the amount of energy leaving the system through natural damping. The energy dissipated via natural damping is given by Eq. 3.21. It can therefore be concluded that the energy provided to the system is proportional to the square of vibration. Thus, via Eq 3.27, the energy provided to a system is proportional to the square of the magnitude of the applied moment,

$$Energy \propto M^2$$

(3.28)

We will assume that the mechanical energy provided to a structure by a PZT actuator is proportional to the square of the amplitude of the applied moment in the PZT. Appendix C shows that the net forcing of the beam is equivalent to two equal and opposite moments applied to the beam at the endpoints of the PZT patch. It is also shown that the moment induced in the structure by the PZT actuator is proportional to the applied voltage

(Devasia, *et al.*, 1992). Therefore, we will propose that the mechanical energy provided by the PZT actuator is proportional to the square of the applied voltage and is given by,

$$E_{PZT} \propto V^2 \qquad (3.29)$$

Solving Eq. 3.29 for voltage and substituting into Eq. 3.26 yields a relationship between the required PZT voltage and the desired structural damping ratio,

$$V \propto \sqrt{\left\{ E_d - \left(\frac{\pi F_o^2}{k} \right) \frac{1}{\gamma} \right\}} \qquad (3.30)$$

The actuator apparent electrical power is related to voltage via,

$$P_a = \frac{V^2}{Z_{PZT}} \qquad (3.31)$$

where P_a and Z_{PZT} represent the PZT electrical apparent power and impedance. Combining Eq. 3.30 and Eq. 3.31, an expression is developed relating the apparent power and the amount of desired damping,

$$P_a \propto \frac{1}{Z_{PZT}} \left\{ E_d - \left(\frac{\pi F_o^2}{k} \right) \frac{1}{\gamma} \right\} \qquad (3.32)$$

3.4 Summary

A theoretical development of the series and parallel resonant circuit has been presented. Both circuits can be applied to the PZT actuator to reduce the demands on the amplifier.

A relationship between PZT actuator apparent power and the amount of structural damping in a structure has been developed. The experiments required to verify the concepts presented in Chapter 3 are described next.

Chapter 4

Experimental Setup

4.1 Introduction

This chapter describes the required equipment and procedure used to show a relationship between PZT consumed power and added structural damping, and to verify the properties of the series and parallel PZT resonant circuits.

A cantilever beam is chosen as the test structure because it is easy to excite, record the response, and it represents a common mechanical structure. It is also chosen because a cantilever beam natural frequency can be altered simply by varying the position of the clamp holding its root. This is important because the LC resonant frequency of the circuits is based on the capacitance of the PZT and the inductance of the inductors readily available. It is advantageous to have the LC resonant frequency slightly higher than the mechanical resonant frequency. This facilitates tuning the LC resonance to the structural resonance simply by adding capacitance to the PZT actuator. To provide a disturbance a shaker is chosen because it provides a harmonic excitation in which the force imparted onto the structure is easily measured. Current and voltage measurements are also required to measure the power consumed by the PZT actuator. Therefore, electronic circuitry to measure current and voltage is required. An accelerometer is also needed to measure the amplitude of vibration. The accelerance is used in the determination of the amount of damping in the beam and the mechanical energy provided by the shaker to the beam. With the equipment described above it is possible to answer our questions.

4.2 Physical Description: Structure, Sensors, and Actuators

The cantilever beam chosen is fabricated from 6061 aluminum with a modulus of elasticity of approximately 70 GPa and a Poison's ratio of 0.3. The length of the beam is 33.97 cm, the width is 4.0 cm, and the thickness is 0.3 cm. Two piezoceramic patches are used to actuate the structure and are mounted on either side of the beam, 4.47 cm from the root. The patches are attached to the beam using conducting glue (epo-tek H20E). The outside of the PZT corresponds to the supply side while the inside is connected to the beam which is the electrical ground. A single patch is 3.65 cm long, 1.9 cm wide and 0.03 cm thick. The disturbance is provided by a shaker acting through a "stinger" located 3.1 cm from the root of the beam. Two polyvinylidene fluoride (PVDF) sensors are attached to the structure with store-purchased, double-sided "carpet" tape and are located on either side, 9.9 cm from the root of the beam. A single PVDF sensor is 5.95 cm long, 3.45 cm wide, and 52μ m thick. The accelerometer (Kistler Model 8616A500) is positioned at the tip of the beam. All components are placed symmetrically about the centerline along the beam's length. Figure 4.1 shows the instrumented structure.

The Kistler Model 9712A50 force transducer and accelerometer have two functions. They are used together to obtain frequency response functions of accelerance with respect to the applied force. The frequency response functions are used to determine the damping in the beam for various control gains. The integrated accelerance and force signal are also used to determine the amount of energy provided to the beam by the shaker (Ling Dynamic Systems Ltd. model V203). The PVDF sensors are configured measure the strain rate in the beam. The signal from the film is conditioned and is fed back to the PZT actuators. The PZT actuation counteracts the excitation caused by the disturbance and also provides active damping to the beam.

a. Top View

PZT Actuator

PVDF Sensor

Accelerometer

Force Transducer

Shaker

Force Transducer

PZT Actuator

PVDF Sensor

Accelerometer
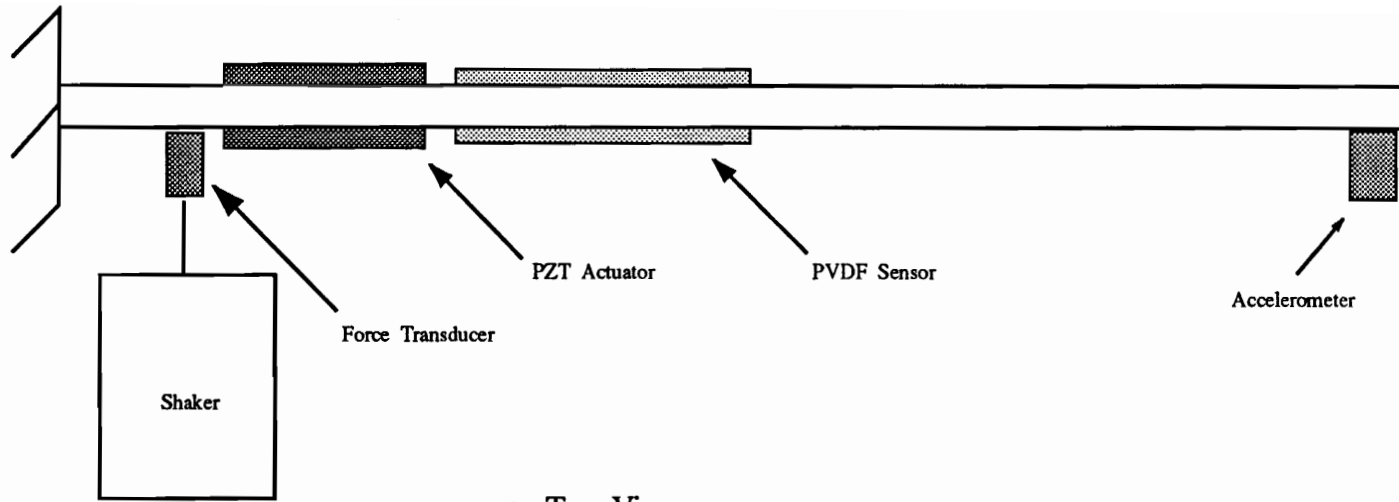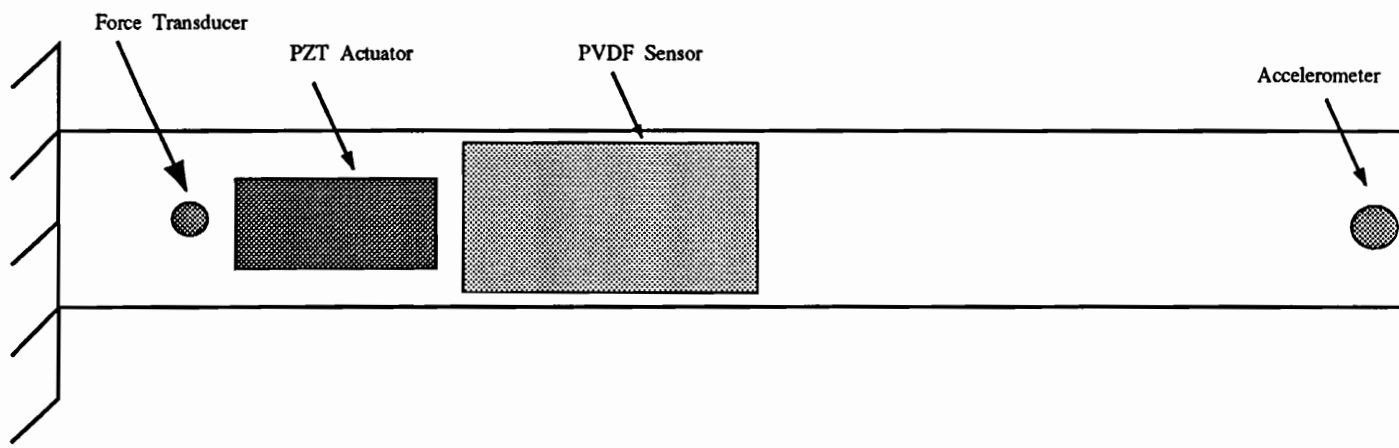
b. Side View

Figure 4.1 Schematic of Structure

4.3 Strain Rate Circuit

A PVDF sensor generates a charge across its film that is proportional to strain. When the impedance on the output of the sensor is infinite, the charge is proportional to the voltage across the film. Thus the PVDF voltage is proportional to strain. When the impedance on the output of the sensor is zero, the charge developed within the film (caused by strain) is free to migrate and generates a current. In a capacitive element, the charge migration leads the element's developed charge by ninety degrees. Thus for harmonic excitation, the current developed by a PVDF sensor is proportional to strain rate since strain rate leads strain by ninety degrees (Sumali, 1992). The strain rate circuit used in this experiment is similar to a standard current to voltage converter (Smith, 1984). An extra capacitor (15 pF) is added in parallel with the feedback resistor as shown in Fig. 4.2. The purpose of the capacitor is to eliminate high frequency noise. The addition of the capacitor adds approximately two degrees of phase lag to the strain rate signal at the beam's second mode. This extra phase lag is compensated with a filter (Frequency Devices Model LP02) so that a signal proportional to strain rate is fed back to the PZT actuators.

4.4 System Description

The shaker provides a sinusoidal disturbance force to the beam. Because of the harmonic forcing, the beam vibrates and contains internal sinusoidal strains. The PVDF sensor is mounted to the structure and thus the film is harmonically strained and generates a current proportional to strain rate. The current is converted to a voltage signal nearly proportional to strain rate and is amplified with an inverting operational amplifier (op-amp). The signal is then filtered with a Frequency Devices Model LP02 (eight pole Bessel) low pass filter. The cutoff frequency is set to 136 Hz so the filter adds 178 degrees of phase lag to the signal. The signal is then amplified using a Hewlett Packard

35

R = 470 kΩ

15 pF

PM-355AZ

−

+

PVDF Sensor

Vout
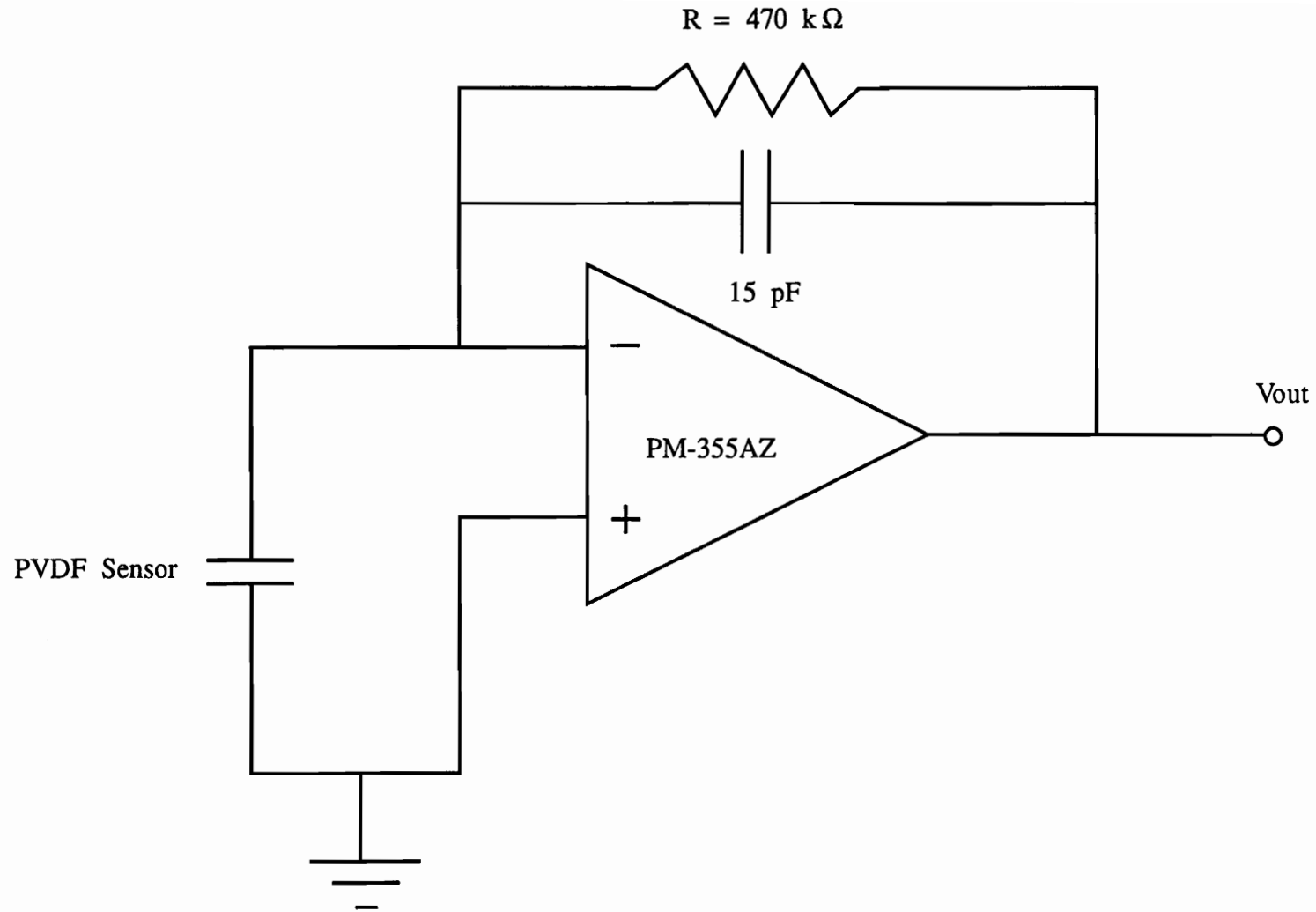
Figure 4.2 Strain Rate Circuit

6824A amplifier and is fed back to the PZT actuators. The block diagram of the system is shown in Fig. 4.3.

4.5 Voltage Measurement

To obtain power measurements, the voltage across the PZT actuator must be measured. Typical voltages applied across a PZT actuator range anywhere from 10 to 100 V (Note: all voltages are expressed in rms Volts). The maximum voltage that is applied to the PZT in this research is 35 V. The maximum voltage is limited by the voltage saturation limits placed on the op-amps by the DC power supplies. If the DC power supply can only generate ± 60 V, then the maximum rms voltage is slightly less than 42.42 V. The Tektronix frequency analyzer can not accept more than 7.07 V (rms), and therefore a voltage reducer (1/10) is implemented using an APEX PA41A op-amp (shown as U2 in Fig. 4.4). When making measurements with an ordinary voltmeter or oscilloscope, the input resistance of the meter is finite. For measurements across loads with a high impedance, the finite resistance of the meter introduces error. Therefore a unity gain buffer is also implemented to isolate the PZT actuator from the voltage reducer using a PA41A op-amp (shown as U1 in Fig. 4.4). The buffer has an input impedance of approximately 1×10^{11} Ω. The circuit diagram of the voltage reducer is shown in Fig 4.4.

An experiment is performed to calibrate the voltage reducer. The Tektronix frequency analyzer is used to apply a 5 V sinusoidal signal to the HP amplifier (the amplifier gain is set to 10). The amplified signal is then applied to the reducer circuit and the output of the reducer circuit is measured by the analyzer. The feedback resistance of the reducer circuit is adjusted until the output and input voltages are identical. The voltage reducer circuit has a gain determined to be 0.1 V/V.

37
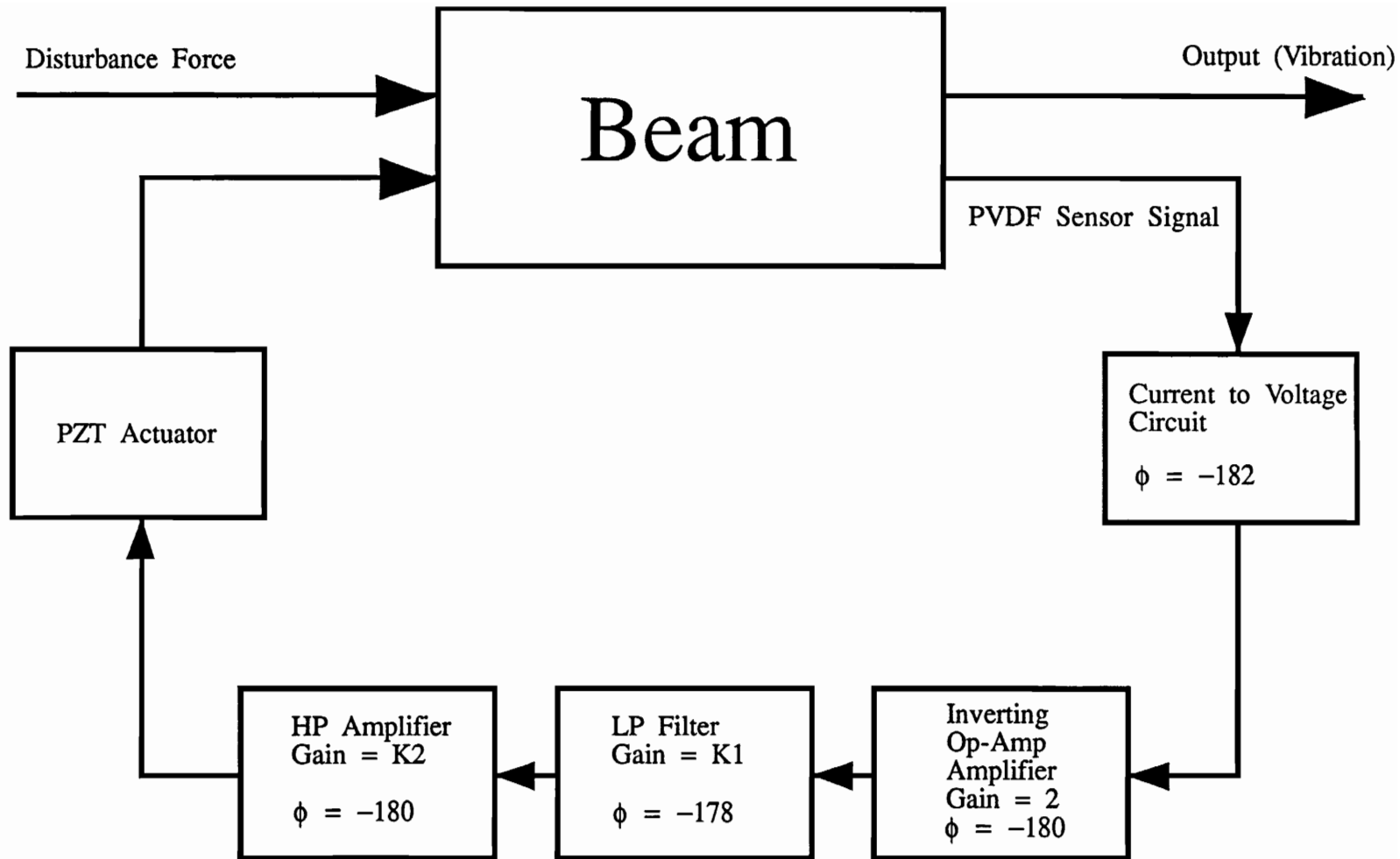
Figure 4.3 Block Diagram of the Strain Rate Feedback

R=1k Ω

R=10 k Ω

V_s

U1

V_s

U2

Reduced Voltage

$-V_s /10$
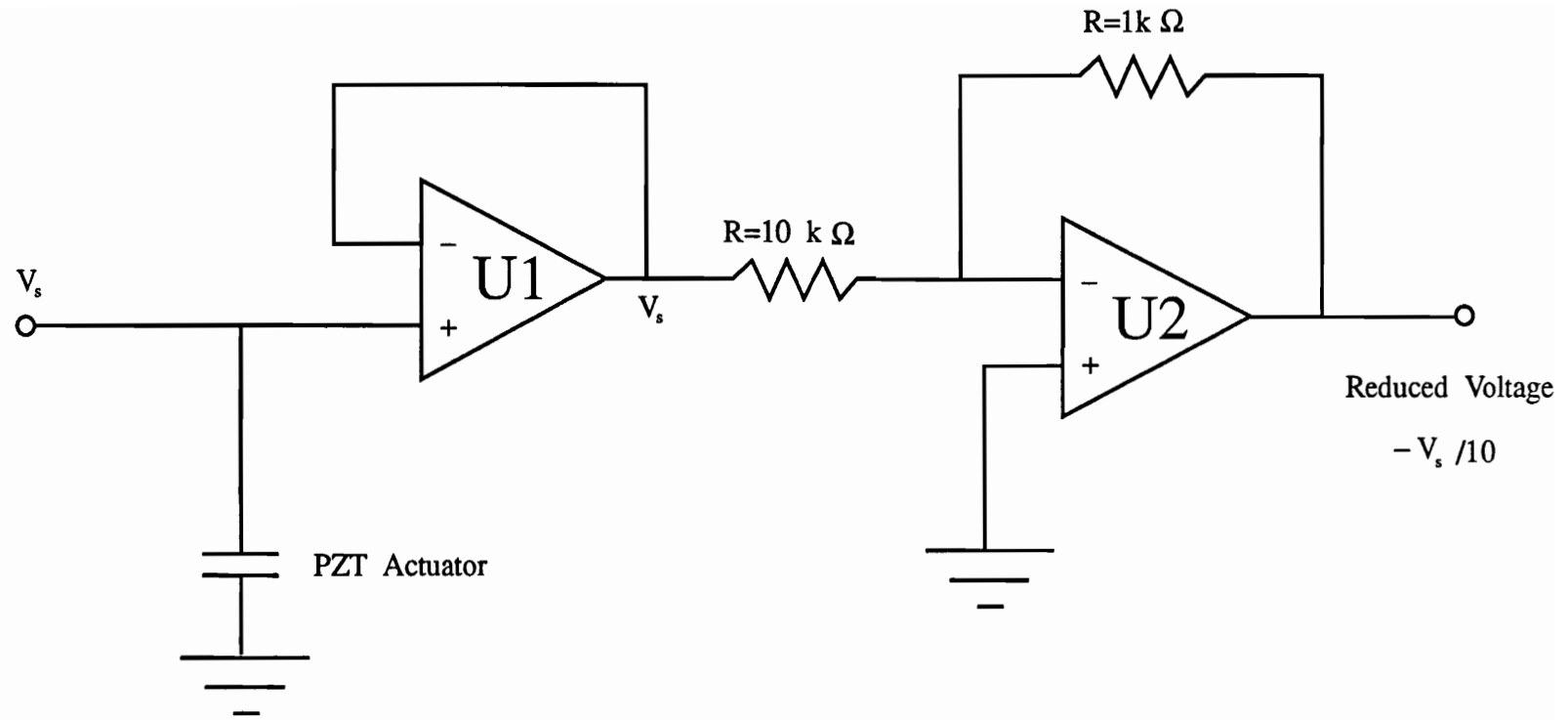
PZT Actuator

Key:
U1 - APEX PA41A Op-Amp
U2 - APEX PA41A Op-Amp

Figure 4.4 Voltage Reducer Circuit

4.6 Current Measurement

A voltage signal proportional to the current passing through the PZT actuator is also required. Therefore a current to voltage converter is needed to obtain a measure of the current. The typical current-to-voltage converter that would normally be used in this application is the circuit already implemented to measure strain rate, shown in Fig. 4.2 (excluding the 15 pF capacitor added to reduce noise). This circuit replaces the load's ground with the op-amp's virtual ground. However the cantilever beam in this research is grounded and allows current to pass through the PZT to ground via the beam. This would normally not be a problem, however the shaker, force transducer, and the accelerometer are also electrically attached to the beam and allow extra paths for current to flow from the beam to ground. The beam is therefore grounded via the two transducers, the shaker, and the virtual ground of the current-to-voltage converter. The multiple ground path introduces errors in current measurement and so a current to voltage converter that measures current on the supply side of the PZT is required. The circuit that is developed is shown in Fig. 4.5. The op-amp U3 produces a voltage which is the sum of the HP amplifier voltage (V_s) and the current passing through the PZT actuator multiplied by the feed resistor R. The output is given by,

$$V_{U3} = V_s + iR \tag{4.1}$$

The op-amp U4 creates a voltage that is equal to the inverted HP amplifier voltage and is given by,

$$V_{U4} = -V_s \tag{4.2}$$
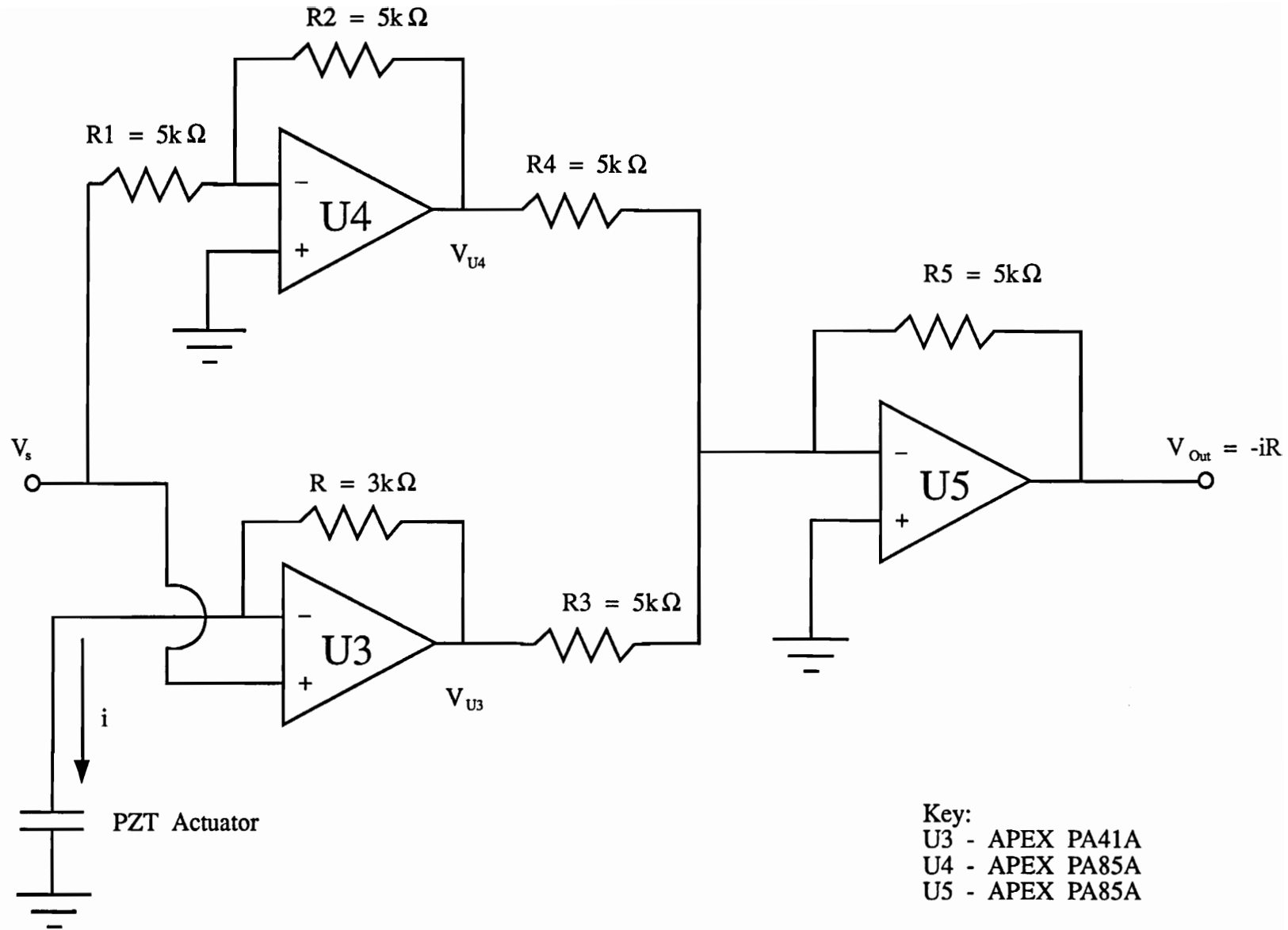
Figure 4.5 Current to Voltage Converter

The op-amp U5 adds the two voltages from the output of U3 & U4. A signal proportional to the PZT current is then obtained at the output of U5 and is given by,

$$V_{U5} = V_{U3} + V_{U4} = -iR \tag{4.3}$$

The complete transfer function of the current-to-voltage converter is given by,

$$V_{Out} = R_5 \left\{ \frac{V_s R_2}{R_1 R_3} - \frac{iR}{R_4} - \frac{V_s}{R_4} \right\} \tag{4.4}$$

To calibrate the resistance values, potentiometers are adjusted using a Fluke multimeter to $\pm 1\Omega$. Once the resistances are adjusted, V_s is set to 35 V and the PZT load in Fig 4.5 is removed. The output of the current to voltage converter is set to zero by trimming R3. This calibrates R1, R2, and R3 with respect to R4. The resistors, R4 and R5, are then calibrated to the same value, and based on Eq. 4.4, the current to voltage converter should provide an accurate measure of the current.

4.7 Voltage Reducer and Current to Voltage Converter Testing

To verify the proper operation of both the voltage reducer and the current to voltage converter, an experiment is performed to determine the resistance of an 18 kΩ resistor. The resistance of a load is defined by Ohm's Law,

$$R = \frac{V}{I} \tag{4.5}$$

Thus the resistance can be obtained by measuring the current through and the voltage across the element. The two circuits are used to determine the resistance as a function of frequency and the applied voltage across the resistor. The sine dwell function of the Tektronix Fourier Analyzer is used to obtain a transfer function of voltage with respect to current. The value of this transfer function represents the resistance of the load being tested. This experiment tests the proper operation of the current-to-voltage converter and the voltage reducer.

4.8 Impedance Testing of the PZT Actuator and the Inductor

In order to tune the PZT actuator, its specific electrical properties must be known. This includes capacitance and internal resistance. Inductors are generally known to behave in a nonlinear fashion and have unreliable nominal values. It is therefore necessary to perform impedance tests on the PZT actuator as well as the correcting inductor. The technique used to determine impedance is identical to the one developed in Section 4.7 using Ohm's Law,

$$Z = \frac{V}{I} \qquad (4.6)$$

The ratio of voltage with respect to current obtained from a sine dwell test represents the complex impedance of the test load. The impedance of the PZT and the inductor are modeled in Fig 3.6 and are given by,

$$Z_{PZT} = R_C - \frac{j}{\omega C} \qquad (4.7)$$

and,

$$Z_L = R_L + j\omega L \qquad (4.8)$$

43

The complex transfer function can easily be converted into an impedance. The real part of the transfer function represents the internal resistance of the test load and the imaginary part of the transfer function corresponds to the imaginary part of the impedance as given by Eq. 4.7 and Eq. 4.8. The electrical impedance of the PZT actuator and the correcting inductor can be easily determined by performing several sine dwell tests. The impedance tests are performed at 15, 20, 25, 30, and 35 V and range in frequency from 115 Hz to 145 Hz. The data from the impedance experiments are used in modeling the behavior of the series and parallel resonant circuits.

The impedance of an unmounted (free) PZT patch is also performed to determine the mechanical coupling effect on the electrical properties of the PZT actuator. The tested free PZT patch has a similar DC (direct current) capacitance and a slightly smaller area compared to the PZT actuator mounted on the beam. The free PZT dimension is $3.15 \times 3.18 \times 0.0305$ cm.

4.9 Power and Damping Measurements

To verify the relationships developed to relate the apparent power of the actuator as a function of added damping, the current passing through and the voltage across the PZT must be measured along with the damping in the beam for various control gains. Nineteen different control gains are chosen and are shown normalized with respect to the fourth control gain in Table 4.1. For each of the nineteen control gains a sine dwell test is performed. The sine dwell tests start at 115 Hz and sweeps up to 145 Hz by 0.15 Hz. The shaker excites that structure at a particular frequency during the sweep and the Tektronix frequency analyzer records the transfer functions, accelerance with respect to force (A/F) and PZT actuator applied voltage with respect to actuator current (V/I).

44

Table 4.1 Normalized Control Gains for Various Sine Dwell Tests

Experiment Number	Control Gain
1	0
2	0.5
3	0.75
4	1.0
5	1.3
6	1.6
7	2.0
8	2.3
9	2.6
10	3.0
11	3.5
12	4.0
13	4.5
14	5.0
15	6.0
16	7.0
17	8.0
18	9.0
19	10.0

From the transfer function of A/F, the amount of damping within the system is determined using a polynomial curve fitting algorithm assuming a structural damping model and also a viscous damping model. The structural damping algorithm is developed by Kochersberger and the viscous damping algorithm is developed by Han (Kochersberger, to appear, Han, 1989). Both of these algorithms are based on work by Adcock (Adcock, 1987). The transfer function of A/F is also used to determine the phase of X/F. The phase is used in determining the mechanical power provided to the beam by the shaker. From the actuator transfer function of V/I, the phase of V/I is extracted. The phase information is used in determining the angle, ϕ, described in Fig 3.1c. The phase angle, ϕ, is used to determine the amount of real and reactive power consumed by the PZT.

Once the sine dwell tests are performed, the magnitudes of the PZT voltage, PZT current, accelerance, and force are determined at the resonant frequency. This is done by obtaining the time averaged rms value of each of the time domain signals while the beam is being controlled. The magnitude of the force and accelerance are used to determine the amount of energy imparted to the beam by the shaker. Because work is defined by the dot product of applied force and displacement, the amount of energy provided to the beam is given by,

$$E_d = FX \cos(\vartheta) \tag{4.9}$$

where E_d, F, and X represent the energy provided by the disturbance (shaker) to the beam, the magnitude of the force, and the amplitude of the vibration, respectively. The term ϑ is the phase angle between displacement and force.

The displacement magnitude is obtained directly by dividing the accelerance magnitude by the square of the vibrating frequency (rad/s). The amount of energy imparted to the beam

46

per cycle can now easily be determined, since X, F, and ϑ are known. From the magnitudes of PZT current and PZT applied voltage, the apparent power is determined at the operating frequency. The real and reactive power is also determined by knowing the magnitude and phase of the transfer function V/I.

4.10 Viscous and Structural Damping Models

A damping model for a structure is typically chosen based on an engineer's intuition or because a particular model simplifies the mathematics. This research uses a structural damping model based on results presented in Chapter 5. Verification of the structural damping model is obtained by studying the frequency response functions obtained as described in Section 4.11. Using two polynomial curve fitting programs the damping ratios for the two damping models are obtained. A program written by Kochersberger is used extract the structural damping ratios while a program written by Han is used to extract the viscous damping ratios (Kochersberger, to appear, Han, 1989).

A single frequency response function (normalized feedback gain = 1.0) is chosen to compare the polynomial fit that the structural damping and viscous damping models produce. From the error between both models and the actual frequency response function the best damping model is chosen.

4.11 Natural Energy Dissipation in the Beam

Verification of the energy balance formulated in Eq. 3.26 can be performed by knowing the energy provided to the beam by the disturbance and the natural energy dissipation in the beam. An equation for the natural energy dissipated by the beam is derived in Chapter 3 and is rewritten here for clarity,

47

$$E_{Beam} = \left(\frac{\pi F_o^2}{k} \right) \frac{1}{\gamma}$$

The terms F_o and γ are measured for each feedback gain as described in Section 4.9. The stiffness of the beam is easily determined for the first mode, but not the second. To determine the stiffness for the second mode of the beam, it is assumed that the modal mass for the first and second mode are the same. For the first mode the stiffness is given by,

$$k_1 = \frac{3EI}{\ell^3} \tag{4.10}$$

where I represents the moment of inertia of the beam. By knowing the first mode natural frequency, the equivalent mass is determined by,

$$m_1 = m_2 = \frac{k_1}{\omega_1^2} \tag{4.11}$$

The equivalent beam stiffness for the second mode is given by,

$$k_2 = m_2 \omega_2^2 \tag{4.12}$$

Combining Eq. 4.10, Eq. 4.11, and Eq. 4.12 results in an expression for the equivalent beam stiffness at the second mode,

$$k_2 = \left(\frac{3EI}{\ell^3} \right) \frac{\omega_2^2}{\omega_1^2} \tag{4.13}$$

By knowing F_o, k_2, and γ, the natural energy dissipation within the beam can be determined and the verification of Eq. 3.26 can be made.

4.12 Parallel LC Resonance

To demonstrate the power factor correction and the reduction of current caused with the addition of a tuned inductor, ten sine dwell tests are performed. The transfer functions of A/V and I/V are recorded with the same range of frequencies and resolution described in Section 4.9. In this part of the experiment the PZT actuators are not being used to control the beam, but instead are simply actuating it. The tests for parallel resonance are performed at five different voltage levels (15, 20, 25, 30, and 35 V). Five of the tests are performed with a correcting inductor and the other five are performed with the PZT acting alone. Because the LC resonant frequency is slightly higher than the mechanical resonant frequency of the beam, a 2 nF capacitor is added in parallel to the PZT actuator to lower the resonant frequency of the LC combination.

4.13 Series LC Resonance

To demonstrate the power factor correction and the voltage increase caused by the addition of a tuned inductor, five sine dwell tests are performed. The transfer function of the capacitor output voltage with respect to the amplifier input voltage (V_{out} / V_{in}) is recorded with the same range of frequencies and resolution described in Section 4.9. As in Section 4.12, the PZT actuators are not controlling the beam but are simply being used for actuation. The tests for series resonance are also performed at five different voltage levels (15, 20, 25, 30, and 35 V). Because the series LC resonant frequency is slightly higher than the mechanical resonant frequency of the beam, a 3 nF capacitor is added in parallel to the PZT to lower the resonant frequency of the LC combination.

4.14 Summary

This chapter presents a description of the required equipment and procedure used to demonstrate the two primary concepts presented. The first is to show a relationship between PZT consumed power and added structural damping. Measured disturbance energy and modeled dissipation energy must be compared along with the amount of apparent power consumed for a given amount of damping. The second is to verify the properties of the series and parallel PZT resonant circuits. This is performed using the circuits developed to measure current and voltage with the use of sine dwell tests. The results of the experiments shall be presented next.

Chapter 5

Results and Discussion

The purpose of this chapter is to present the results of the experiments performed. This includes the testing of series and parallel resonant LC circuits and the experiments that relate PZT consumed power and mechanical damping. The data will be analyzed and deviations from the theory will be discussed.

5.1 Strain Rate Circuit Test

To verify that the signal from the strain rate circuit used in Fig. 4.2 is measuring strain rate, a strain circuit is developed. The strain circuit is configured so that the output of PVDF film is applied to a high input impedance buffer, similar to the op-amp U1 in Fig. 4.4. The PVDF sensors on both sides of the beam are used such that one sensor is configured to measure strain and the other is configured to measure strain rate. Both of the sensor signals are displayed using a digital oscilloscope. Within the frequency range from 100 Hz to 200 Hz, the strain rate signal is observed to lead the strain signal by 90 degrees in the the time traces. Assuming the strain signal is accurate, it can be concluded that the strain rate circuit provides an accurate measure of the strain rate within the structure. These results are also observed in previous experiments in both the time and frequency domain (Finefield, 1992).

5.2 Current to Voltage Converter and Voltage Reducer Experiments

To initially verify the performance of the circuits shown in Fig. 4.4 and Fig. 4.5, qualitative experiments are performed. The current to voltage converter is compared to an ammeter and the voltage reducer is tested using two voltmeters.

To verify the proper operation of the current to voltage converter, the resistance R in the Fig. 4.5 is set to 1 kΩ. This produces a voltage proportional to the current passing through the load (10 mA of current will generate 10 V at the output). As the magnitude and frequency of the applied voltage are changed, the current within the load changes. The ammeter and voltmeter reading have been shown to be identical to within 1.0% for load output voltages larger than approximately 1V. For output voltages less than 1 V, the signal to noise ratio decreases which introduces error.

To verify the proper operation of the voltage reducer, a signal is applied to a load and to the voltage reducer. A voltmeter is used to measure the load voltage and a second voltmeter is used to measure the output of the voltage reducer. The ratio of the voltmeter readings represents the gain of the voltage reducer and is found to be 0.096. It is not expected that both voltmeters are calibrated identically and therefore the gain of the reducer is not exactly 0.1. As the magnitude and frequency of the applied voltage are changed, the gain of the reducer is consistent within 1.0%.

An impedance experiment for a 18 kΩ resistor is also performed. The voltage reducer and current to voltage converter are used to experimentally determine the impedance of a resistor. Figure 5.1 shows the empirical calculated resistance as a function of frequency and voltage. The nominal value of the resistor used is 18 kΩ $\pm 5\%$. A Fluke (model 8050A) multimeter measured the resistance to be 18.14 kΩ. The current to voltage
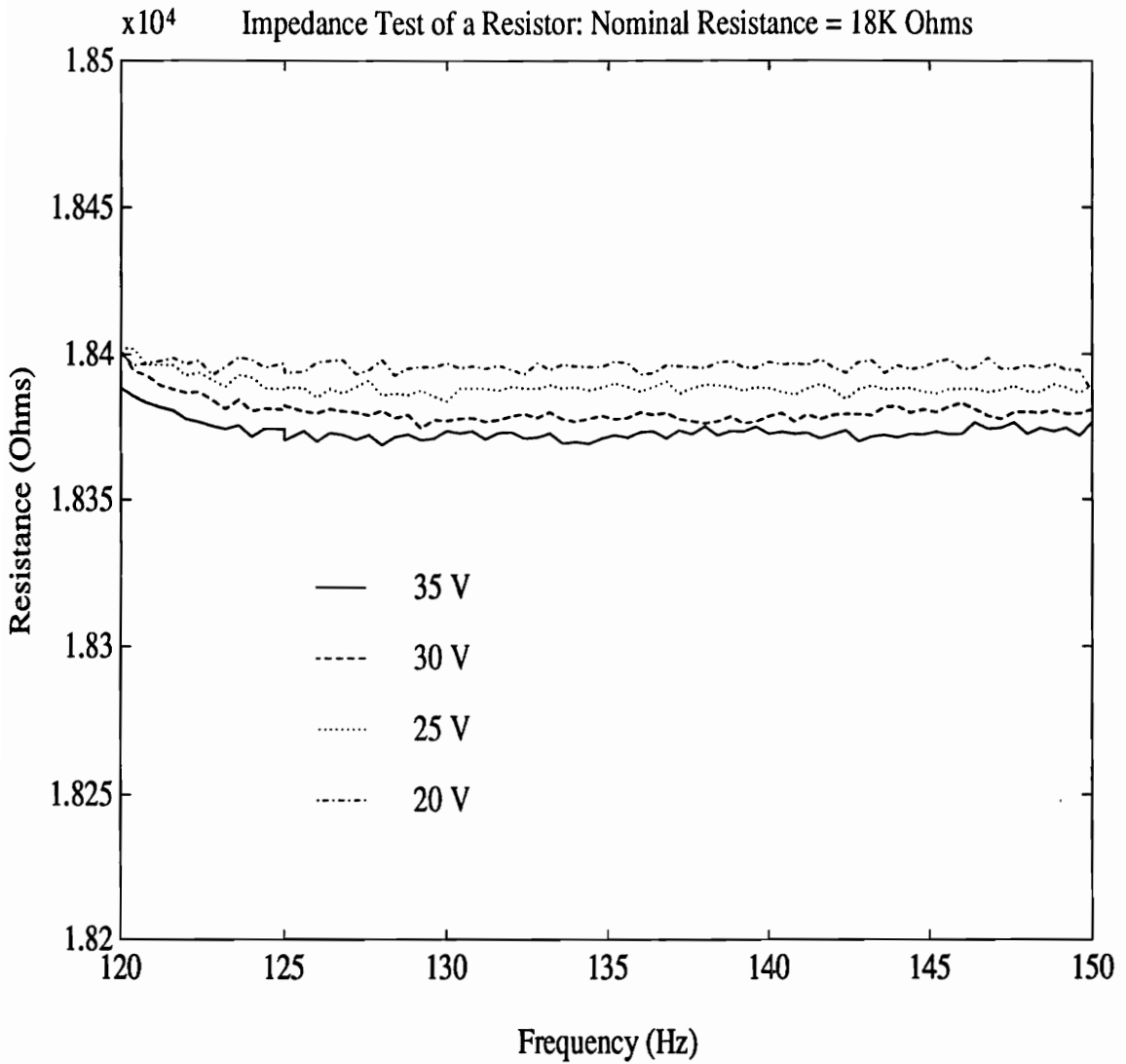
Figure 5.1 Measured Resistance of an 18 kΩ Resistor Using the Current to Voltage

Converter and the Voltage Reducer Circuits

Note: All voltages are expressed in rms Volts

converter in conjunction with the voltage reducer produced a resistance value of 18.38 kΩ $\pm$.015 kΩ. The experimental resistance falls well within the tolerance of the resistor, and compared to the ohmmeter, has a relative error of only 1.4%. The phase of voltage with respect to current is shown in Fig. 5.2. For a purely resistive element there should be no phase difference between the current and voltage in the load. The experiment indicates that the phase difference is approximately -0.1 degrees, which is not significant when compared to the phase match between channels of the analyzer. However, the sign of the phase difference indicates that the current is leading the voltage in the resistor and therefore the load is slightly capacitive. This can easily be accounted for by the parasitic capacitance that is present whenever wires are connected without solder.

Based on the experimental results presented, it can be concluded that the current to voltage converter will provide an accurate measure of the load current for output voltages higher than 1 V. The conversion from current to voltage is based on the feedback resistance R and should be set such that the minimum current measurement produces a voltage of at least 1 V. For the measuring the PZT actuator current in this set of experiments, the value R is chosen to be 3 kΩ. It can also be concluded that the voltage reducer circuit is functioning properly and has a gain of 0.1 V/V. Both of these circuits are used throughout this research.

5.3 Impedance Testing of the PZT Actuator and the Tuning Inductor

Several experiments are performed to determine the electrical impedance of the PZT actuator and the tuning inductor. The test voltages are 15, 20, 25, 30, and 35 V. The measured capacitance of the mounted PZT actuator is shown in Fig. 5.3. The empirical capacitance of the PZT actuator is determined as is described in Section 4.8. The test indicates that the PZT capacitance has a small frequency and voltage dependence. The
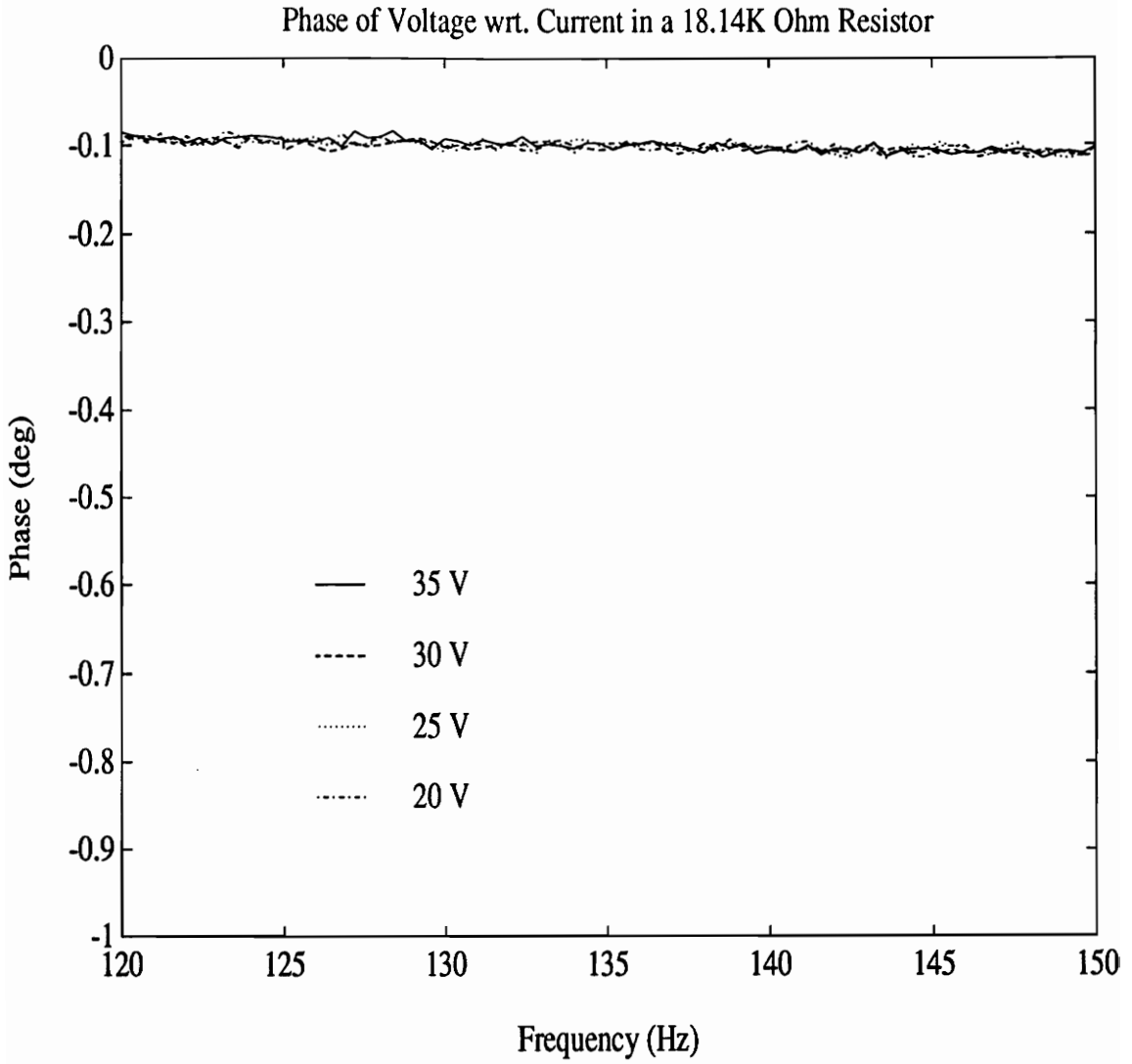
Figure 5.2 Measured Phase of the 18 kΩ Test Resistor

capacitance increases approximately 5 nF for an applied voltage ranging from 15 to 35 V at the beam's second mode. A free PZT actuator is also tested within this frequency range and has similar characteristics as the mounted PZT actuator, except at a resonant frequency of the structure. A Micronta multimeter (model 22-194) is also used to measure the actuator capacitance and is shown to be approximately 52 nF.

Figure 5.4 shows the empirical internal resistance of the PZT actuator for the various voltages as described by Section 4.8. At the second mode the internal resistance varies between 1.32 kΩ and 1.74 kΩ for the range of voltages tested. This internal resistance represents approximately 7% of the PZT actuator total impedance. The internal resistance of the PZT actuator also decreases slightly with frequency. This can be expected since all capacitors have some internal resistance and at higher frequencies the internal resistance becomes negligible. At the beam's second natural frequency (132.4 Hz) the PZT actuator internal resistance increases a significant amount. A free PZT is also shown in Fig. 5.4 and does not possess this behavior. This phenomenon is due to the mechanical coupling between the actuator and the beam.

Impedance tests are also performed on the inductor to determine its electrical properties. Figure 5.5 shows the empirical inductance of the correcting inductor. As expected the inductor exhibits nonlinear behavior. The calculated inductance is frequency and voltage dependent. The second mode inductance value ranges from 21.47 H to 21.97 H, depending on the applied voltage.

Figure 5.6 shows the internal resistance of the inductor as a function of frequency and voltage. The empirical internal resistance is shown to be slightly voltage dependent and strongly frequency dependent. The internal resistance of the inductor used is approximately 3 kΩ and represents 17% of the total impedance of the inductor. A model

Figure 5.3 Impedance Test for the PZT Actuator (Capacitance)

Note: The free PZT test is performed at 30 V and had similar DC capacitance as the mounted PZT. The dimensions of the free patch are $3.15 \times 3.18 \times 0.03$ cm, the dimensions of a single mounted PZT patch are $3.65 \times 1.9 \times 0.03$ cm.

Extracted Internal Resistance of the PZT Actuator

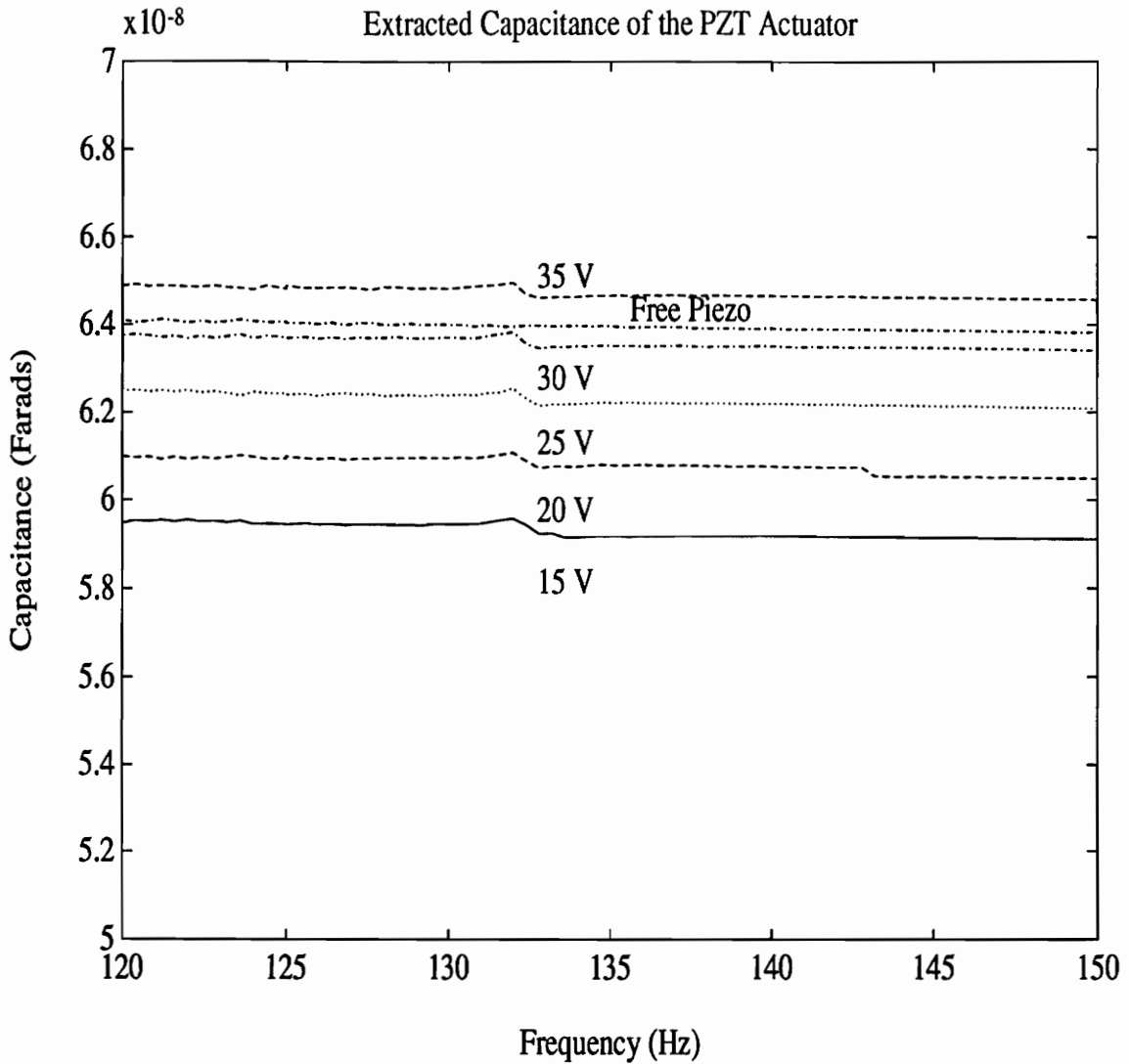Figure 5.4 Impedance Test for the PZT Actuator (Resistance)

Note: The free PZT test is performed at 30 V and had similar DC capacitance as the mounted PZT. The dimensions of the free patch are 3.15×3.18×0.03 cm, the dimensions of a single mounted PZT patch are 3.65×1.9×0.03 cm.
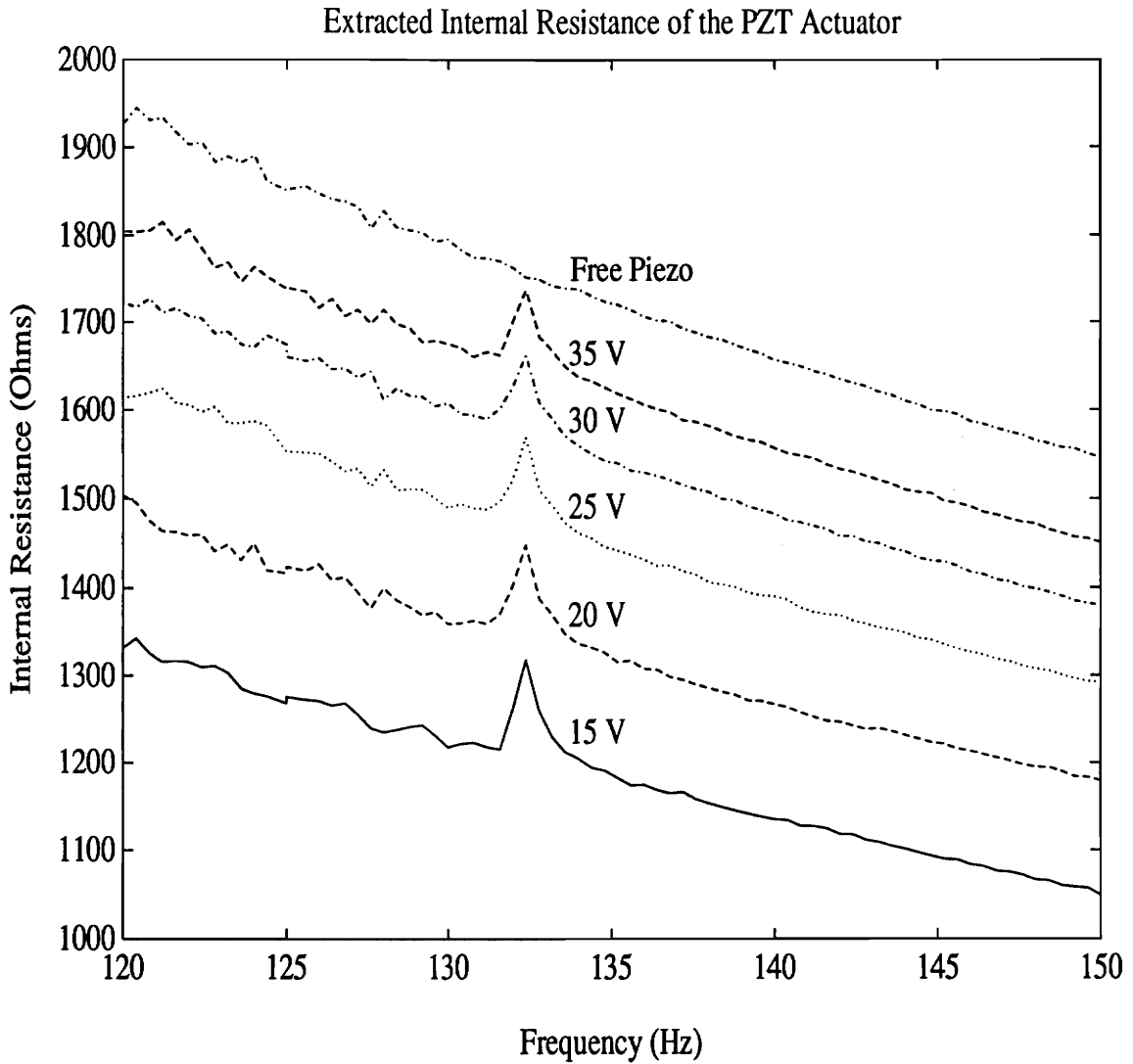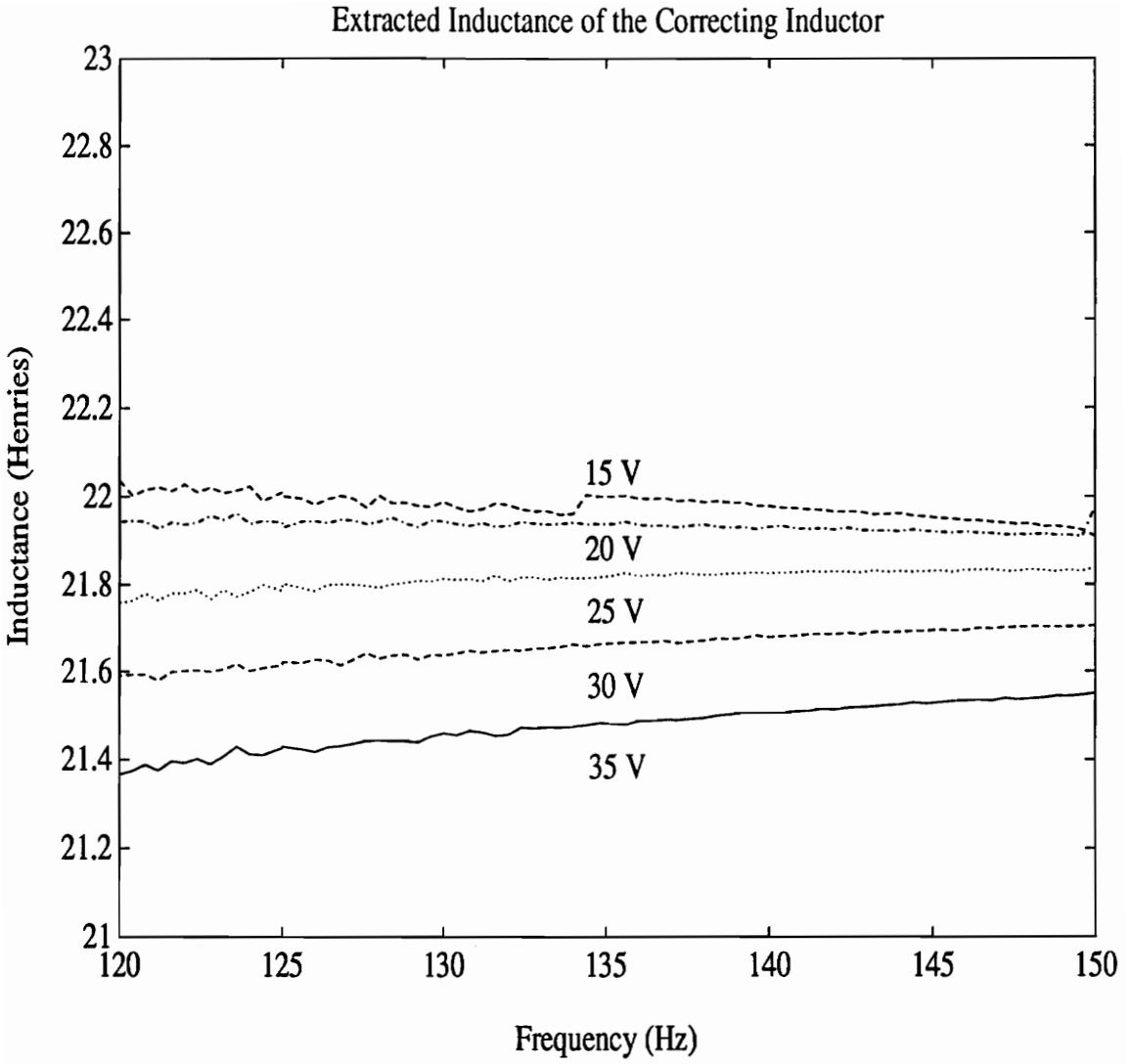
Figure 5.5 Impedance Test for the Correcting Inductor (Inductance)
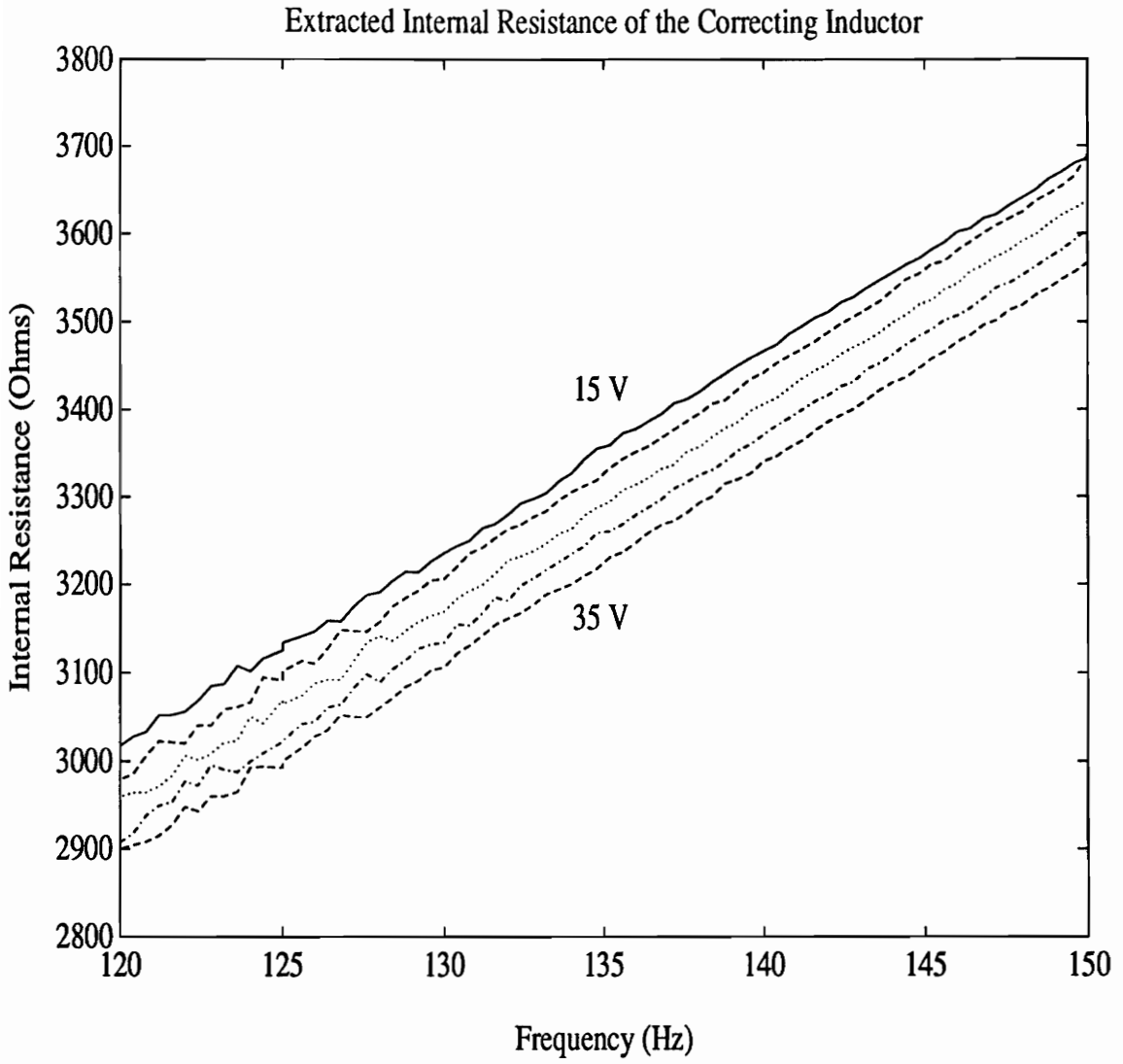
Figure 5.6 Impedance Test for the Correcting Inductor (Resistance)

neglecting the internal resistances of the inductor and the PZT actuator is certain to be inaccurate.

5.4 Relationship Between Consumed Power and Added Damping

To verify the concepts developed in Chapter 3, experiments relating PZT consumed power and structural damping are performed. This section presents the results of the various experiments performed and attempts to explain the deviations of the results from the developed theory.

5.4.1 Frequency Response Functions for Various Control Gains

Figures 5.7 and 5.8 show the frequency response functions for the nineteen different control gains. The sharpest peak corresponds to the uncontrolled case while the flattest peak is associated with the highest feedback gain. As expected, the PZT actuators provide more damping to the system as the feedback gain is increased. The system damping is extracted from the frequency response functions.

5.4.2 Choice of Damping Model & Extraction of the Damping Ratios

Damping ratios were obtained from two curve fitting routines which used a structural damping and a viscous damping model. Our expectation is that the energy dissipation mechanism, obtained by feeding back a strain rate measurement, will be more closely modeled by a structural damping model. Our purpose in using two models in the curve fitting process is to check this expectation. Figure 5.9 shows the frequency response function of the accelerance with respect to force (normalized feedback gain of 1.0 is used) along with each polynomial curve fit assuming a viscous and a structural damping model,
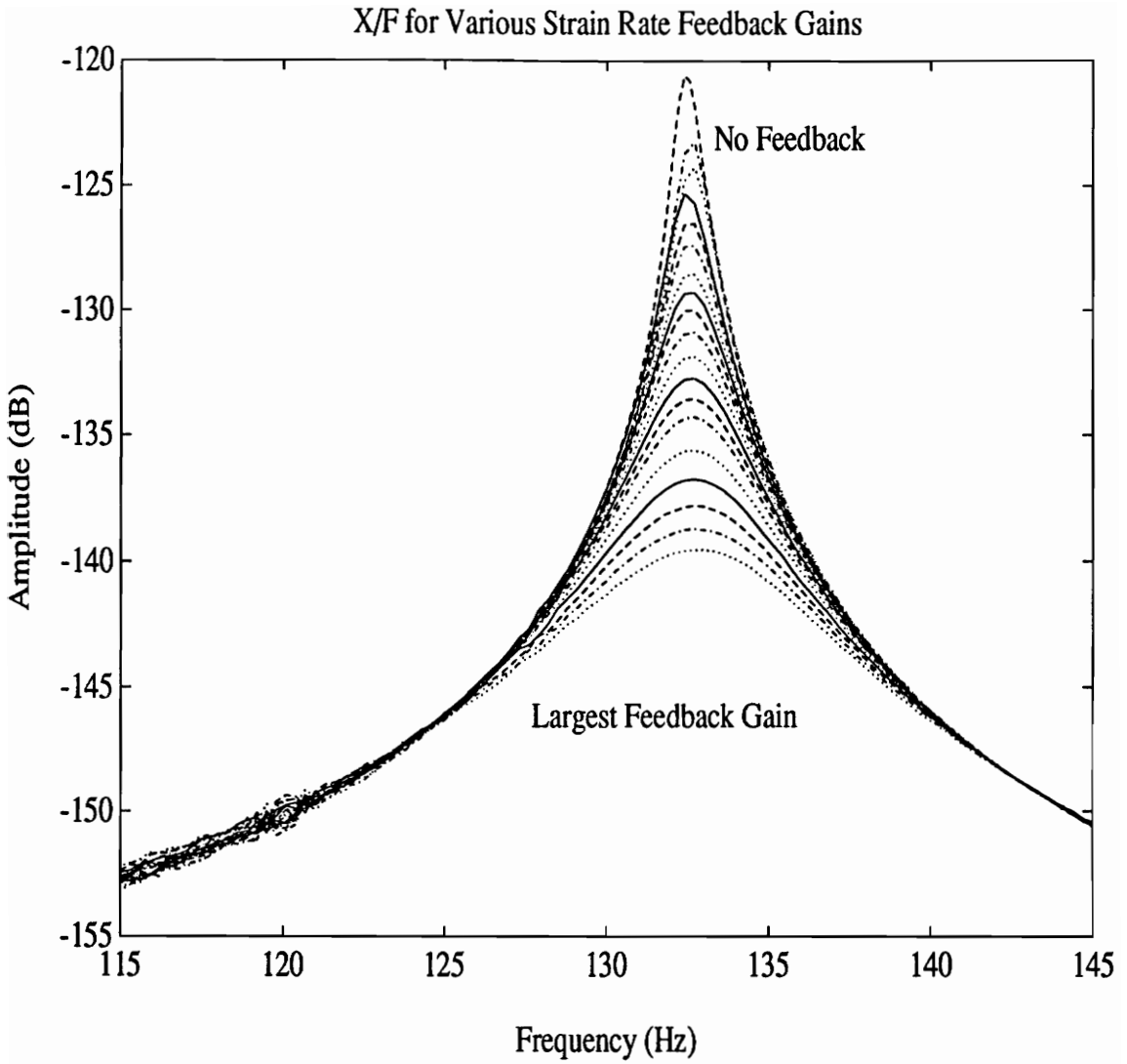
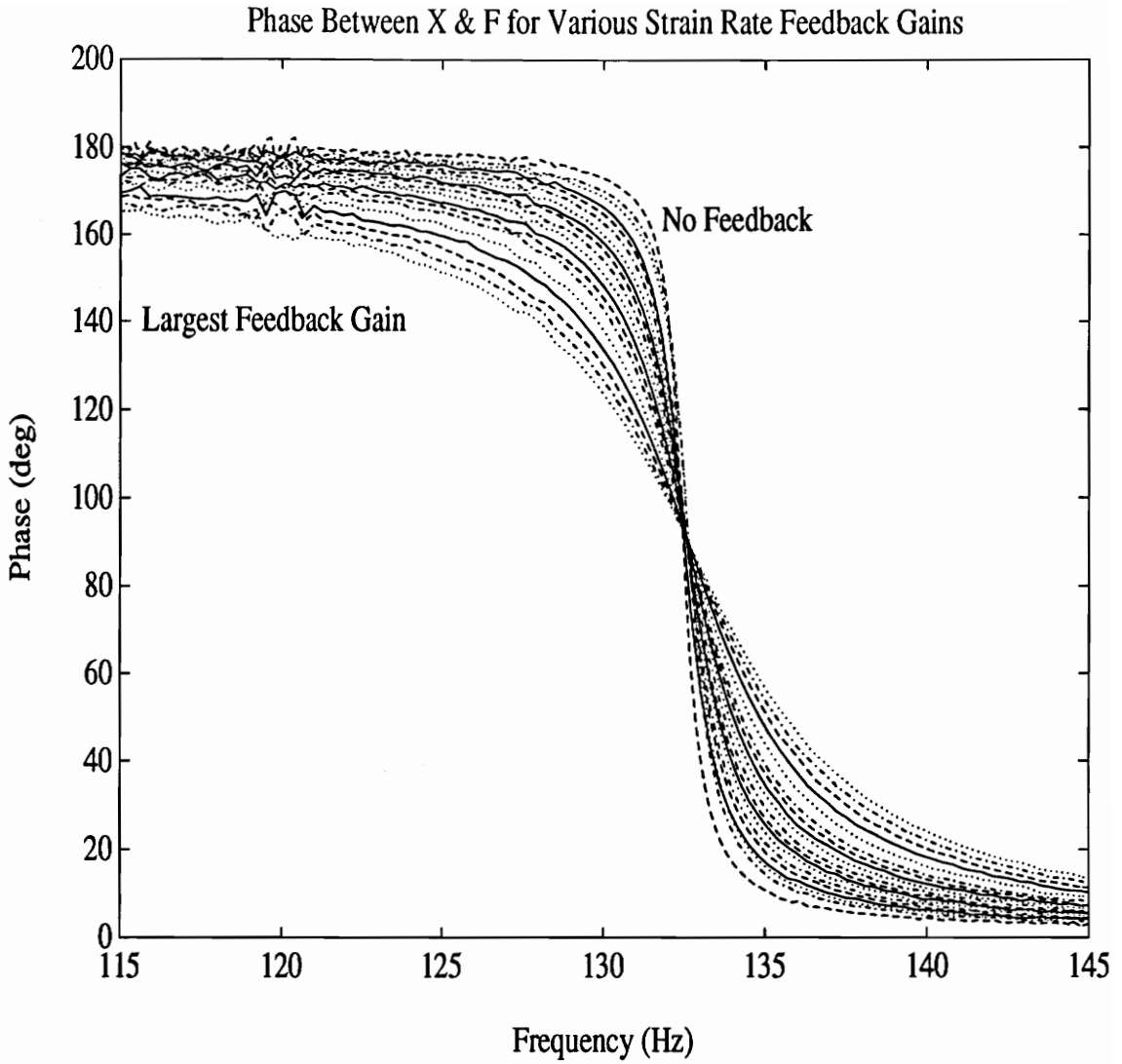Figure 5.7 Frequency Response Functions for Various Feedback Gains

Figure 5.8 Frequency Response Functions for Various Feedback Gains (Phase)

respectively. Both models assume a single pole within the frequency range of interest. The viscous damping model has a total error approximately 326% larger than the structural damping model. The absolute error is determined by taking the difference between the curve fit and the actual frequency response function at each frequency. The relative error is simply the magnitude of the absolute error divided by the actual value of the frequency response function. The total error is determined by summing all of the absolute errors at each frequency for both models and comparing them. Figure 5.10 shows the absolute and relative error of both the structural damping and the viscous damping models. The error in both models is clearly deterministic with only minor random error. The magnitude of the error of the structural damping model is always smaller than the viscous damping model except in the range of the natural frequency. This effect may be caused by random error in the actual frequency response function. Based on the data presented it can be concluded that a structural damping model is a more accurate representation of the energy dissipation within the beam.

To extract the structural damping ratios from the various frequency response functions a program developed by Kochersberger is used (Kochersberger, to appear). The structural damping model is described in Section 3.3.2. Table 5.1 shows the structural damping ratios as a function of the normalized feedback gains. The gains are normalized with respect to the fourth feedback gain.

5.4.3 Voltage, Current, Accelerance, and Force for Various Control Gains

As the control gain is altered, the root mean square (rms) value of the PZT voltage, PZT current, disturbance accelerance, and disturbance applied force are measured. The measured values are shown in Table 5.2 as a function of the normalized control gain. The data obtained in Table 5.2 is used to calculate the apparent power used by the PZT

64
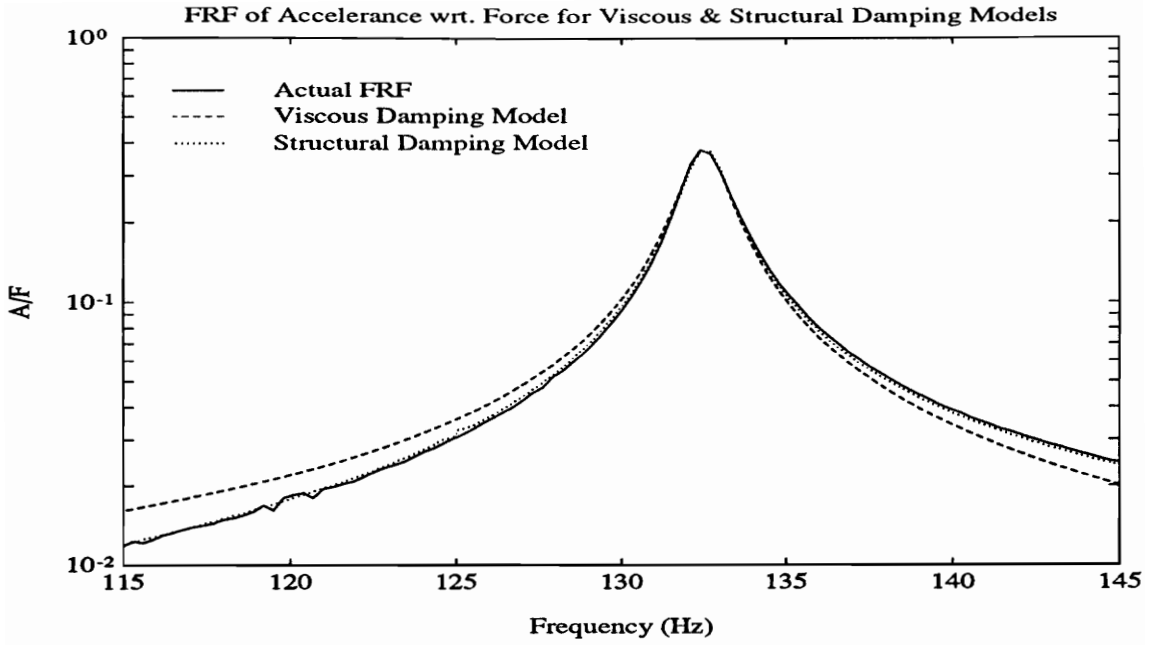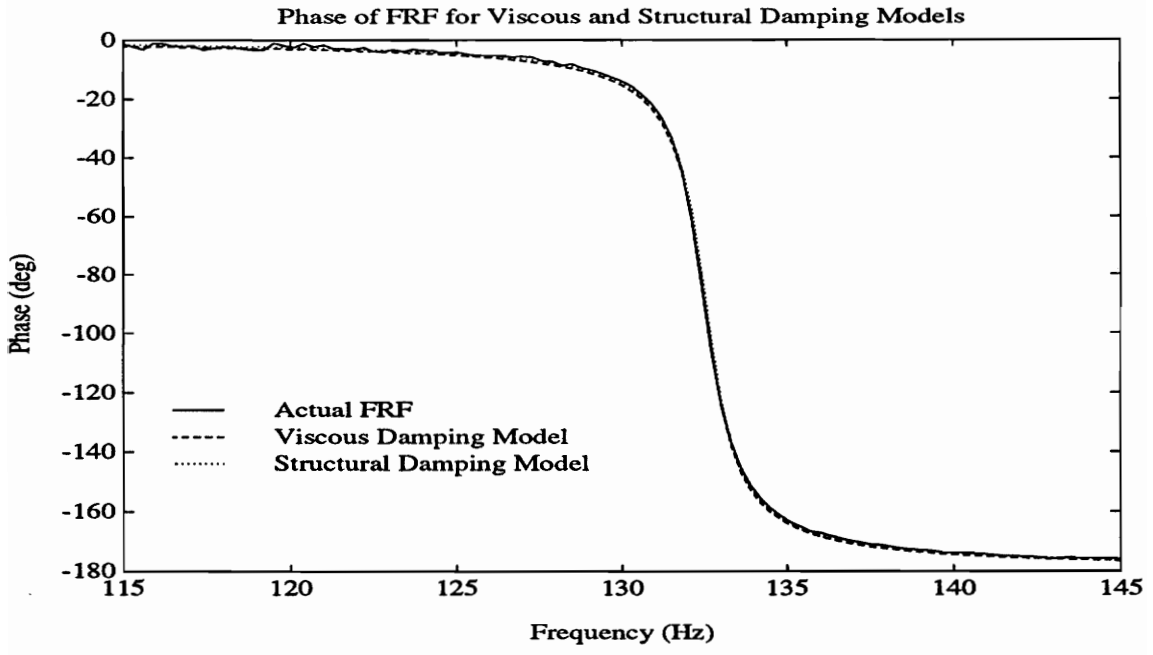
Figure 5.9 Actual FRF and Damping Model Curve Fit

a. Magnitude of FRF

b. Phase of FRF
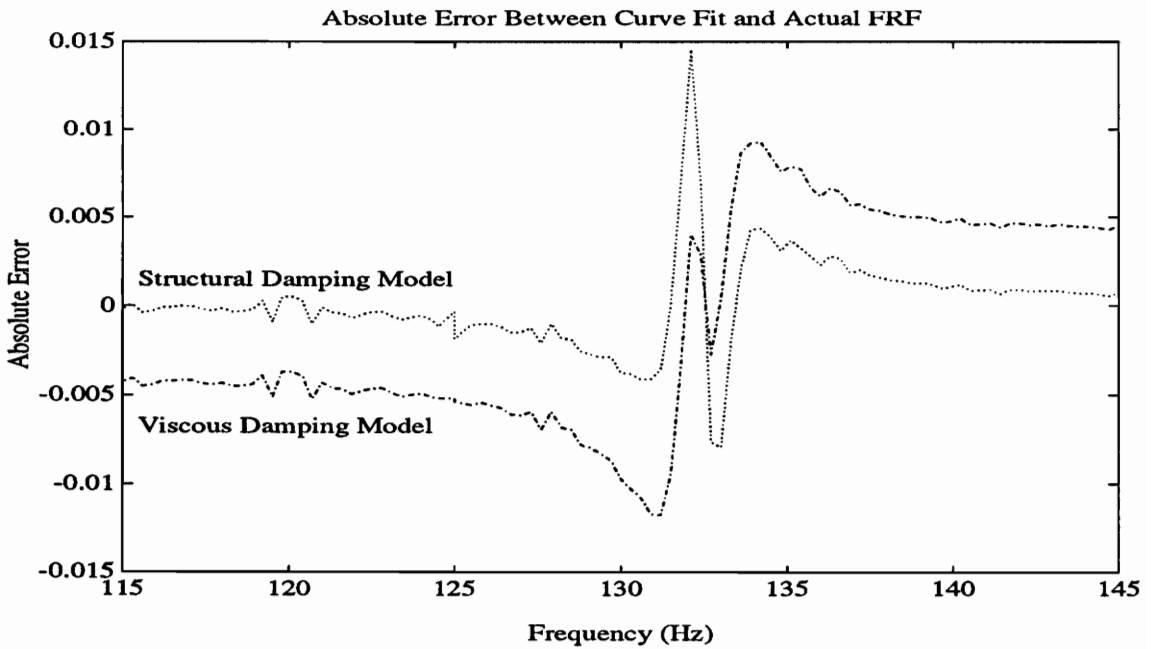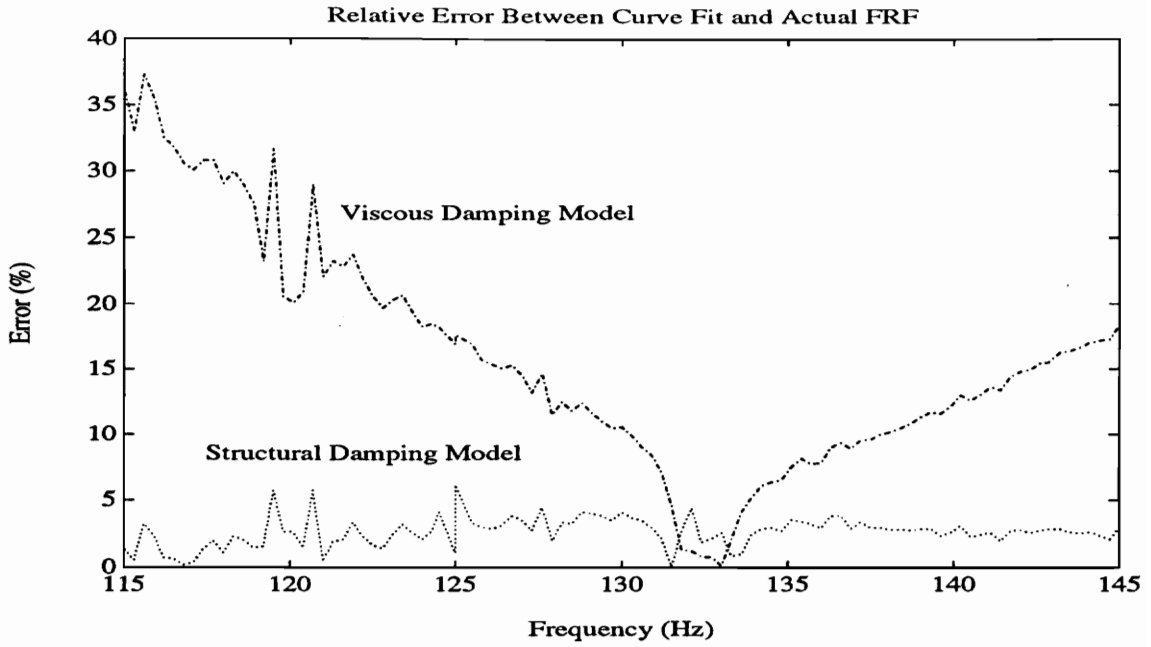
Figure 5.10 Error of the Structural and Viscous Damping Models

a. Relative Error

b. Absolute Error

actuator and the energy delivered to the beam by the shaker. A conversion must be made from the voltage signals that the transducers produce to the physical force and acceleration values.

5.4.4 Power and Damping Relationships

The information in Table 5.1 and Table 5.2 is used to relate the PZT consumed power to the amount of damping in the structure. The PZT actuator real and reactive power as a function of the structural damping ratio is shown in Fig. 5.11 and Fig. 5.12, respectively. As expected the magnitude of the real and reactive power increases as the amount of active damping added to the beam increases.

The model developed in Chapter 3 relating PZT apparent power and the amount of structural damping within a structure predicts that the PZT apparent power will asymptotically approach a finite value for an infinite amount of damping. An infinite amount of damping implies that all the energy provided to the beam by the disturbance is being removed by the PZT actuator. Therefore the beam will not vibrate. Figure 5.13 shows the empirical relationship between the PZT apparent power and the amount of structural damping in the system. The experimental result and the model developed are physically in agreement. When no feedback is provided, the structural damping ratio is defined by the beam's physical properties and the PZT apparent power is zero. As the amount of damping increases the PZT apparent power also increases and begins to approach an asymptote as the model predicts. This indicates that the developed model is physically justified.

The model relating PZT apparent power and structural damping is based on the energy balance performed on the beam. For steady state operation the sum of the energy entering

Table 5.1 Structural Damping for Various Control Gains

Normalized Control Gain	Structural Damping Ratio
0	0.00613
0.5	0.00817
0.75	0.00926
1.0	0.01055
1.3	0.01189
1.6	0.01323
2.0	0.01517
2.3	0.01658
2.6	0.01801
3.0	0.01997
3.5	0.02248
4.0	0.02488
4.5	0.02745
5.0	0.02994
6.0	0.03525
7.0	0.04046
8.0	0.04604
9.0	0.05137
10.0	0.05697

Table 5.2 Measured PZT Power and Shaker Energy Data

| Normalized Control Gain	Force (mV)	Accelerance (mV)	PZT Voltage (V)	PZT Current (V)
0	126.2	83.2	0	0
0.5	133.7	75.9	0.252	0.343
0.75	145.9	66.9	0.359	0.492
1.0	154.3	62.2	0.533	0.733
1.3	168.8	54.5	0.622	0.860
1.6	178.1	50.6	0.730	1.016
2.0	186.1	46.8	0.855	1.196
2.3	201.8	40.1	0.934	1.314
2.6	207.1	37.6	1.014	1.432
3.0	213.7	35.0	1.103	1.564
3.5	220.5	32.3	1.202	1.714
4.0	226.4	29.8	1.285	1.842
4.5	231.4	27.9	1.361	1.959
5.0	235.9	26.3	1.427	2.060
6.0	243.1	23.4	1.538	2.232
7.0	248.8	21.3	1.632	2.379
8.0	253.5	19.8	1.705	2.493
9.0	257.3	18.6	1.767	2.591
10.0	260.4	17.5	1.822	2.676
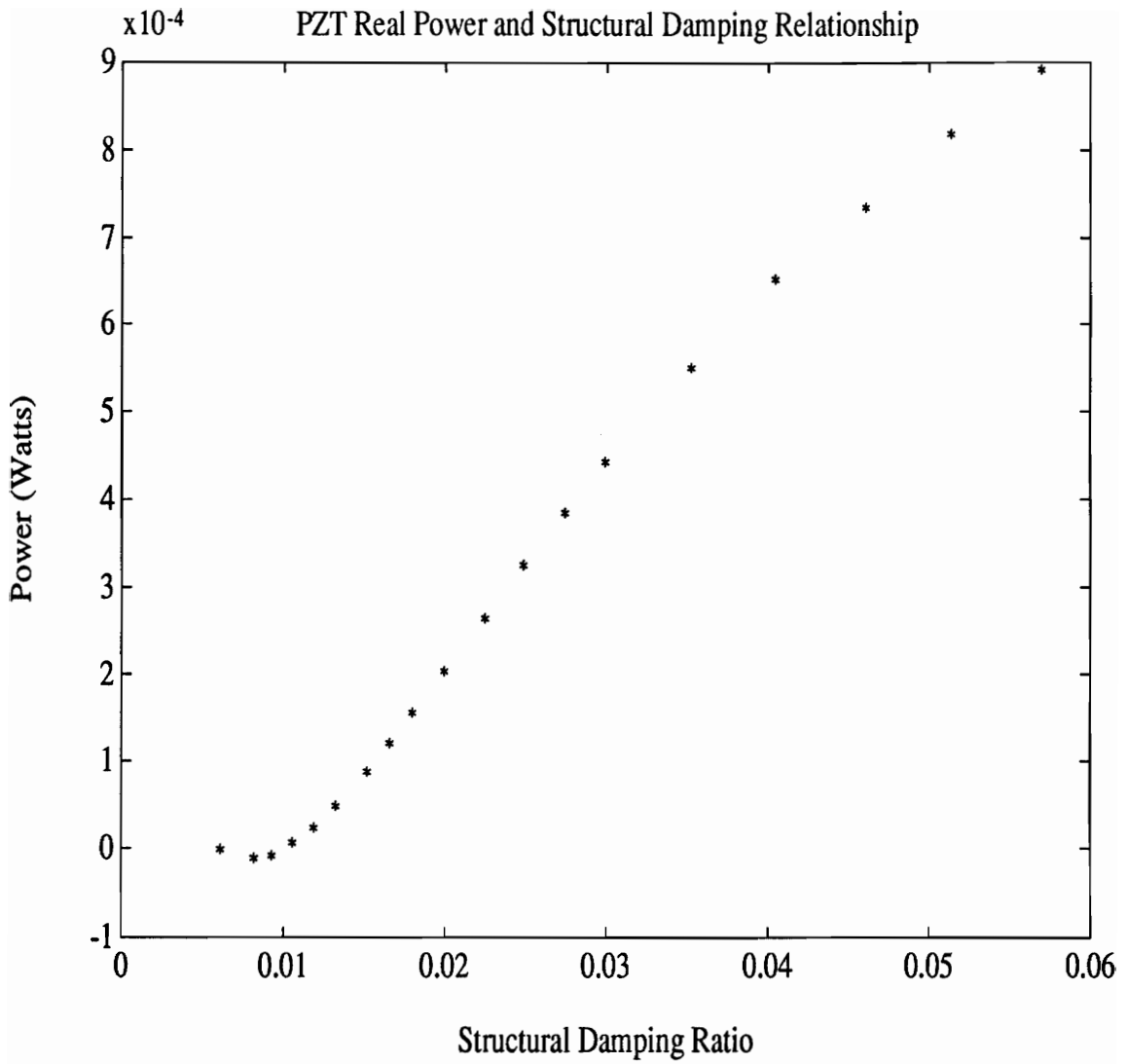
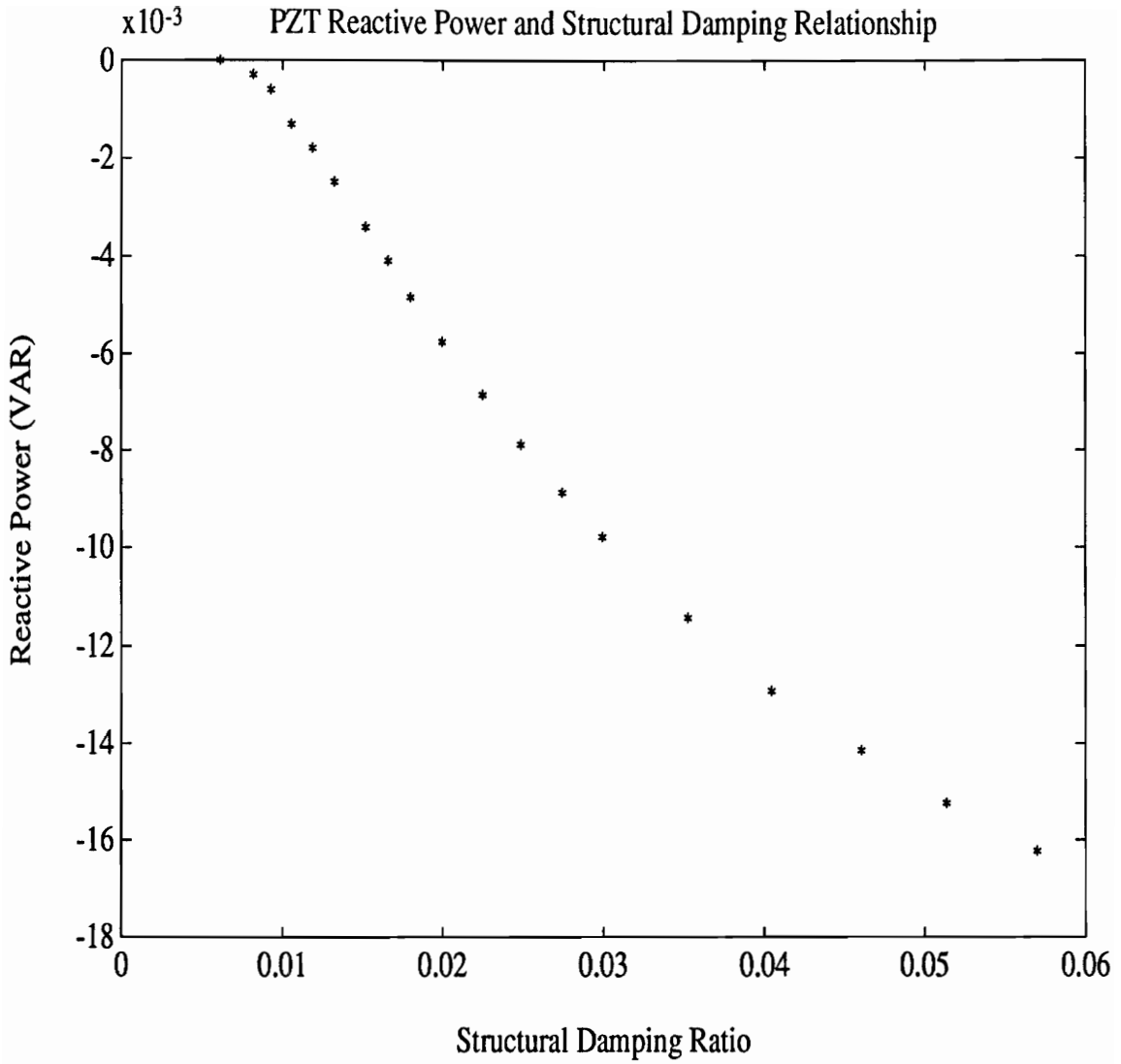Figure 5.11 PZT Real Power Related to Structural Damping

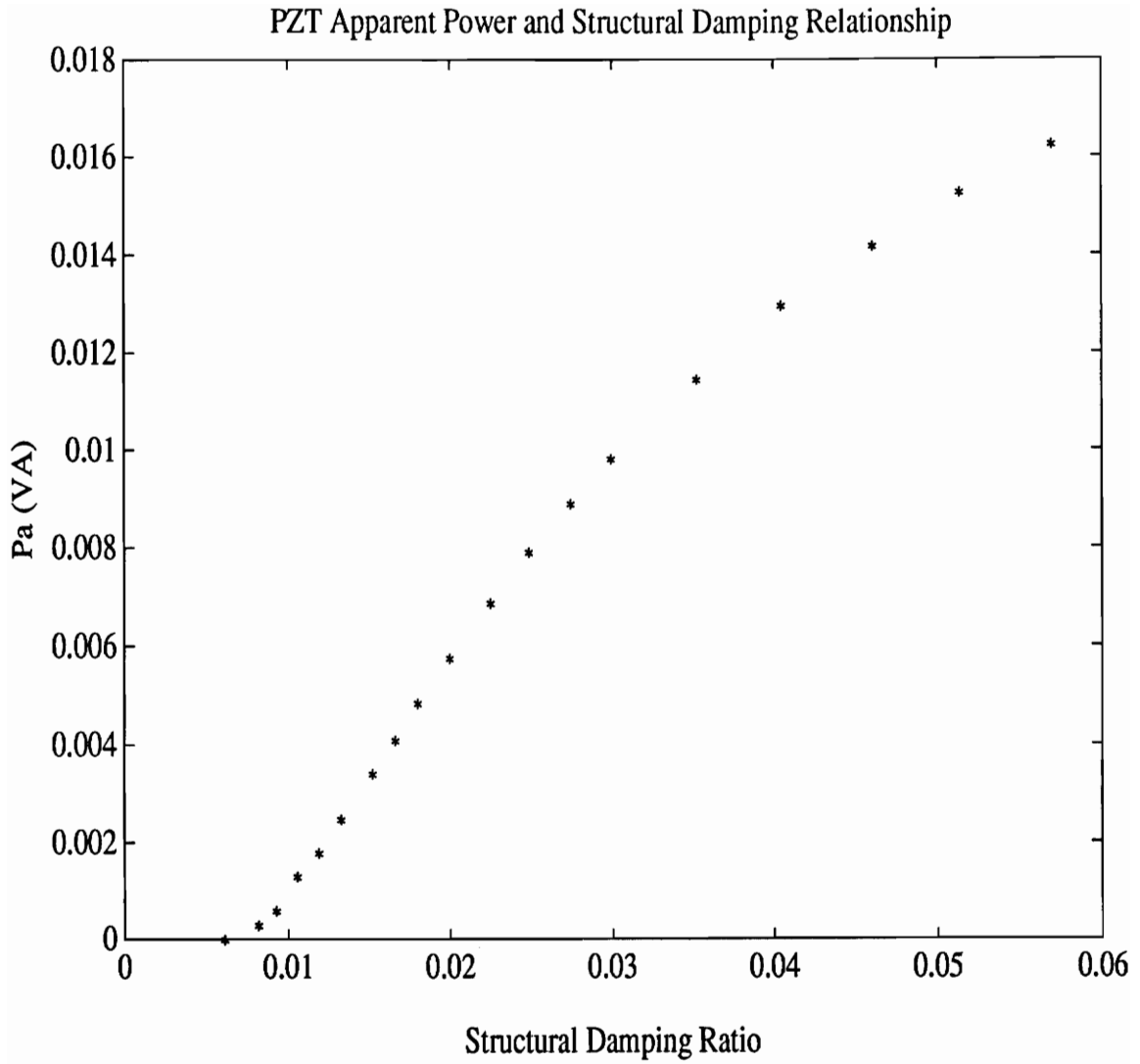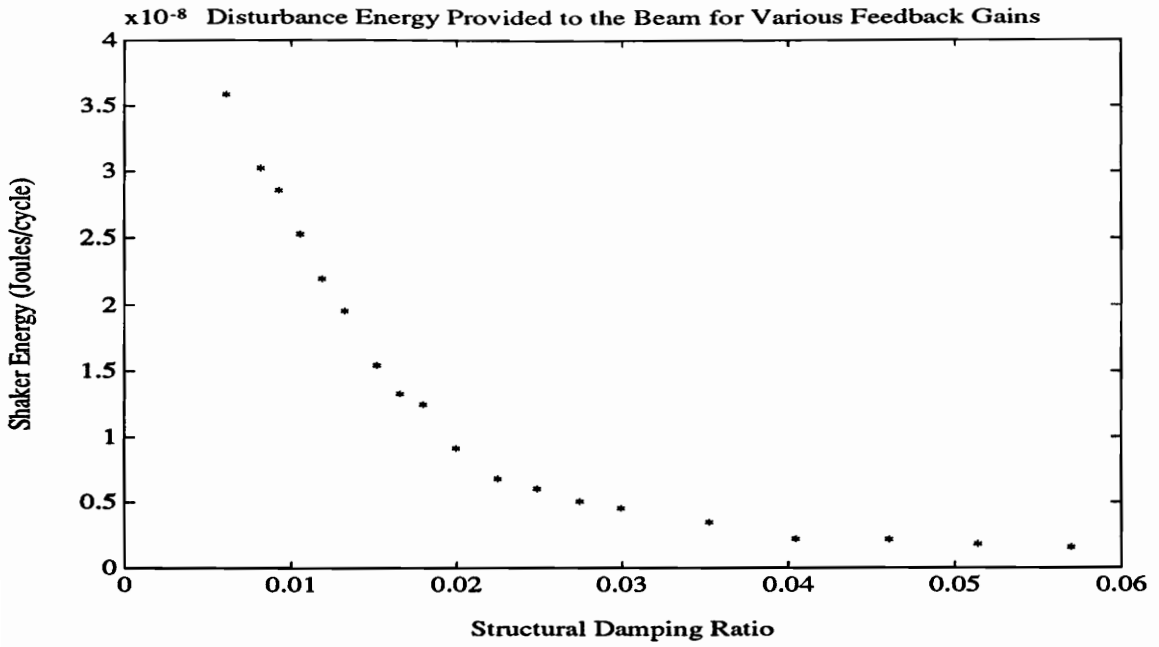Figure 5.12 PZT Reactive Power Related to Structural Damping

Figure 5.13 PZT Apparent Power Related to Structural Damping

and leaving the system must equal to zero. Using Eq. 3.26, the energy dissipated by the PZT can be calculated if the amount of energy provided to the beam by the disturbance is known. Figure 5.14a shows the empirical energy provided to the beam by the shaker as determined by Eq. 4.9. The plot is physically justified since the amplitude of the vibration is decreased as the damping is increased and thus the work done by the shaker is reduced. The second term in Eq. 3.26 is used to determine the energy naturally dissipated within the beam for a given vibration amplitude. Figure 5.14b shows the calculated beam energy dissipated by natural damping. It is expected that the sum of the energy dissipated by the beam naturally and the energy dissipated through active damping is equal to the energy provided by the disturbance. The energy dissipated naturally within the beam should always be less than or equal to the energy provided by the disturbance, depending upon the amount of active damping. This effect is not verified by Fig. 5.14 and it can be concluded that the experimental result is inaccurate. Errors may be introduced from the calibration of the transducers, the assumed beam stiffness, or the modulus of elasticity used. Regardless of the calibration, if the natural energy dissipation within the beam is scaled such that the dissipation and disturbance energies in the open loop case are equated, the experimental data remains flawed. It is interesting to note that for the open loop case the predicted natural energy dissipation and the disturbance energy are almost identical. This indicates that the model developed for the inherent energy dissipation within the beam could be correct.

5.5 Power Factor Correction Using a Parallel LC Resonant Circuit

This section presents the results of the parallel LC resonant circuit applied to the PZT actuator. The correcting inductor is shown to have no effect on the mechanical actuation of the beam, but it does reduce the current consumption of the PZT actuator and corrects the power factor. The predicted and measured results are also compared.

73

x10⁻⁸   Disturbance Energy Provided to the Beam for Various Feedback Gains

a.Energy Provided by the Disturbance (Shaker)

x10⁻⁸   Calculated Natural Energy Dissipation for Various Feedback Gains
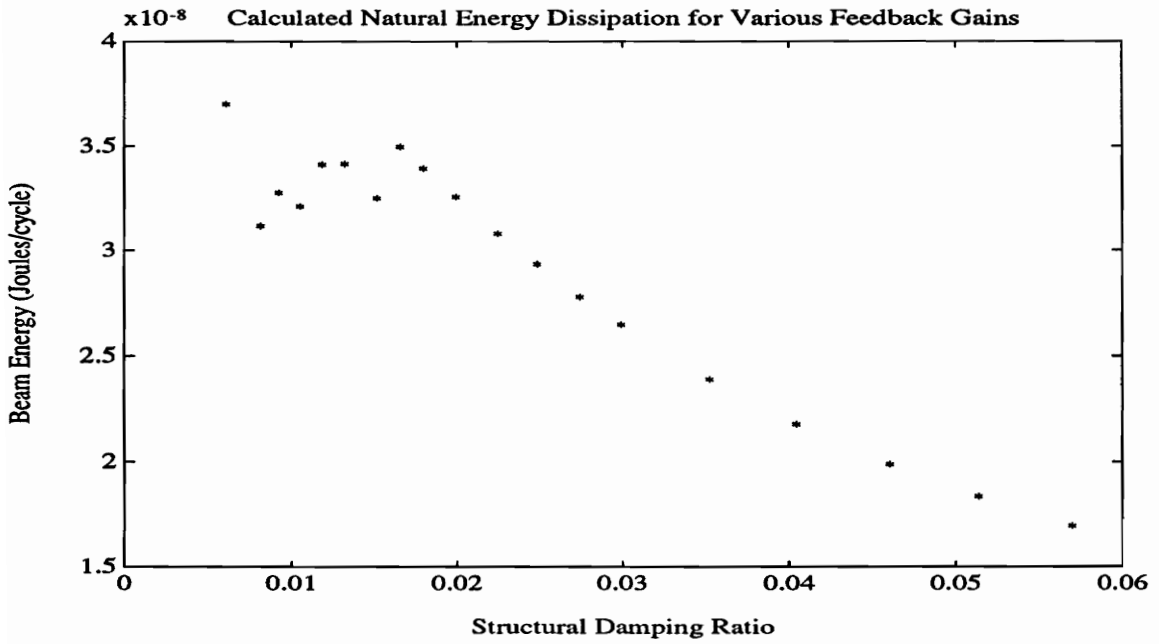
b.Energy Dissipated through Natural Damping

Figure 5.14 Energy Associated with the Beam in terms of a Control Volume

74

5.5.1 Actuation Effect of Parallel Resonance

It is necessary to show how the introduction of the correcting inductor affects the actuating abilities of the PZT patch. Figure 5.15 shows the frequency response function of displacement with respect to PZT voltage with and without a correcting inductor at 35 V. The plot shows no noticeable difference between the two frequency response functions. This is expected since the amount of PZT actuation is voltage dependent and the voltage across the PZT is fixed in both cases. The frequency response functions at other voltages showed similar results and are not shown. It is concluded that correcting the power factor of the PZT actuator with a parallel inductor does not affect the actuating ability.

5.5.2 Experimental Results of Parallel LC Resonant Circuit

The ratio of actuator current to applied PZT voltage is compared at five different voltage levels (35, 30, 25, 20, and 15 V) for both the PZT patch actuating alone and the PZT actuating with the correcting inductor. With the addition of the tuned inductor, the magnitude of the actuator current is reduced by approximately 12 dB compared to the actuator current without the tuned inductor as shown in Fig. 5.16. Not all the LC combinations are tuned exactly to the second mode because the LC resonant frequency is slightly voltage dependent. The phase of the actuator current with respect to the applied PZT voltage is shown in Fig. 5.17. As expected, the voltage and current signal of the corrected PZT actuator are in phase. The power factor is corrected from near zero to near unity. Figure 5.18 shows the current supplied by the amplifier loaded by the PZT actuating alone and the PZT actuating with the tuned inductor. The correcting inductor reduces the current consumption of the actuator 72-75%, depending upon the applied
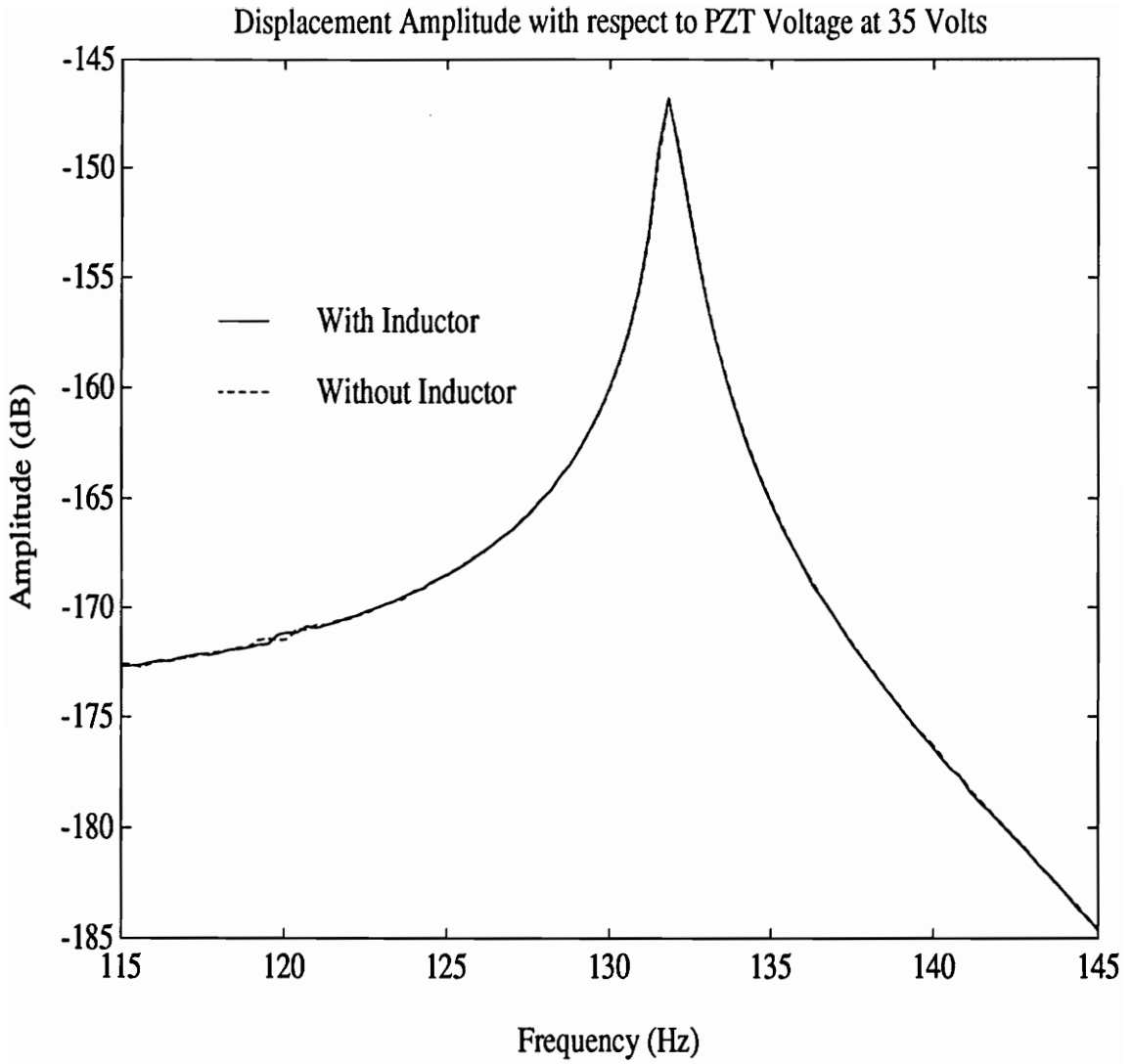
Figure 5.15 FRF of Displacement With Respect to Actuator Voltage
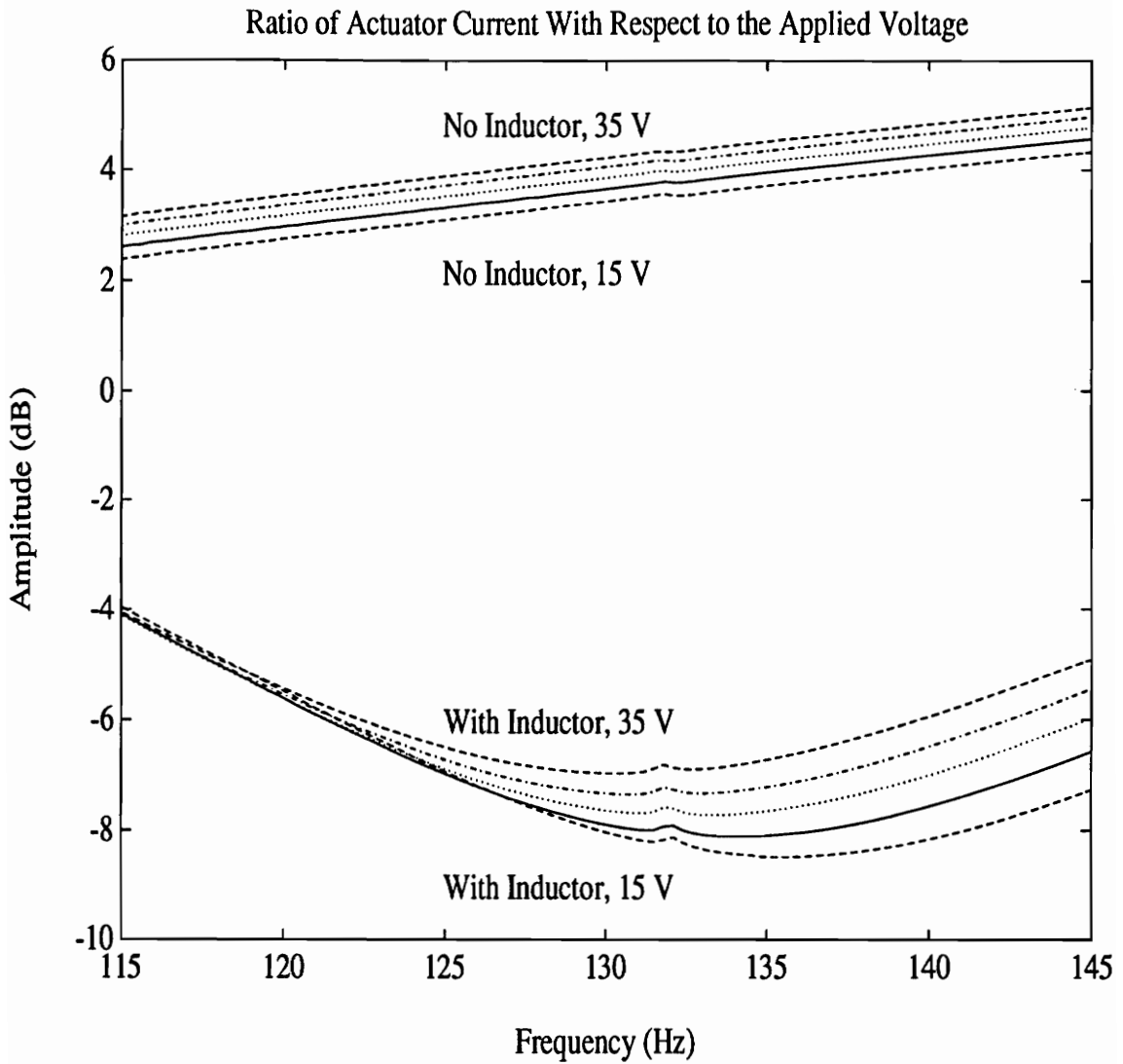
Figure 5.16 Measured Ratio of Actuator Current With Respect to Voltage for Parallel Resonance: Tests Performed at 35, 30, 25, 20, and 15 V
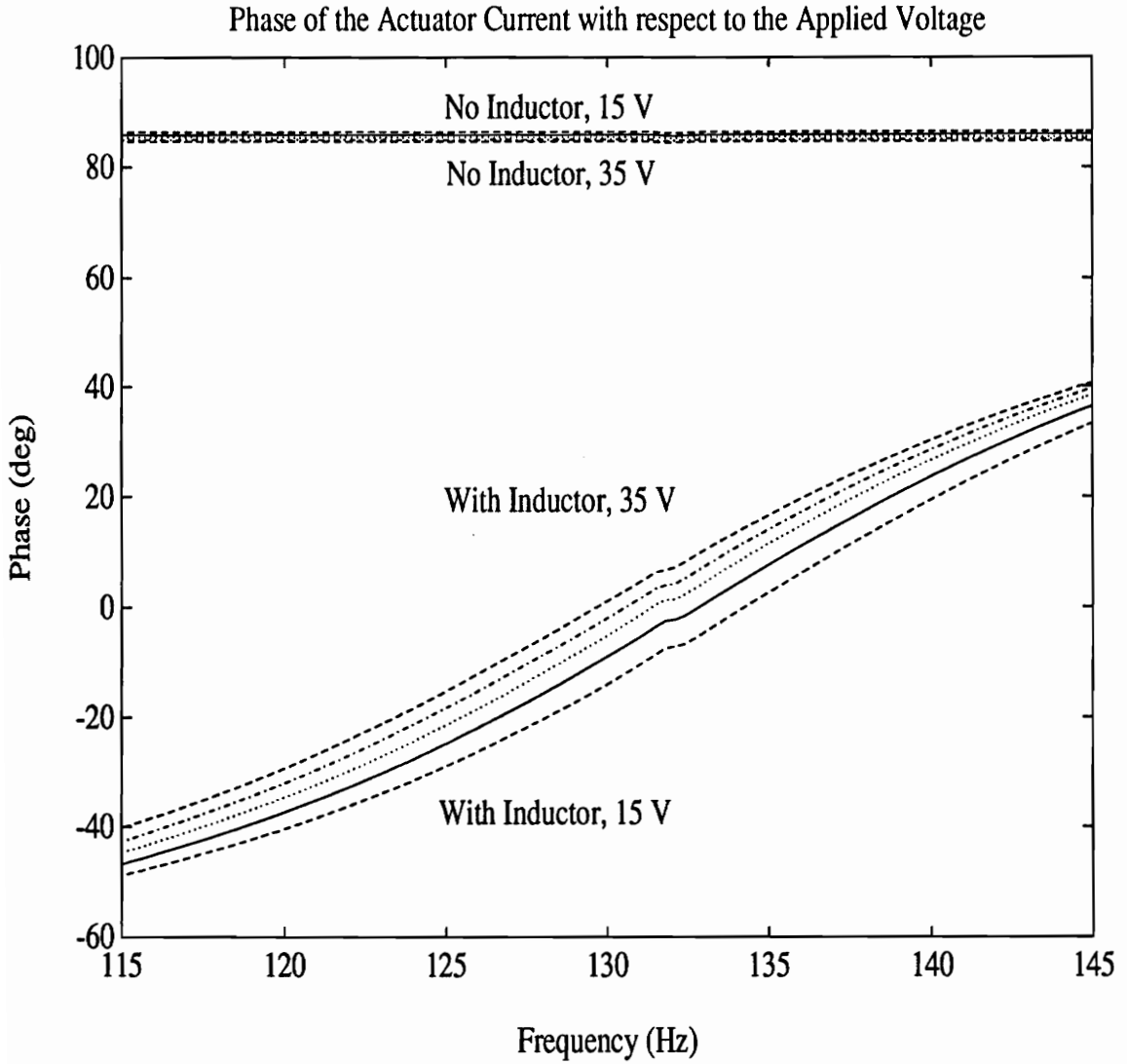
Figure 5.17 Measured Phase of Actuator Current With Respect to Voltage for Parallel

Resonance: Tests Performed at 35, 30, 25, 20, and 15 V
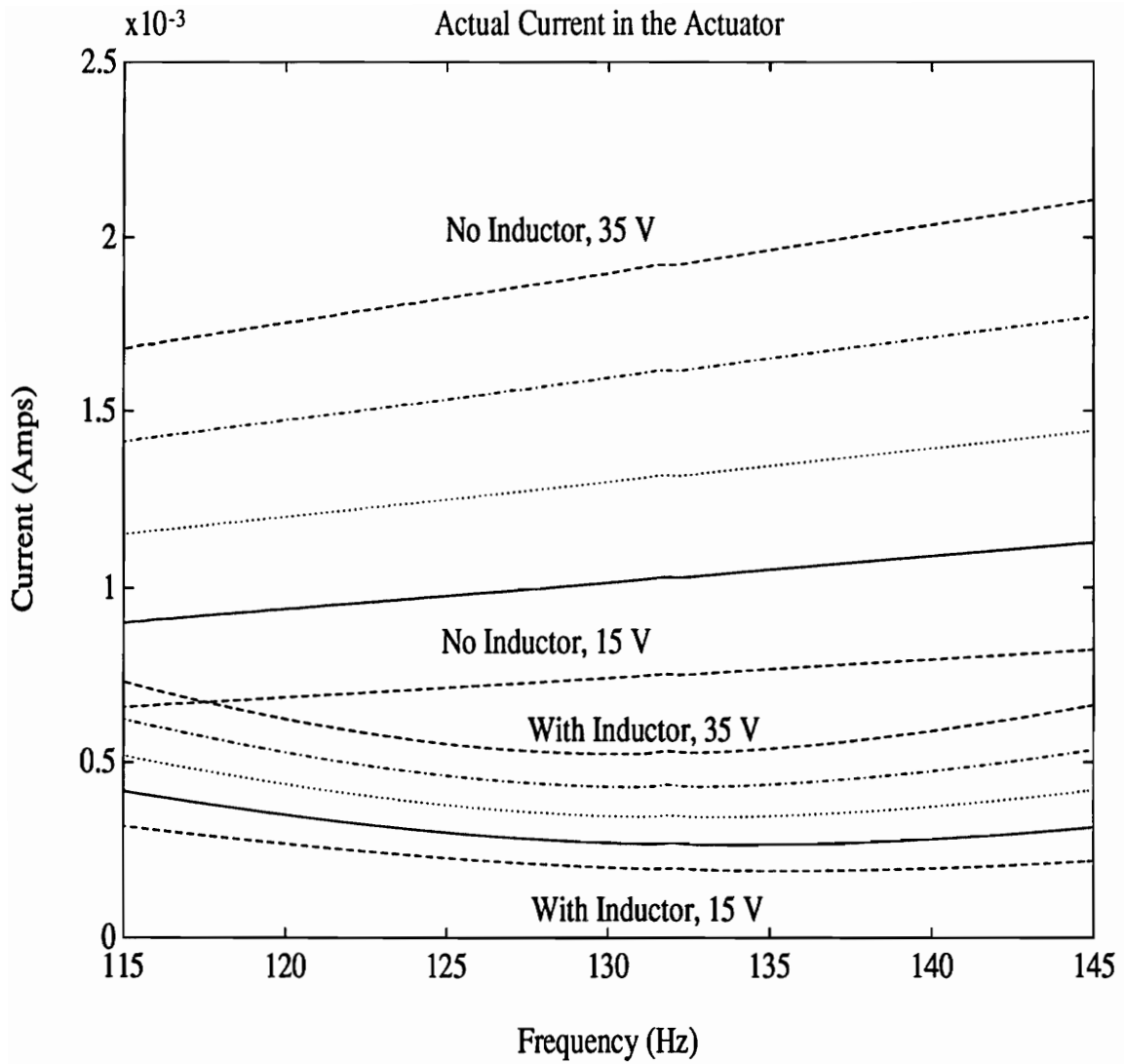
Figure 5.18 Measured Actuator Current for Parallel Resonance

Tests Performed at 35, 30, 25, 20, and 15 V

voltage. Since the current is reduced for a fixed voltage, the PZT apparent power is also reduced 72-75%.

5.5.3 Parallel LC Resonance Comparison with Theoretical Results

The electrical characteristics determined from the impedance tests are used to model the behavior of the PZT actuator and the interaction it has when used with a correcting inductor. The physical constants used are obtained from Fig. 5.3 through Fig. 5.6 at 132.4 Hz. The parallel LC electrical circuit used is shown in Fig. 3.6 and is modeled using a program in Matlab. Figure 5.19 shows the theoretical ratio of the actuator current with respect to the applied voltage for both the PZT patch actuating alone and the PZT patch actuating with the correcting inductor. Figure 5.20 shows the corresponding theoretical phase plot. The model predicts the magnitude of the current to be reduced by approximately 11dB with respect to the current in the PZT actuator. The model also predicts the PZT current and voltage to be in phase at the second mode frequency for the PZT patch with the tuned inductor.

Figure 5.21 displays both the theoretical and experimental ratio of the actuator current to PZT applied voltage for a corrected PZT load. The experimental data and theoretical model produce very similar results. The theoretical model predicts the LC resonant frequencies to be slightly larger than the actual values. The probable cause of this deviation is due to the lack of perfect models for the inductor and PZT patch used. The inductance and capacitance values in the model are based on the results of the impedance test shown in Section 5.3. If the extracted inductance and capacitance are smaller than the actual values, then the model's LC resonant frequency will be slightly higher than the actual value. The theoretical model also predicts the PZT current to be reduced approximately 0.25 dB less than it actually is. This deviation is probably also caused by

80

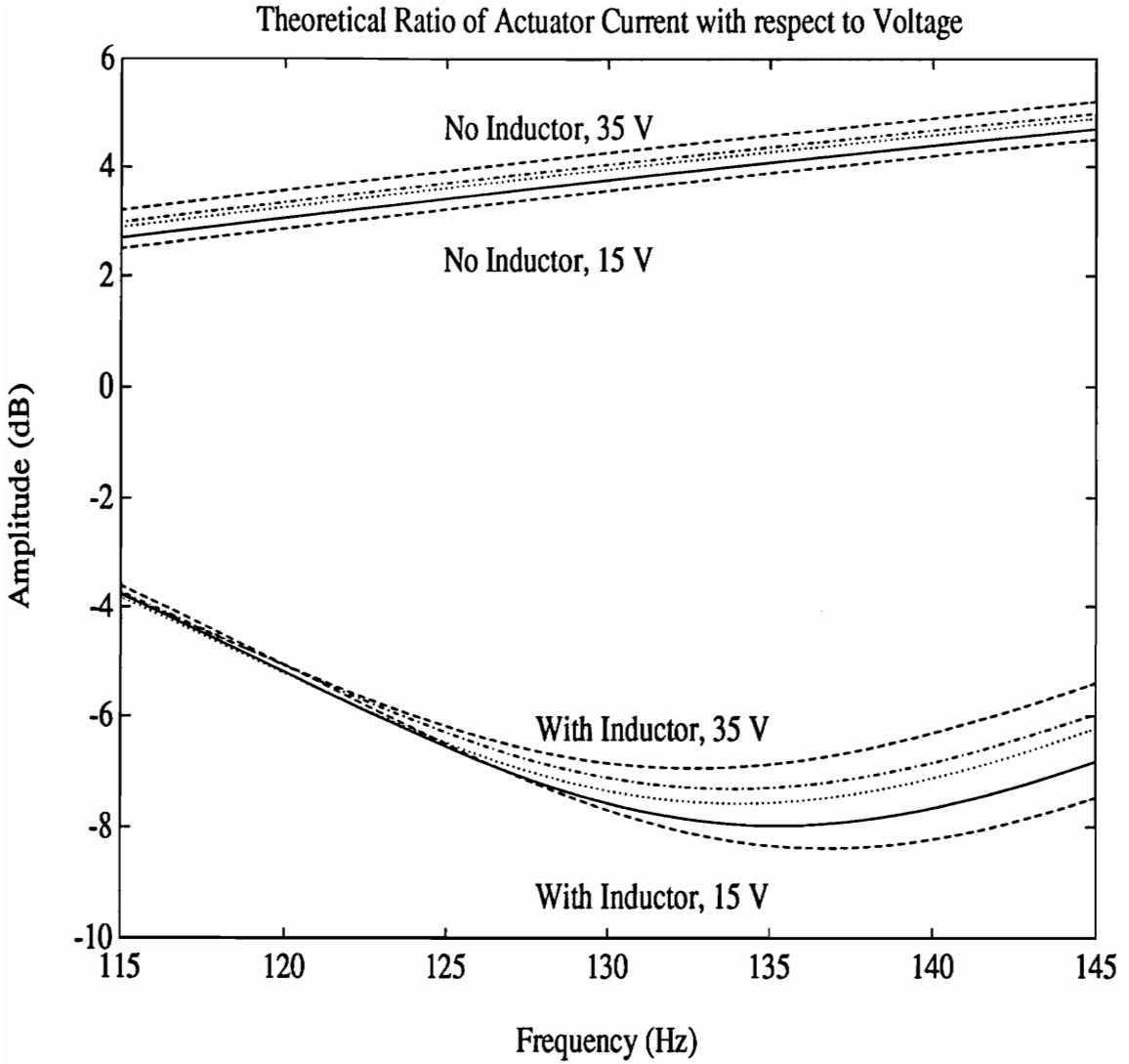Figure 5.19 Theoretical Ratio of Current With Respect to Voltage for Parallel Resonance

Modeled at 35, 30, 25, 20, and 15 V
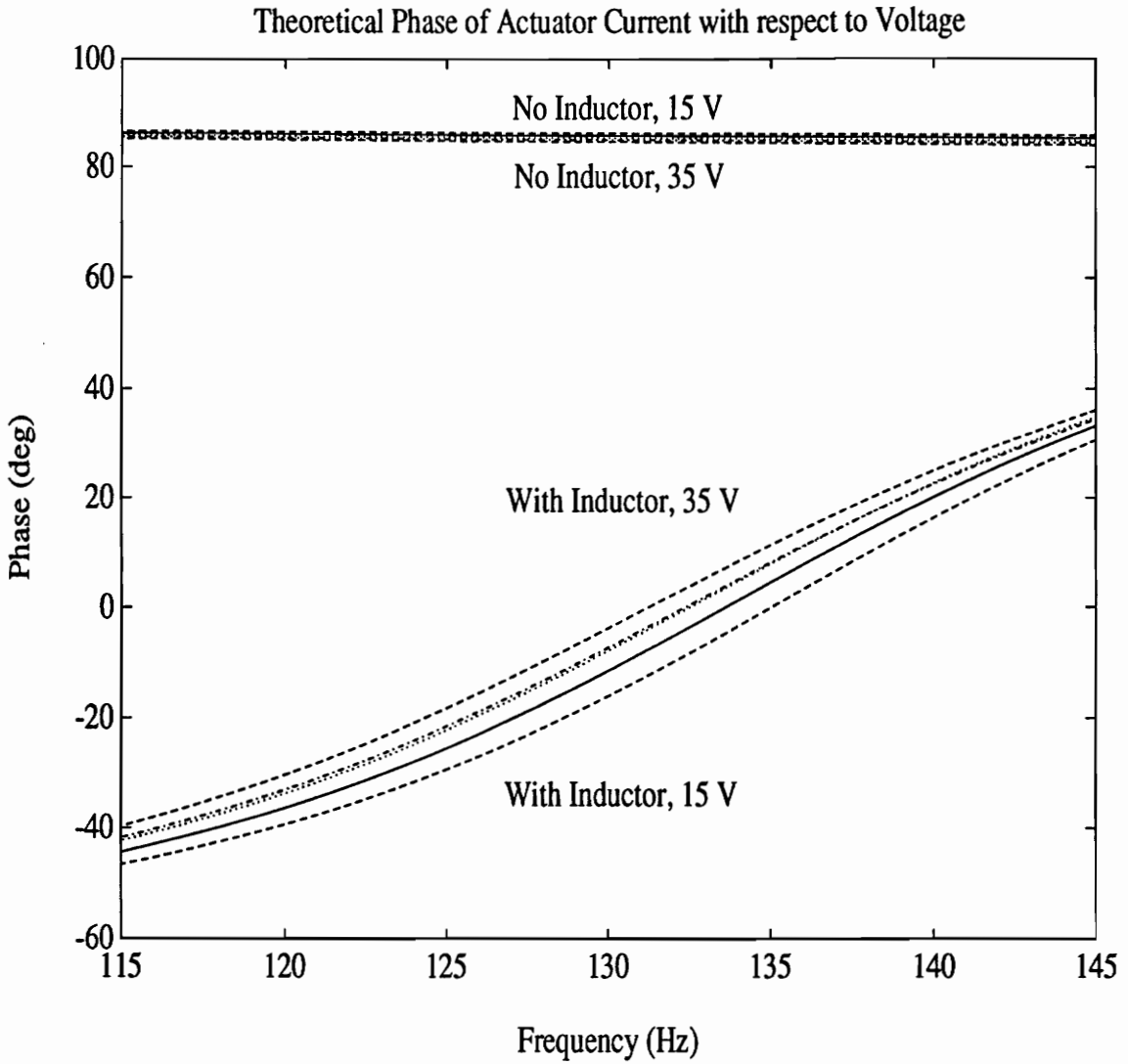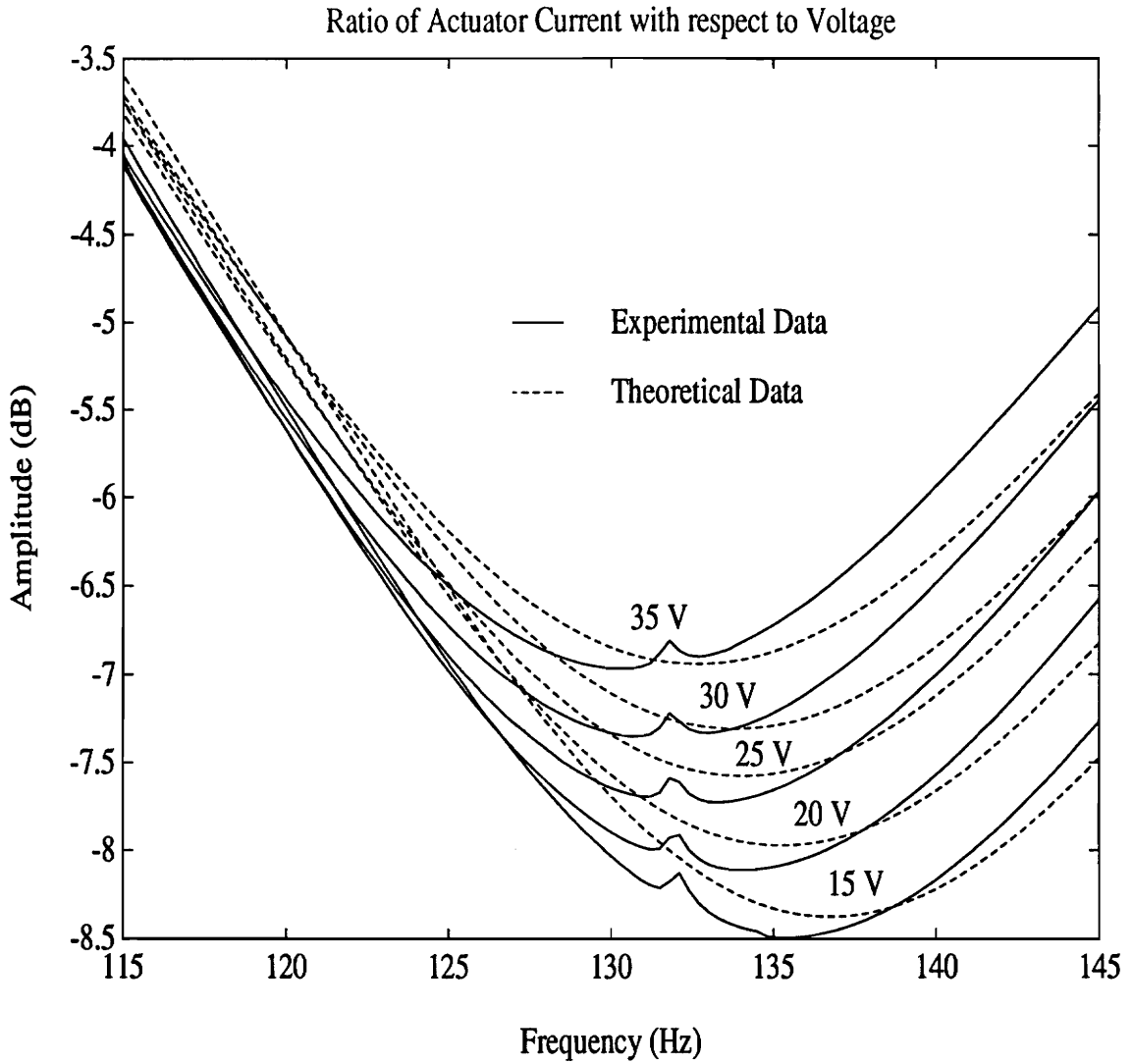
Figure 5.20 Theoretical Phase of Actuator Current With Respect to Voltage for Parallel Resonance: Modeled at 35, 30, 25, 20, and 15 V

Ratio of Actuator Current with respect to Voltage

Figure 5.21 Comparison of Theoretical and Experimental Actuator Current
With Respect to Voltage for Parallel Resonance

errors in modeling the internal resistance of the inductor and the PZT patch. The modeled internal resistance for the PZT actuator is obtained at the second mode frequency. At this frequency the internal resistance of the PZT patch increases 5-10% above normal due to mechanical coupling. The internal resistance of the PZT patch is most likely higher than the actual value and so the model predicts less current reduction due to higher electrical damping. The relative error between the empirical and theoretical LC resonant frequency is approximately 2% while the relative error in the amount of current reduction is approximately 10%. Based on the results presented, it can be concluded that the experimental results are valid and that the circuit used to model the LC parallel resonance is reasonably accurate.

Table 5.3 displays the inductance values extracted from the impedance test described in Section 5.3. The table also shows the predicted inductance needed to correct the power factor as defined by Eq. 3.10. The predicted inductance is based on the internal resistance of the inductor and PZT actuator as well as the operating frequency and the capacitance of the PZT actuator. For the experiments performed at 30 V, the predicted correcting inductance and the actual inductor modeled from the impedance test are most closely related. It is therefore expected that the model at 30 V is the most accurate at the second mode frequency.

5.6 Series LC Resonance

This section presents the results of the series LC resonant circuit applied to the PZT actuator. The correcting inductor is shown to increase the voltage across the PZT patch and correct the power factor. The theoretical and experimental results are also compared.

84

Table 5.3 Experimental and Theoretical Correcting Inductances for Parallel LC Resonance

PZT Voltage (V)	Experimental Inductance from Impedance Test (H)	Theoretical Inductance from Eq 3.10 (H)
35	21.47	21.08
30	21.65	21.64
25	21.82	21.85
20	21.94	22.35
15	21.97	22.87

5.6.1 Experimental Results of Series LC Resonant Circuits

The ratio of the PZT output voltage to the amplifier input voltage is compared for five different voltage inputs (10, 8, 6, 4, and 2 V) and is shown in Fig. 5.22. The addition of the correcting inductor causes the LC combination to resonate at the second mode and causes the PZT voltage to exceed the amplifier input voltage by approximately 12 dB. The corresponding phase plot is shown in Fig. 5.23. Near the second mode frequency the PZT voltage lags the amplifier voltage by 90 degrees. Because the PZT acts essentially like a capacitor, the PZT voltage should also lag the current passing through the PZT by 90 degrees. This implies that the amplifier input voltage and current are in phase and so the power factor is corrected from approximately zero to near unity. Figure 5.24 shows the actual PZT output voltages for the five different input voltages. For an amplifier supply voltage of 10 V the PZT output voltage at resonance is approximately 38 V. The increase in PZT voltage ranges from 280 to 350%, depending upon the input voltage.

For a given PZT voltage, the PZT current is a fixed quantity defined by Ohm's Law. Therefore for a fixed PZT voltage, the current passing through the actuator is the same for the PZT patch actuating alone or with the tuned inductor. However, the amplifier input voltage is reduced by 12 dB for the PZT actuating with the tuned inductor at resonance. The apparent power of the PZT tuned actuator is therefore reduced by 12 dB when compared to a PZT patch actuating alone.

5.6.2 Series LC Resonance Comparison with Theoretical Results

The electrical characteristics determined from the impedance tests are used to model the behavior of the PZT actuator and the interaction it has when used with a correcting inductor. The electrical values used are obtained from Fig. 5.3 through Fig. 5.6 at 132.4

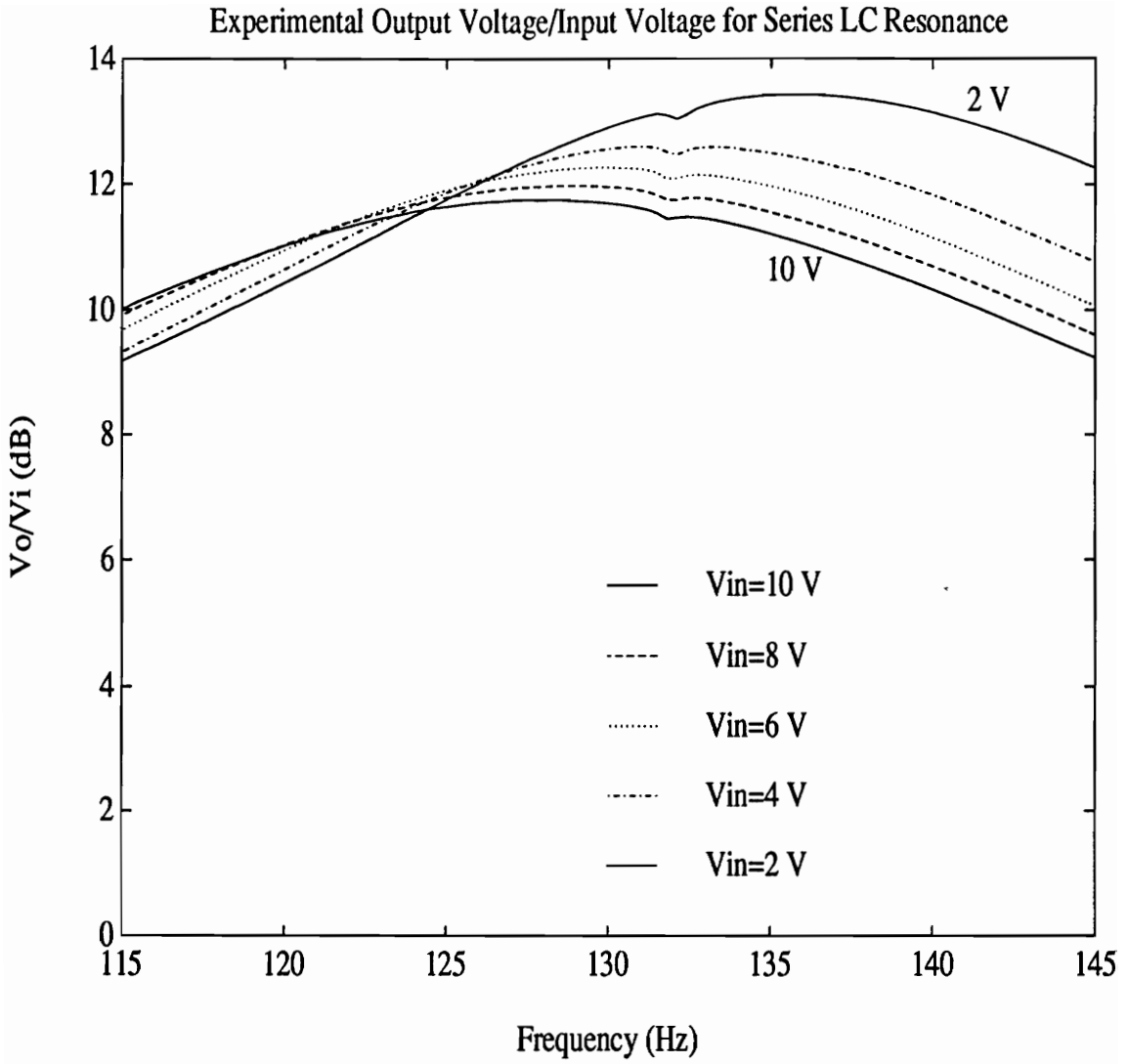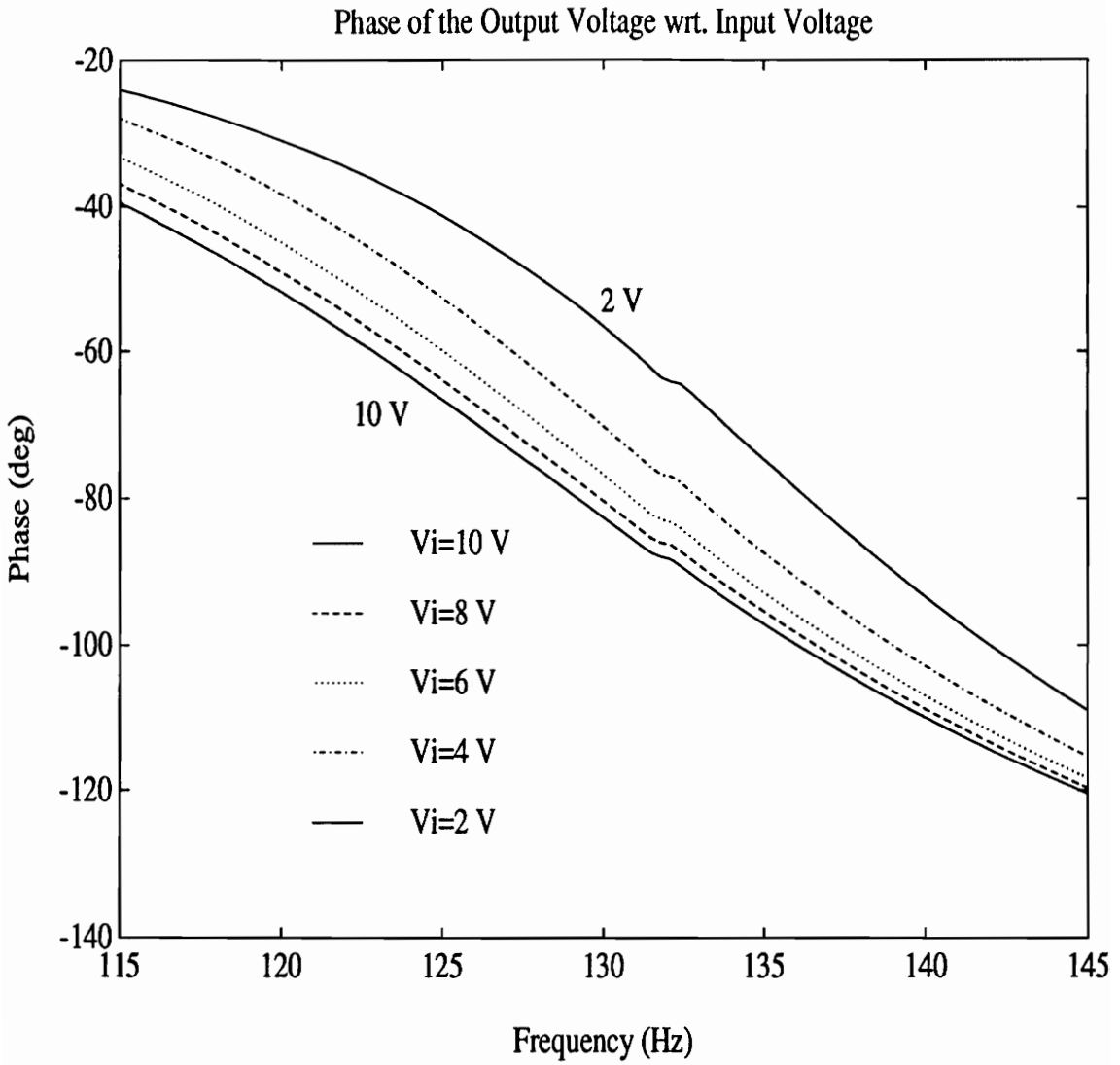Experimental Output Voltage/Input Voltage for Series LC Resonance

Figure 5.22 Measured Ratio of PZT to Input Voltage for Series LC Resonance

87

Figure 5.23 Measured Phase of PZT Voltage With Respect to
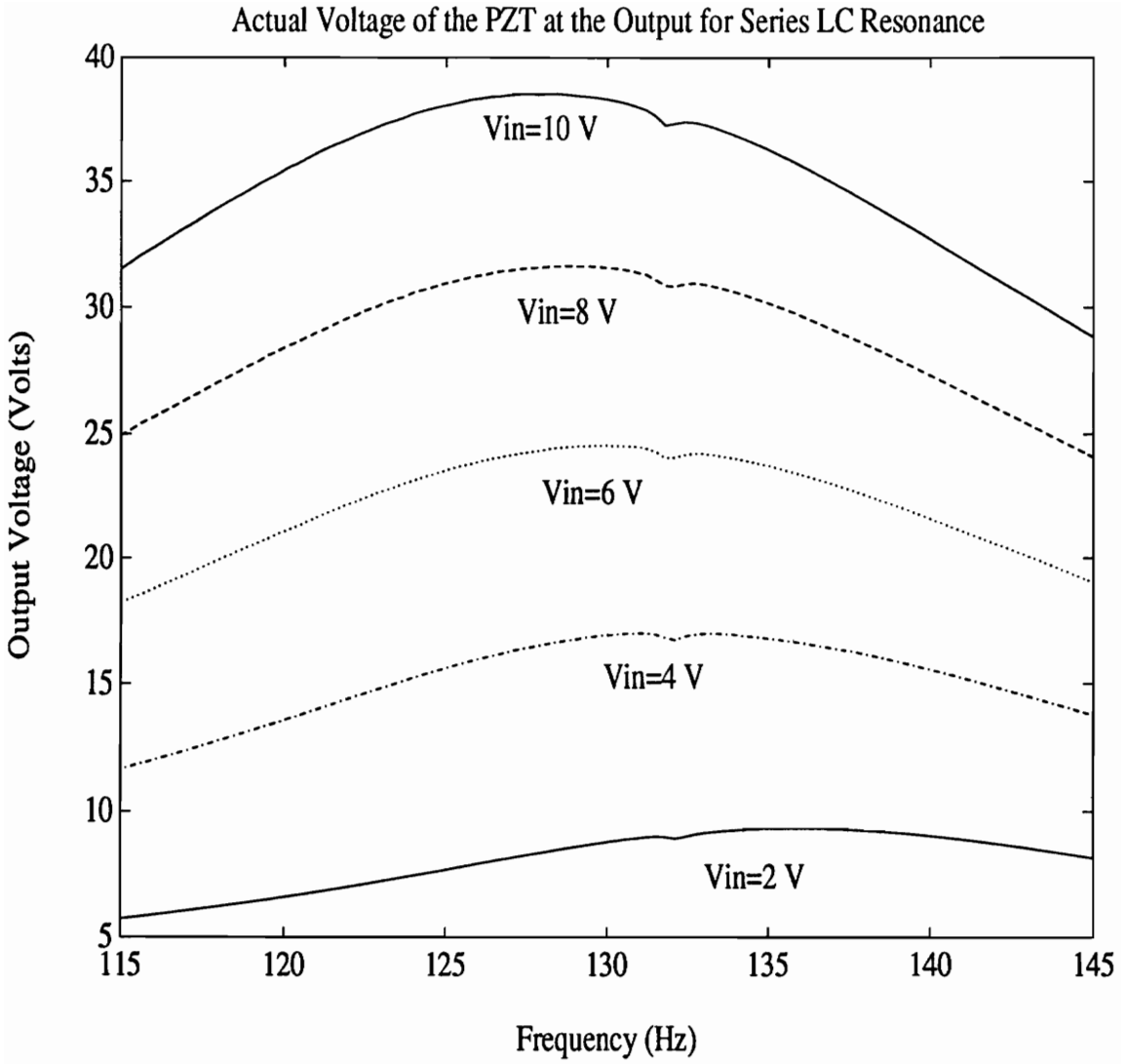Input Voltage for Series LC Resonance

Figure 5.24 Measured PZT Voltages for Series LC Resonance

Hz. The series LC electrical circuit used is shown in Fig. 3.6 and is modeled using a program in Matlab. Figure 5.25 shows the theoretical ratio of the PZT output voltage to the amplifier input voltage at five different voltage levels (10, 8, 6, 4, and 2 V). Figure 5.26 shows the corresponding theoretical phase plot. The model predicts that the PZT output voltage is larger than the amplifier input voltage by approximately 12 dB. The model also predicts that the phase of the PZT voltage lags the amplifier voltage by 90 degrees near the second mode frequency. This implies that the predicted power factor near the second mode is approximately unity. In both the theoretical and experimental phase plots the phase crosses -90 degrees at slightly above the beams second mode frequency. Ideally the phase plot should cross -90 degrees at the resonant frequency, however, the PZT has some internal resistance and the transfer function of PZT output voltage to the amplifier input voltage is measured incorporating the internal resistance of the PZT patch. This causes the -90 degree phase crossover frequency to be slightly higher than the LC resonant frequency.

Figure 5.27 shows a comparison of the experimental and theoretical ratio of PZT output voltage to the amplifier input voltage. As was seen in the parallel resonant case the internal resistance in the model is slightly higher than the actual internal resistance. This causes the deviation between the magnitudes of the experimental and theoretical data. The LC resonant frequencies of the theoretical model are also slightly higher than the actual values. The inductance and capacitance extracted from the impedance tests in Section 5.3 are most likely lower than the actual values and cause the deviation. Based on the results presented, it can be concluded that the experimental results are valid and that the circuit used to model the LC series resonance is reasonably accurate.

Table 5.4 displays the inductance values extracted from the impedance test described in Section 5.3. The table also shows the predicted inductance needed to correct the power

Theoretical Output Voltage/Input Voltage for Series LC Resonance
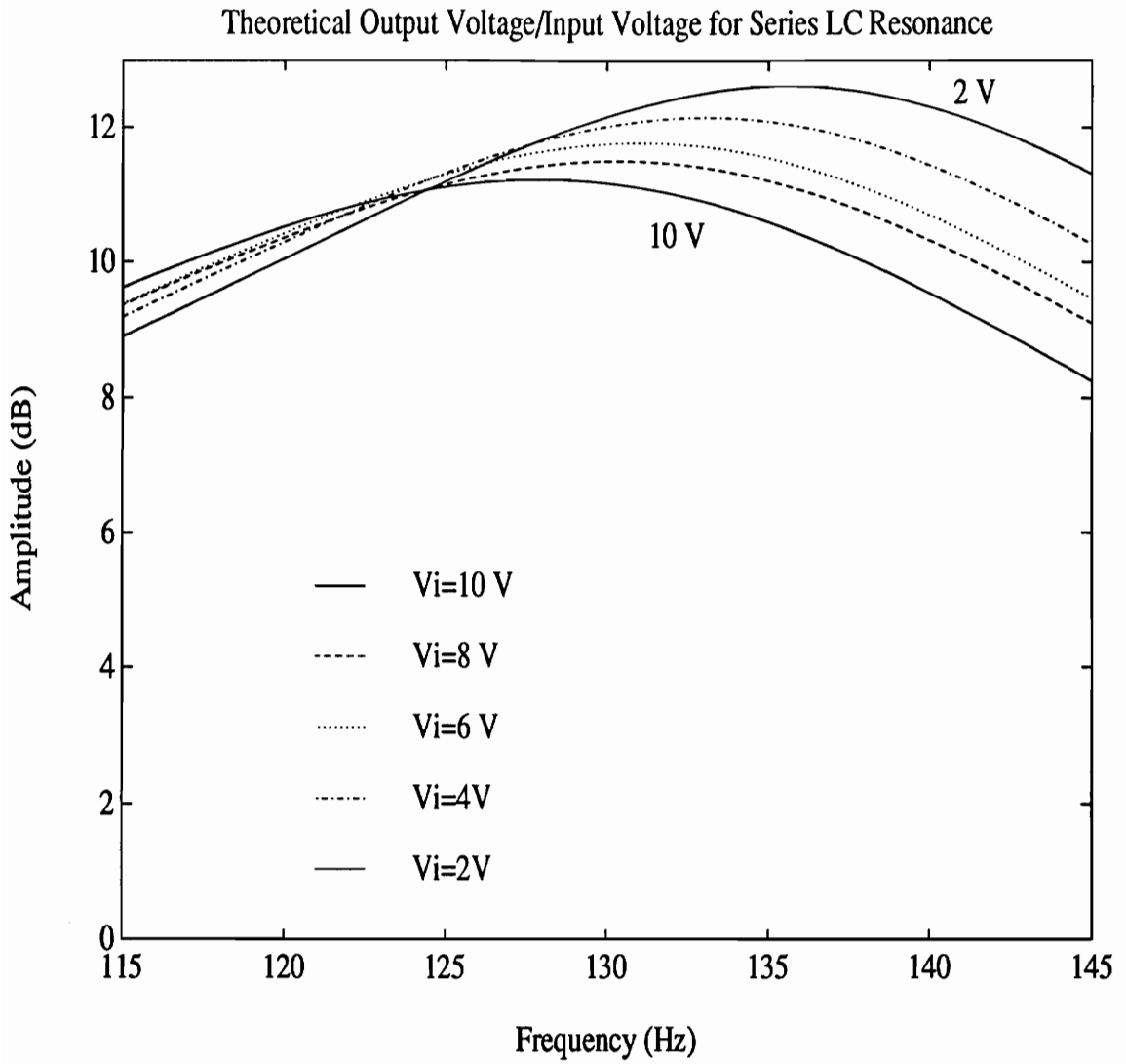
Figure 5.25 Theoretical Ratio of PZT Voltage to Input Voltage for Series LC Resonance
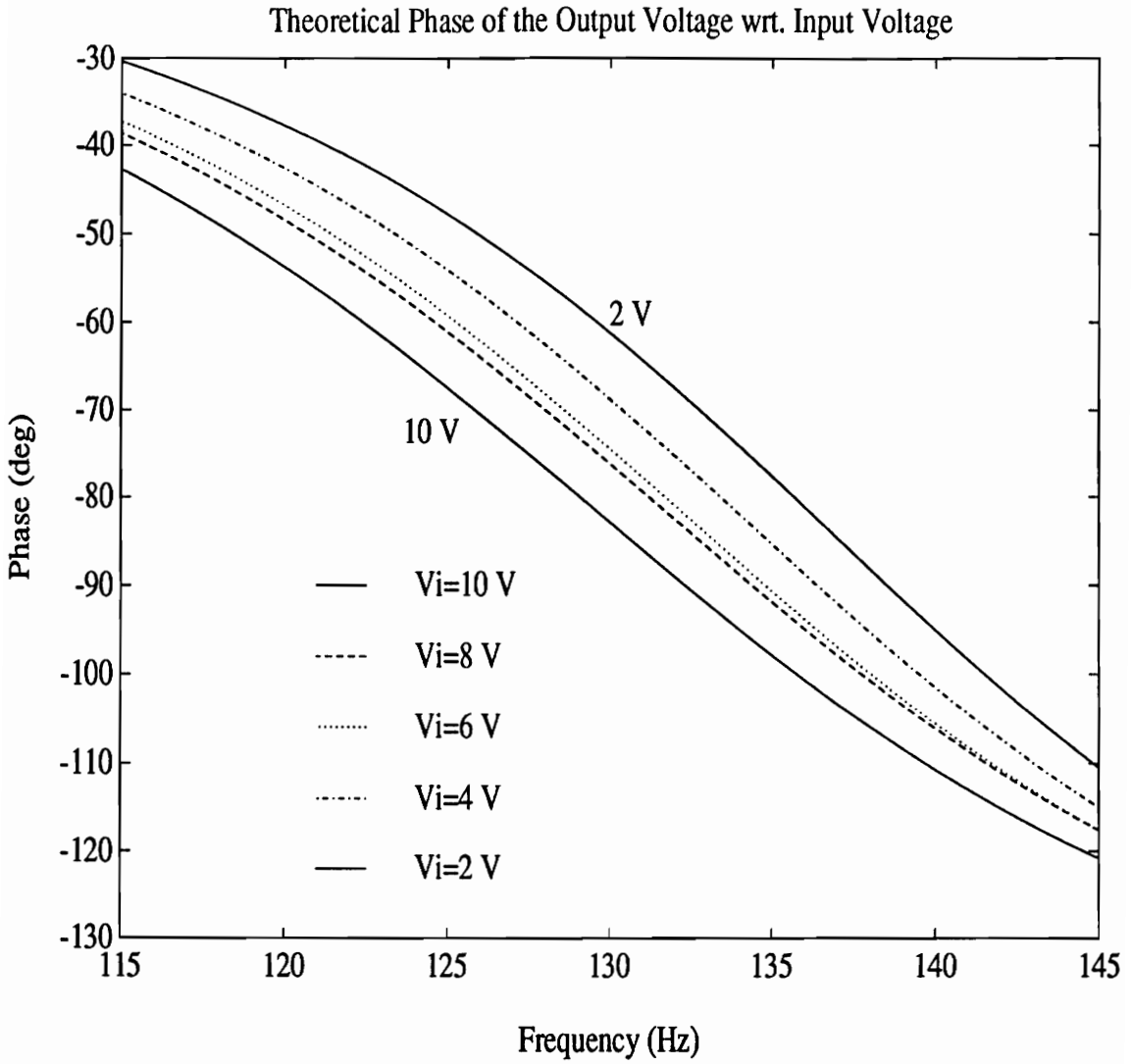
Figure 5.26 Theoretical Phase of PZT Voltage With Respect to Input

Voltage for Series LC Resonance
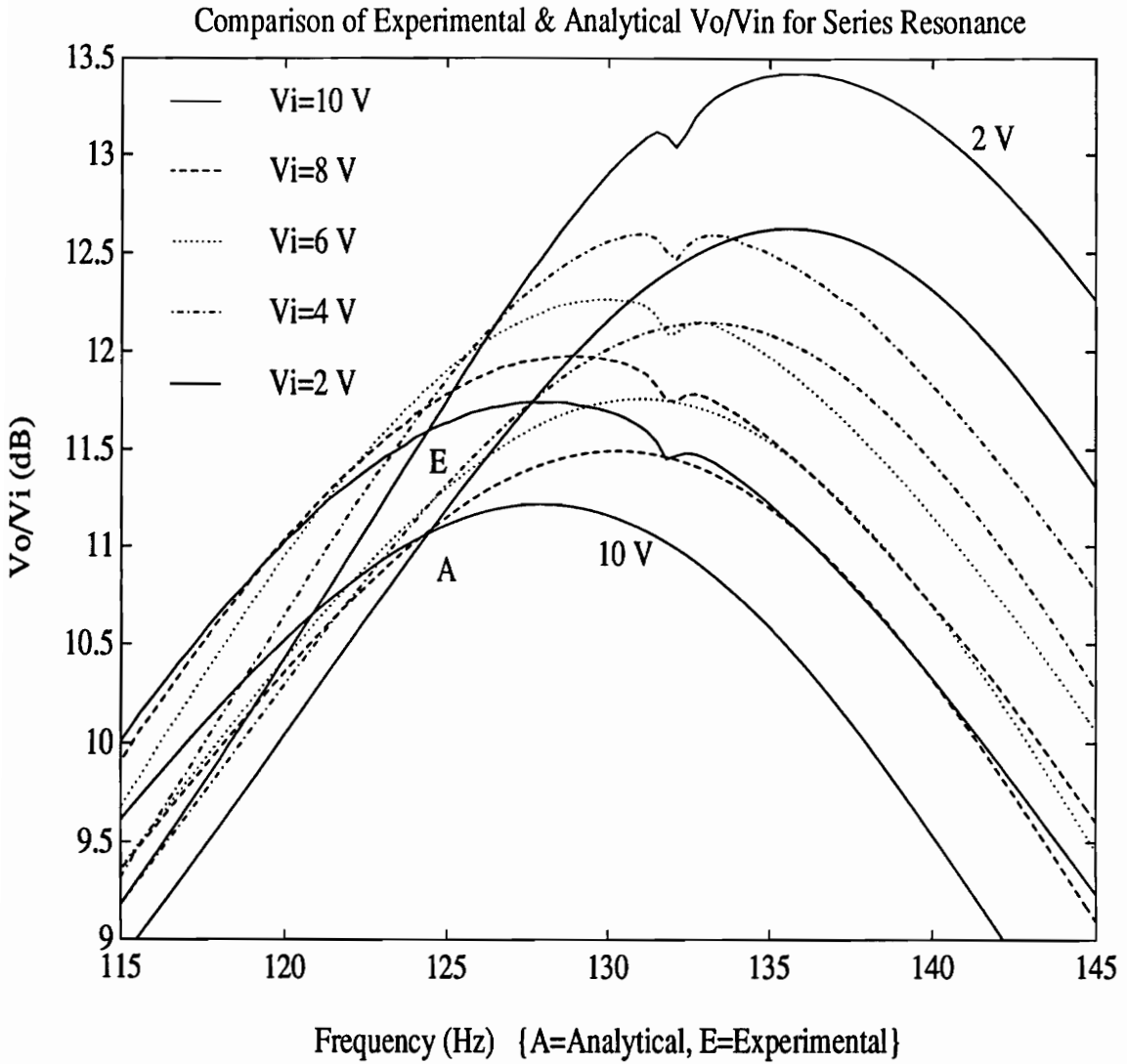
Figure 5.27 Comparison of Theoretical and Experimental Ratio of PZT to Input Voltage

Table 5.4 Experimental and Theoretical Correcting Inductances for Series LC Resonance

Input Voltage (V)	Experimental Inductance from Impedance Test (H)	Theoretical Inductance from Eq 3.16 (H)
10	21.57	21.57
8	21.60	21.57
6	21.85	21.57
4	21.95	22.57
2	22.00	22.57

factor as defined by Eq. 3.16. The predicted inductance is based only on the operating frequency and the capacitance of the PZT actuator. For the experiments performed with an input voltage of 10 V, the predicted correcting inductance and the actual inductor modeled from the impedance test are most closely related. It is therefore expected that the model at 10 V is the most accurate at the second mode frequency. This is effect is seen in Fig. 5.27 where the experimental and modeled LC resonant frequencies are virtually identical.

5.7 Summary

The results show that the model developed relating structural damping and apparent power consumed by the PZT actuator is qualitatively verified and is physically justified. Implementing the parallel LC resonant circuit reduced the actuator current consumption by 75% while implementing the series LC resonant circuit produced a 300% increase in the voltage applied to the actuator compared to the case when no inductor was used. In both cases the power factor has been corrected and the apparent power has been reduced 12 dB. The conclusions and recommendations are presented next.

Chapter 6

Conclusions and Recommendations

6.1 Conclusions

A study of applying power factor correction methods to piezoceramic actuators has been performed. The research investigated power factor correction with the use of series and parallel inductor-capacitor resonant circuits. A relationship between the PZT actuator apparent power and the structural damping within a system is also developed. The model is compared to experimental results of an energy balance performed on a cantilever beam. On the basis of the discussions in Chapter 5 the following conclusions are drawn.

6.1.1 Choice of Damping Models

Structural and viscous damping models have been compared for an aluminum cantilever beam. Figure 5.9 and Fig 5.10 show polynomial curve fits to the actual frequency response function and the error associated with each model. The structural damping curve fit clearly has less error than the viscous damping model. It is therefore concluded that a structural damping model provides the best representation of the damping within the beam, when strain rate feedback is used.

6.1.2 Power and Structural Damping Relationship

A relationship between the PZT actuator apparent power and the structural damping within a system has been developed and is given by Eq. 3.31. Figure 5.13 shows the experimental relationship between the PZT apparent power and the structural damping

96

ratio. It is expected that for a finite amount of power the PZT actuator will cancel the vibration caused by the disturbance and also provide an infinite amount of damping to the structure. The measured apparent power begins to asymptotically approach a finite value as the damping is increased. This agrees with the developed model and therefore Eq. 3.31 is qualitatively verified experimentally and is physically justified.

The developed model is based on the energy balance described by Eq. 3.26. To verify the energy balance, the energy provided to the beam by the disturbance is measured and compared to the predicted energy dissipated naturally within the beam. The results of the energy balance are shown in Fig. 5.14 and are physically unrealistic. The model predicts that the energy naturally dissipated within the beam is larger than the energy provided to the beam by the disturbance. The quantitative results of the energy balance are therefore inconclusive.

6.13 Parallel LC Resonance

Power factor correction techniques have been applied to a mounted PZT actuator. Correcting the power factor of the PZT actuator results in a reduced current and power consumption as compared to a PZT patch actuating alone. This effect is demonstrated in Fig. 5.16 and Fig. 5.17. The addition of the tuned inductor corrects the power factor to near unity and reduces the current consumption approximately 75% at the beam's second mode frequency. Due to the reduction in current, the PZT apparent power is also reduced by 75%. The theoretical and experimental results are almost identical and can be seen in Fig. 5.21.

The primary advantage of using a tuned inductor in parallel with the PZT actuator is the reduction of current consumption. Since PZT patches do not consume a significant

amount of power, the power reduction caused by power factor correction is not important. The reduction of the current consumption is significant because many amplifiers are current limited. By using a tuned inductor in parallel with the PZT patch, a smaller amplifier can be used to power the actuator. The addition of the parallel inductor also allows the PZT patch a path to discharge through, thus protecting the amplifier from capacitive flyback voltages.

The results presented are based on tests performed at low frequencies and with an inductor having high internal resistance. The magnitude of the PZT current is proportional to the operating frequency and so at higher frequencies the PZT actuator uses more current. However, the impedance of the LC parallel resonant circuit is only dependent on the internal resistance of the LC elements and at higher frequencies will produce larger current reductions than the results presented. An inductor with a smaller internal resistance can also help to reduce the current consumption even further.

6.14 Series LC Resonance

Correcting the power factor of the PZT actuator using a series resonant circuit results in an increased actuation voltage and a reduced power consumption as compared to a PZT patch actuating alone. This effect is demonstrated in Fig. 5.22 and Fig. 5.23. The addition of the tuned inductor corrects the power factor to near unity and increases the PZT voltage approximately 300% at the beam's second mode frequency. Due to the increase in voltage, the PZT apparent power is also reduced by 75%. The theoretical model and the experimental results are almost identical and can be seen in Fig. 5.27.

The primary advantage of using a tuned inductor in series with the PZT actuator is the increase in PZT voltage. Since PZT patches do not consume a significant amount of

power, the power reduction caused by power factor correction is not important. The increase in voltage is significant because many amplifiers are voltage limited. By using a tuned inductor in series with the PZT patch, a smaller amplifier can be used to power the actuator. The addition of the series inductor also provides inherent filtering to high frequency noise and protects the amplifier from large currents caused by stepped voltages in capacitive loads.

For the same reasons described in Section 6.13, the voltage increase of the PZT actuator would be much larger if the operating frequency was higher and the inductor internal resistance was lower.

6.2 Recommendations

Future work can be performed in verifying the relationship developed between PZT power and structural damping. The concepts presented are physically justified however accurate experimental data is required to validate the model. Improvements can be made in the experimental setup such that the energy provided to the structure by the disturbance is readily and accurately determined.

The realistic model for the PZT actuator was assumed to be a resistor and a capacitor connected in series. This was chosen because the real and imaginary components extracted from the impedance test are most easily converted into a series impedance model. A parallel internal resistance model can be considered and may produce better results in a broader frequency range.

References

Adcock, J. L., 1987, "Curve Fitter for Pole Zero Analysis," *Hewlett Packard Journal*, January, pp. 33-36.

Bailey, T., and Hubbard, J. E., 1985, "Distributed Piezoelectric-Polymer Active Vibration Control of a Cantilever Beam," *J. Guidance, Control and Dynamics*, Vol. 8(5), pp. 605-610.

Blevins, R.D., 1987, Formulas for Natural Frequency and Mode Shape, Robert E. Krieger Publishing Co., Malabar, Florida.

Chapman, S. J., 1985, Electric Machinery Fundamentals, McGraw-Hill, New York.

Clark, R. L. and Fuller, C. R., 1992, "Experiments on Active Control of Structurally Radiated Sound Using Multiple Piezoceramic Actuators," *The J. of the Acoustical Society of America*, Vol. 91(6), pp. 3313-3320.

Clark, W. W., Robertshaw, H. H. and Warrington, T. J., 1989, "A Planar Comparison of Actuators for Vibration Control Flexible Structures," AIAA Paper No. 89-1330.

Crawley, E. F. and Anderson, E. H., 1990, "Detailed Models of Piezoceramic Actuation of Beams," *J. of Intell. Mater. Syst. and Struct.*, Vol. 1(1), pp. 4-25.

Crawley, E. F. and de Luis, J., 1987. "Use of Piezoelectric Actuators as Elements of Intelligent Structures," *AIAA Journal*, Vol. 25(10), pp. 2000-2010.

Cudney, H. H., 1989, "Distributed Control Using Multilayered Piezoelectric Actuators," Dissertation, State University of New York, Buffalo, NY.

Devasia, S., Meressi, T., Paden, B., Bayo, E., 1992, "Piezo-Electric Actuator Design for Vibration Suppression: Placement and Sizing," *Proceedings of the 31st IEEE Conference on Decision and Control*, Paper No. 92-651.

Finefield, J. K., 1992, "Investigation of Combined Feedback and Adaptive Control of Cylinder Vibrations," Master Thesis, Mechanical Engineering, VPI&SU, Blacksburg, Virginia.

Hagwood, N. W. and von Flotow, A., 1989, "Damping of Structural Vibrations with Piezoelectric Materials and Passive Electric Networks," *Proceedings of the Damping '89 Conference*, West Palm Beach, Florida, February 8-10.

Han, M. C., 1989, "On the Application of Forsythe Orthogonal Polynomials for Global Modal Parameter Estimation," *Proceedings of the Seventh International Modal Analysis Conference*, Las Vegas, Nevada, pp. 628-630.

Hsu, D. S. and Lin, H. H., 1987, "Optimal Control with Control Force Constraints," *Proceedings of the Sessions at Structures Congress '87*, Orlando, Florida, pp. 622-636.

Johnson, D.E., Hilburn, J. L., and, Johnson, J. R.,1986, Basic Electrical Circuit Analysis, Prentice-Hall, Englewood Cliffs, New Jersey, pp. 378-382.

Knisely, J. R., 1988, "Power Factor Improvement Provides Multiple Benefits," *The Magazine of Electrical Design Construction and Maintenance*, Vol. 87(6), pp. 60-64.

Kochersberger, K., 1992, "Structurally Damped Mobility Curve Fitter," unpublished, VPI&SU, Blacksburg, Virginia.

Lee, C. K., Chiang, W. W., and O'Sullivan, T. C., 1989, "Piezoelectric Modal Sensors and Actuators Achieving Critical Active Damping on a Cantilever Plate," *Proceedings of the Structures, Structural Dynamics, and Materials Conference,* Mobile, Alabama, pp. 2018-2026.

Rao, S. S., 1990, Mechanical Vibrations, Addison-Wesley Publishing Co., New York.

Schulz, G. and Heimbold, G., 1983, "Dislocated Actuator/Sensor Positioning and Feedback Design for Flexible Structures," *J. Guidance, Control and Dynamics*, Vol. 6(5), pp. 361-367.

Skidmore, G. R. and Hallauer, W. L., 1985, "Experimental-Theoretical Study of Active Damping with Dual Sensors and Actuators," AIAA Paper No. 85-1921.

Smith, R. J., 1983, <u>Circuits Devices and Systems</u>, John Wiley and Sons, New York.

Sumali, H., 1992, "Active Structural Acoustic Control of Cylinders," Master Thesis, Mechanical Engineering, VPI&SU, Blacksburg, Virginia.

Trek, Inc., 1991, "Operator's Manual for the Trek Model 50/750 High Voltage Amplifier," New York.

Thomson, W. T., 1981, <u>Theory of Vibration with Applications</u>, Prentice-Hall, Englewood Cliffs, New Jersey.

Xu, Y. L., Kwok, K. C. S. and Samali, B., 1990, "Wind-Induced Vibration of Tall Buildings and Its Control by Tuned Mass Dampers," *Proceedings of the Australian Vibration and Noise Conference*, Melbourne, Australia, pp. 73-80.

Zhou, N., 1992, "Active Control of Sound Transmission Through Plates in a Reverberant Environment," Master Thesis, Mechanical Engineering, VPI&SU, Blacksburg, Virginia.

Appendix A:

Coherence Function

Coherence of the FRF for Fig.7 and Fig. 5.8
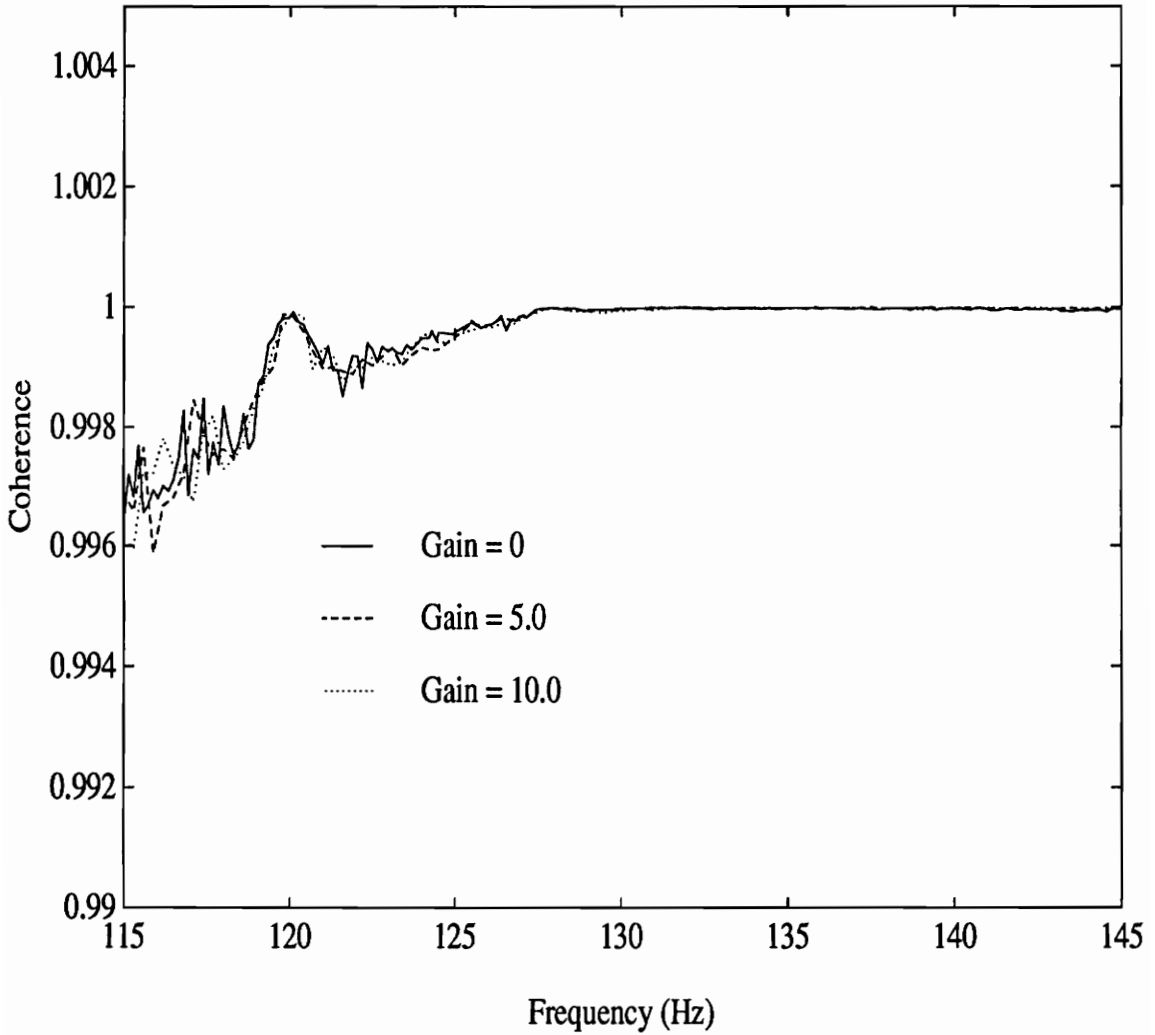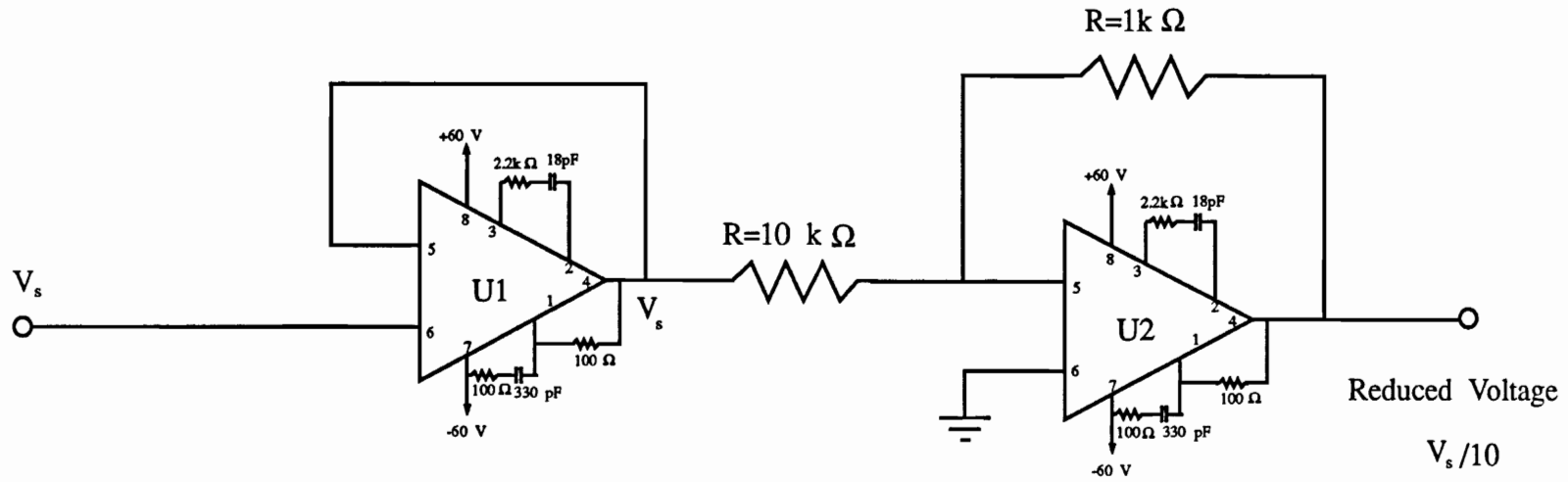

Figure A.1 Coherence for Fig. 5.7 and Fig. 5.8 at Normalized Gain 0, 5.0, and 10.0

Appendix B:

Complete Circuit Diagrams

$$R=1k\ \Omega$$

$$V_s$$

$$R=10\ k\ \Omega$$

U1

U2

$$V_s$$

Reduced Voltage

$$V_s\,/10$$

Key:
U1 - APEX PA41A Op-Amp
U2 - APEX PA41A Op-Amp

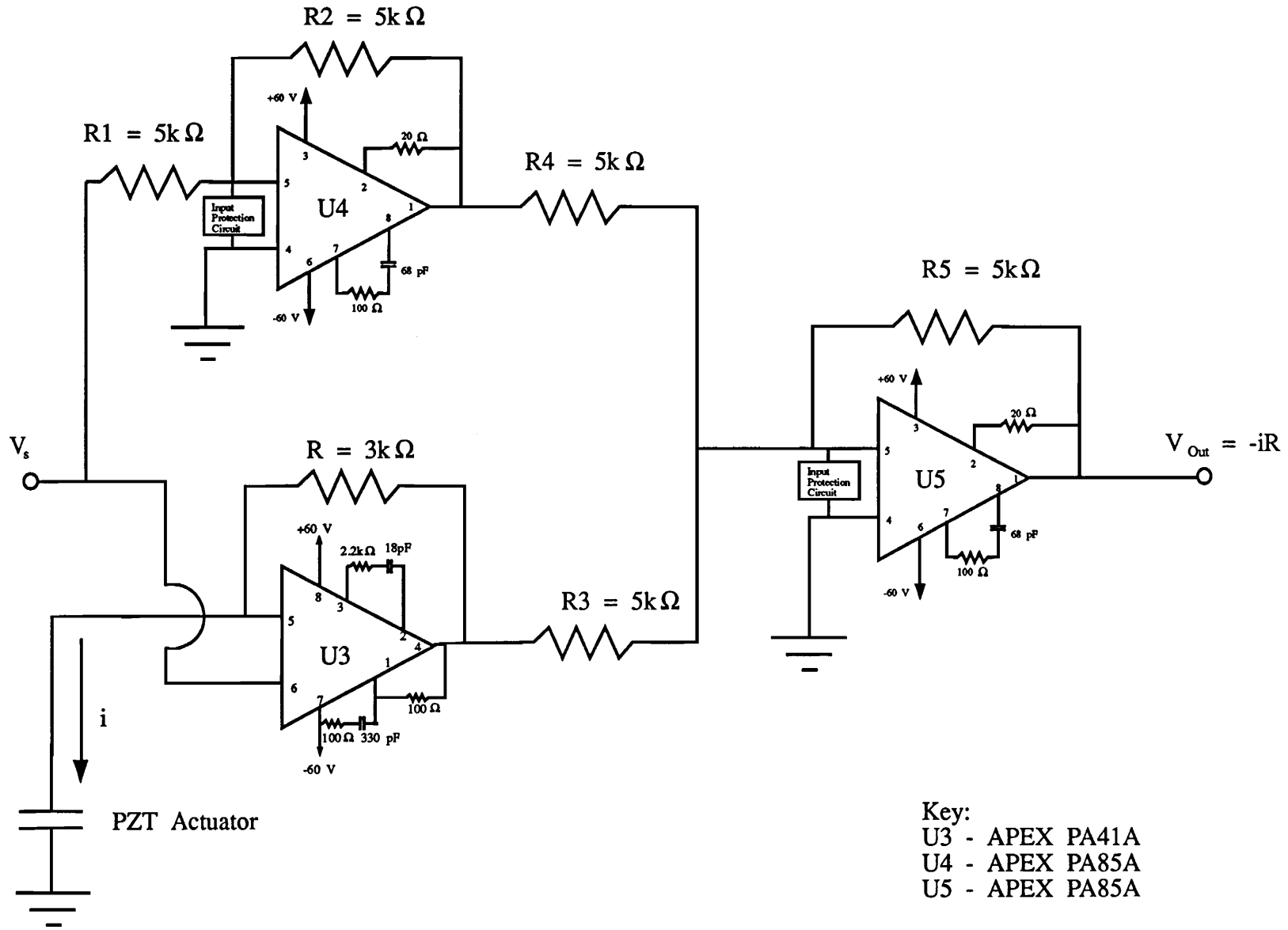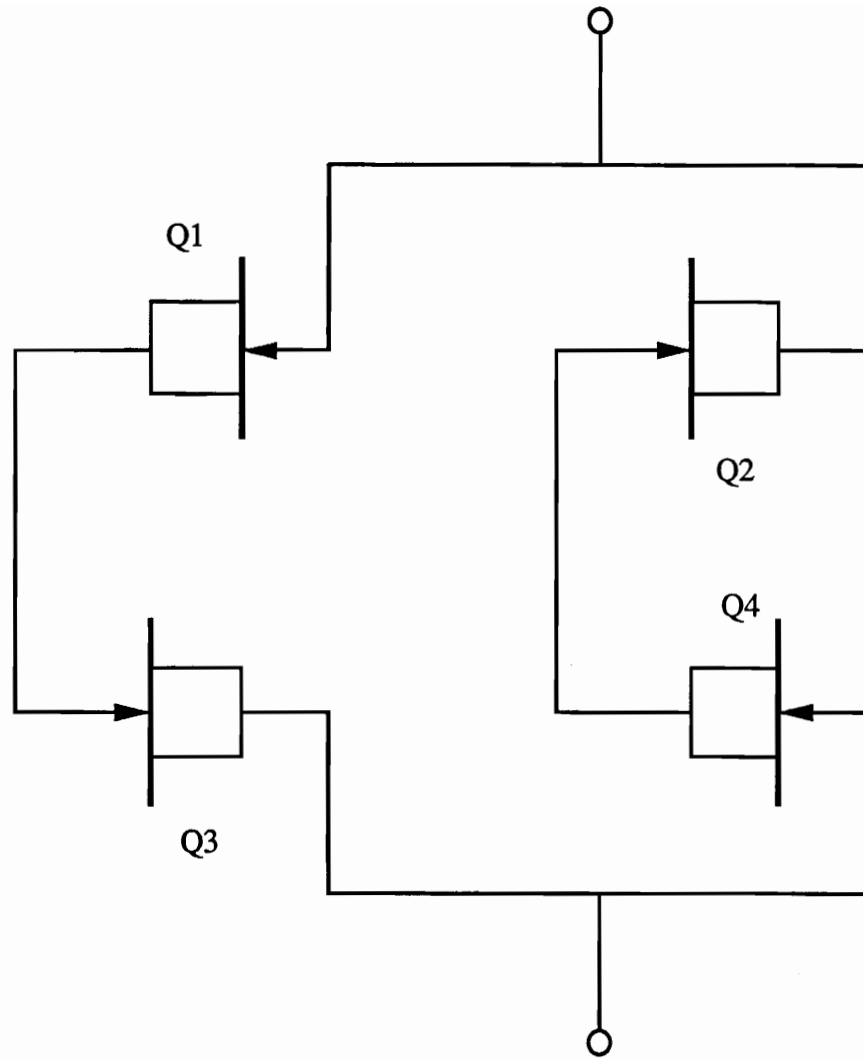Figure B1. Complete Circuit Diagram of Voltage Reducer

Figure B.2 Complete Circuit Diagram of Current to Voltage Converter

Q1

Q2

Q4

Q3

Key:
Q1 - 2N4416 JFET
Q2 - 2N4416 JFET
Q3 - 2N4416 JFET
Q4 - 2N4416 JFET

Figure B.3 Input Protection Circuit

Appendix C:

Moment Voltage Relationship

A relationship between induced moment on the beam by the actuator and the applied voltage to the PZT patch is developed in this section. The following relationships are based on work done by Devasia, *et al*. (1992).

The free strain of the k-th actuator is given by,

$$\Lambda_k = \frac{d_{31} V_k}{t_p}, \qquad k = 1, 2. \tag{C.1}$$

where d_{31}, V_{ak}, and t_{ak} represent the piezoelectric constant, the voltage applied across the actuator, and the thickness of the actuator, respectively.

Assuming a Bernoulli-Euler beam approach, the moment generated by the applied voltage is given by,

$$M^* = bt_p E_p \left\{ (\Lambda_1 - \Lambda_2)\left(\frac{t_b}{2} + t_a + \frac{t_p}{2}\right) \right\} \tag{C.2}$$

Thus,

$$M^* = bE_p d_{31} \left[\frac{t_b}{2} + t_a + \frac{t_p}{2}\right](V_1 - V_2) \equiv \frac{K^*}{2}(V_1 - V_2) \tag{C.3}$$

where M^* is the effective bonding moment acting on a beam of equivalent area moment of inertia and is given by,

$$I_{Eq} = \frac{bt_b^3}{12} + 2\frac{b_a t_a^3}{12} + 2b_a t_a \left[\frac{t_b}{2} + \frac{t_a}{2}\right]^2 + 2\frac{b_p t_p^3}{12} + 2b_p t_p \left[\frac{t_b}{2} + \frac{t_p}{2} + t_a\right]^2 \tag{C.4}$$

where $b_a = b\left(\dfrac{E_a}{E_b}\right)$ and $b_p = b\left(\dfrac{E_p}{E_b}\right)$ are the equivalent adhesive and PZT patch widths, respectively. If the voltages applied to the top and bottom layers are equal in magnitude and opposite in sign, then Eq. C.3 reduces to,

$$M^* = K^* V \qquad (C.4)$$

The effect of the PZT actuator on the beam can be written as two equal and opposite concentrated moments whose magnitude is given by,

$$M = KV \qquad (C.5)$$

where, the constant K is given by,

$$K \equiv K^* \frac{b t_b{}^3}{12 I_{Eq}} \qquad (C.6)$$

Appendix D:

Broad Band Tests

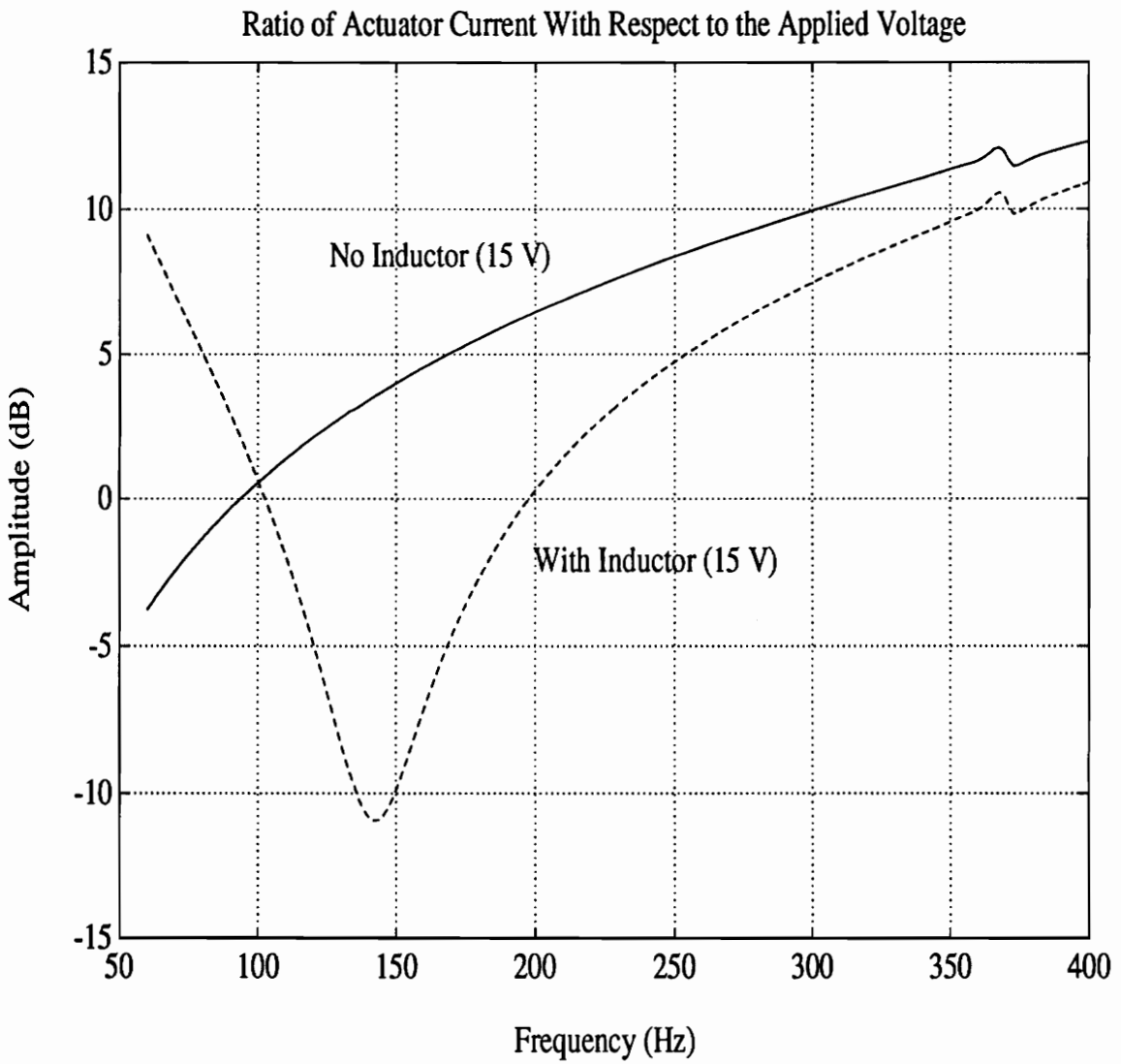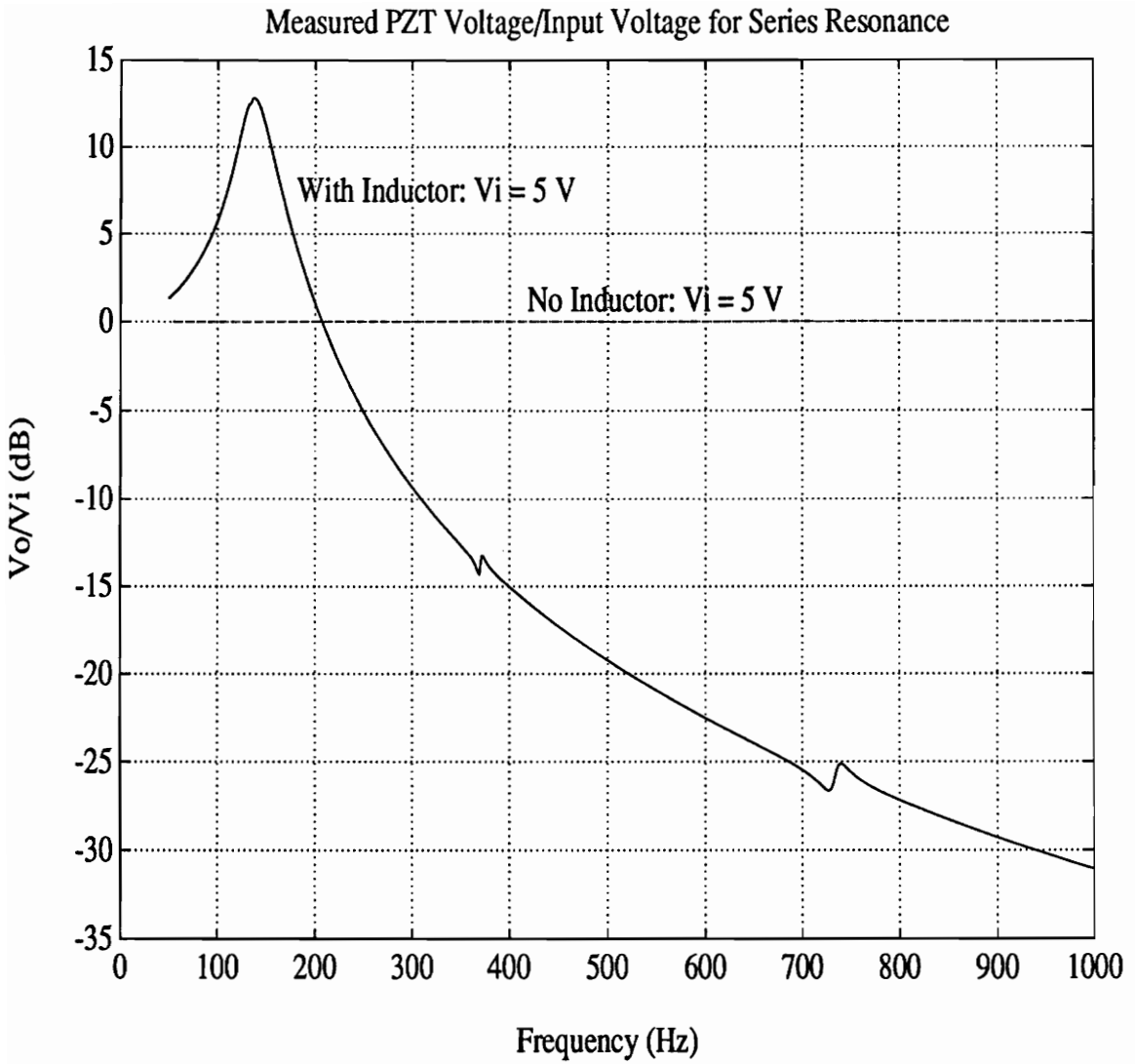Ratio of Actuator Current With Respect to the Applied Voltage

Figure D.1 Measured Broad Band Ratio of Actuator Current With Respect to the Applied

Voltage (Performed at 15 V)

110

Figure D.2 Measured Broad Band Ratio of the PZT Actuator Voltage With Respect to the

Applied Amplifier Input Voltage

Vita

Christopher Niezrecki was born on May 28, 1968 and raised in Orange, CT. After graduating from Amity High School, he attended the University of Connecticut and graduated in 1991 and received a Bachelor of Science degree in Mechanical and also Electrical Engineering. The author has been attending Virginia Polytechnic Institute and State University since August 1991 and expects to finish his Master of Science degree in September of 1992. His intentions are to pursue a PhD degree after working for a time in Connecticut.